CHEMICAL REVIEWS

Review

Cite This: *Chem. Rev.* XXXX, XXX, XXX–XXX

pubs.acs.org/CR

Oxygen Reduction by Homogeneous Molecular Catalysts and Electrocatalysts

Michael L. Pegis,[†] Catherine F. Wise,[†] Daniel J. Martin, and James M. Mayer*

Department of Chemistry, Yale University, New Haven, Connecticut 06520, United States

ABSTRACT: The oxygen reduction reaction (ORR) is a key component of biological processes and energy technologies. This Review provides a comprehensive report of soluble molecular catalysts and electrocatalysts for the ORR. The precise synthetic control and relative ease of mechanistic study for homogeneous molecular catalysts, as compared to heterogeneous materials or surface-adsorbed species, enables a detailed understanding of the individual steps of ORR catalysis. Thus, the Review places particular emphasis on ORR mechanism and thermodynamics. First, the thermochemistry of oxygen reduction and the factors influencing ORR efficiency are described to contextualize the discussion of catalytic studies that follows. Reports of ORR catalysis are presented in terms of their mechanism, with separate sections for catalysis proceeding via initial outer- and inner-sphere electron transfer to O_2. The rates and selectivities (for production of H_2O_2 vs H_2O) of these catalysts are provided, along with suggested methods for accurately comparing catalysts of different metals and ligand scaffolds that were examined under different experimental conditions.

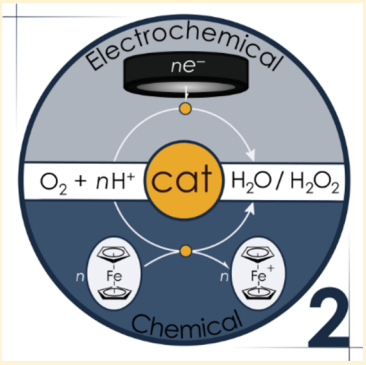

CONTENTS

Special Issue: Oxygen Reduction and Activation in Catalysis

Received: September 7, 2017

DOI: 10.1021/acs.chemrev.7b00542
Chem. Rev. XXXX, XXX, XXX–XXX

1. INTRODUCTION

1.1. Background, Significance, and Scope of This Review

The catalytic reduction of dioxygen (O_2) is a critical component of biological processes and emerging energy technologies. The biological respiratory chain couples O_2 reduction to transmembrane proton transfer and drives the synthesis of ATP.[1] Fuel cells and metal−air batteries are important next-generation energy technologies that use O_2 as an electron/cation acceptor. Such processes typically combine O_2 reduction with the oxidation of a fuel (e.g., H_2) to generate an electromotive force that can power electronics, homes, or vehicles. Because these processes convert chemical to electrical energies, catalysis of the oxygen reduction reaction (ORR) needs to occur with high rates, high selectivity, and high energy efficiency. Despite decades of research, a rapid, robust, inexpensive, and efficient ORR electrocatalyst remains undiscovered. Consequently, the ORR continues to be one of the largest challenges in chemical energy research.

The requirement for energy efficiency separates the ORR from otherwise closely related reactions that involve O_2 as an oxidant (in other words, the reduction of O_2). For example, traditional platinum on carbon and soluble cobalt macrocycles have been used for the ORR and have loose analogies to supported silver catalysts and cobalt salts used as catalysts for the aerobic oxidation of ethylene and cyclohexane.[2,3] The ORR catalyst in the mitochondrial electron transport chain, cytochrome *c* oxidase,[4] shares many commonalities with metalloproteins and metalloenzymes that transport O_2 and that utilize O_2, such as hemoglobins and cytochrome P450s.

This Review covers the field of soluble molecular oxygen reduction catalysis. This includes homogeneous catalysis using soluble reductants and electrochemical methods, both in aqueous and nonaqueous media. This Review surveys many combinations of catalysts, solvents, and sources of protons and electrons. Molecular catalysts attached to electrode surfaces are covered in a separate Review in this issue.[5] This Review attempts to be comprehensive and takes a thermochemical and mechanistic view. It builds on excellent prior reviews that cover this topic from somewhat different perpsectives.[6−11]

In protic media, O_2 reduction can proceed by the two-proton/two-electron ($2H^+/2e^-$) reduction to hydrogen peroxide (H_2O_2) or by the four-proton/four-electron ($4H^+/4e^-$) reduction to water (H_2O) (reactions (i) and (ii) in Scheme 1, respectively). Many

Scheme 1. Half-reactions for O_2 Reduction to H_2O_2 (i) and H_2O (ii)

$$O_2 + 2H^+ + 2e^- \rightleftharpoons H_2O_2 \quad \text{(i)}$$

$$O_2 + 4H^+ + 4e^- \rightleftharpoons 2H_2O \quad \text{(ii)}$$

catalytic processes involve a combination of these two half-reactions, either competitively or sequentially. While both processes look simple, the formation of H_2O_2 is a catalytic reaction with five substrates (O_2, $2e^-$, and $2H^+$), and the catalytic cycle for H_2O production involves *nine* substrates. For most practical energy applications, it is important that the ORR be accomplished with high selectivity for H_2O, as the $2H^+/2e^-$ ORR provides much less free energy. While deleterious for applications that convert chemical energy to electrical energy (e.g., fuel cells), the production of H_2O_2 from O_2 is important for other applications such as paper bleaching, wastewater treatment, and use as a chemical feedstock.[12,13]

The production of H_2O_2 and/or H_2O from O_2, H^+, and e^- always proceeds through mechanistic steps that contain e^- and H^+ stoichiometries smaller than the net $2H^+/2e^-$ and $4H^+/4e^-$ reductions shown in Scheme 1. For instance, a common first step for both H_2O and H_2O_2 production is electron transfer to O_2 to form superoxide ($O_2^{\bullet-}$), which, in some cases, is coordinated to a metal center. This reaction and the following electron transfer (ET), proton transfer (PT), or proton-coupled electron transfer (PCET) steps are less thermodynamically favorable than the overall reduction to H_2O, as discussed later in section 2. For this reason and others, the partially reduced intermediates are often highly reactive and are collectively referred to as reactive oxygen species (ROS). The formation and reactivity of ROS intermediates are critical to the rate and selectivity of ORR catalysis because side reactions of these intermediates can destroy catalysts and other components of a device, such as polyelectrolyte membranes.[14] The same issues arise in biological systems, which have an extensive set of mechanisms to remove ROS.[15,16]

The complexity of O_2 reduction and the formation of high-energy intermediates have made efficient ORR catalysis very challenging. Consequently, most catalysts operate at high overpotentials, meaning that there is a large difference between the applied potential required for catalysis at a reasonable current density or turnover frequency (TOF) and the ORR thermodynamic potential under the experimental conditions. Among the most efficient catalysts used in low-temperature fuel cells are carbon-supported noble metal nanoparticles, typically platinum.[17] There have been substantial advances in this area; however, even the best catalysts operate at considerable overpotentials at viable current densities.[17] New carbonaceous materials containing nitrogen and often iron have shown great promise,[18] and it seems likely that the eventual technological solution will be similar engineered or multicomponent electrode materials or oxides.[19] The soluble electrocatalysts described in this Review are less likely to be practical. In many cases, most of the catalyst is far from the electrode and inactive at any given time, and catalyst separation is an added concern. The studies described in this Review are not aimed toward achieving the Department of Energy (DOE) targets for ORR catalysis; rather, they provide a fundamental understanding of the various rate-limiting, overpotential-regulating, and selectivity-determining steps of the catalytic cycles. The tools of molecular chemistry can be used to understand mechanism and develop structure−activity relationships with much greater detail than is currently available for heterogeneous catalysts. The understanding derived from these studies will likely underpin the step-change in technology that is required to achieve efficient O_2 reduction in fuel cells and other devices.

Studies with soluble ORR catalysts have shown that the nature of the metal, ligands, acid, and solvent can all modulate the thermodynamics of elementary steps to affect catalytic rates, selectivity, and overpotential. These are interdependent quantities, as will be discussed later. Much of the early work in this field was inspired by natural systems, especially cytochrome *c* oxidase, myoglobin, hemoglobin, and cytochrome P450s. Although these

DOI: 10.1021/acs.chemrev.7b00542
Chem. Rev. XXXX, XXX, XXX−XXX

four systems have closely related primary coordination spheres, they react with O_2 in different ways. Myoglobin and hemoglobin engage only in O_2 binding, while cytochrome *c* oxidase reduces O_2 to H_2O and P450s create a highly active iron-oxo ("ferryl") oxidant. This difference in O_2 reactivity largely reflects variations in the secondary coordination sphere and beyond. Specifically, the protein structures stabilize metal−oxygen intermediates differently and control site-specific delivery of H^+ and e^-.

Despite such control, it should be noted that cytochrome *c* oxidase does not perform the ORR near the thermodynamic potential. Rather, it uses lower potentials and captures some of the free energy of the reaction to pump protons across the membrane.[4,20] The tricopper enzyme laccase is currently the best metalloprotein for the ORR and, by some metrics, can outperform platinum when adsorbed on electrodes, although its native function is substrate oxidation.[5,21,22] Such enzyme-like activity is only beginning to be possible with synthetic catalysts.[5]

Inspiration from enzymatic systems and the development of new electroanalytical techniques have stimulated recent work toward improved synthetic ORR catalysts. One very popular approach is to include proton and hydrogen-bond donor groups in the secondary coordination sphere. The "hangman" macrocycles developed by Nocera and co-workers were early examples of such potential "proton relay" catalysts and built upon biomimetic models and the groundbreaking work of Collman, Chang, Anson, Borovik, and others (section 4.2).[23] The development of new methods to evaluate ORR efficiency for soluble catalysts make this a promising time for discovering new catalysts and new concepts for the ORR.

1.2. Outline of the Review

Because the energy efficiency of ORR catalysis is critical and the mechanistic principles reflect the thermodynamic landscape, this Review begins by presenting the thermochemical parameters relevant for O_2 reduction under different conditions (section 2). We provide overall thermodynamic values for the ORR and the thermochemistry for various interconversions of O_2-derived intermediates, as well as the solubility of O_2 in various solvents. Following this introduction, ORR catalysts are divided by mechanism. Section 3 presents studies of O_2 reduction reactions that are initiated by *outer-sphere* electron transfer to O_2. Section 4, the largest portion, describes ORR catalysts that bind directly with O_2 via *inner-sphere* mechanisms, forming metal−oxygen bonds that stabilize reduced, high-energy, and reactive oxygen intermediates. Each section is further divided into subsections as appropriate, for instance, by ligand type, metal, reaction conditions, etc.

2. THERMODYNAMICS OF DIOXYGEN REDUCTION

The ultimate goal of ORR catalysts is to achieve fast rates and high selectivity (H_2O vs H_2O_2) at potentials close to the thermodynamic potential. The thermodynamic potential for the ORR depends on the product(s) formed, either H_2O_2 from the $2H^+/2e^-$ reduction ($O_2 + 2H^+ + 2e^- \rightarrow H_2O_2$) or H_2O from the $4H^+/4e^-$ reduction ($O_2 + 4H^+ + 4e^- \rightarrow 2H_2O$). Additionally, the $2H^+/2e^-$ reduction of H_2O_2 is known ($H_2O_2 + 2H^+ + 2e^- \rightarrow 2H_2O$). Molecular catalysts can often catalyze more than one of these reactions. For example, a relatively common combination is known as the 2 + 2 mechanism, which yields H_2O via H_2O_2 ($O_2 + 2H^+ + 2e^- \rightarrow H_2O_2$, + $2H^+ + 2e^- \rightarrow 2H_2O$). Thus, knowledge of the product(s) formed is necessary to evaluate and compare ORR catalysts. This section summarizes the relevant thermochemistry for both the O_2/H_2O and O_2/H_2O_2 half-reactions required to evaluate ORR catalysts in a variety of media.

2.1. Aqueous Thermochemistry of Dioxygen Reduction

The aqueous thermochemistry of O_2 reduction to H_2O and H_2O_2 has long been established (Table 1). The potentials for unstable odd-electron intermediates derived from O_2 are discussed in section 2.4. Aqueous standard reduction potentials are reported versus the standard hydrogen electrode (SHE, $2H^+ + 2e^- \rightarrow H_{2(g)}$). The strict definition of these standard conditions specifies 298.15 K, 1 atm pressure for gases, and unit activity for solutes (1 M solutions with the properties of the solute at infinite dilution).[24] Typically, however, ORR literature almost always uses 1 M rather than unit activity as the standard state for solutes.

Table 1. Standard Potentials for Aqueous ORR Half-reactions[a]

half-reaction	$E^\circ_{(aqueous)}$[a] (V vs SHE)
$O_{2(g)} + 4H^+ + 4e^- \rightleftharpoons 2H_2O$	1.229
$O_{2(g)} + 2H^+ + 2e^- \rightleftharpoons H_2O_2$	0.695
$H_2O_2 + 2H^+ + 2e^- \rightleftharpoons 2H_2O$	1.763

[a]From ref 25.

Many ORR experiments are done under nonstandard conditions, typically at solution pH's that differ from the standard condition of pH 0. Potentials under nonstandard conditions are called *equilibrium potentials*. The thermodynamic ORR and H^+/H_2 potentials shift according to the Nernst equation (eq 1), where Q is the equilibrium quotient illustrated for the $4H^+/4e^-$ ORR in eq 2. ORR studies often reference their potentials to the H^+/H_2 potential at the same pH, a reference potential that is referred to as the "reversible hydrogen electrode" or RHE. Both O_2/H_2O and H^+/H_2 reactions involve an equal number of protons and electrons, so their potentials each decrease by 0.0592 V per unit change in pH (per decade decrease in proton activity, 0.0592 V = 2.303RT/F at 298 K, where 2.303 is the conversion from ln to log). Therefore, the overall cell potential for water splitting ($2H_2O \rightarrow 2H_2 + O_2$) is 1.229 V and is independent of pH. ORR potentials are much less sensitive to P_{O_2} than to pH, varying only as $P_{O_2}^{1/4}$ for the $4H^+/4e^-$ ORR (e.g., a 10-fold change in P_{O_2} shifts E by only ∼15 mV).

$$E = E^\circ - \frac{RT}{nF} \ln Q \tag{1}$$

$$E = E^\circ - 0.0148 \log(P_{O_2}{}^{-1}[H^+]^{-4}) = E^\circ - 0.0591 \log(P_{O_2}{}^{-1/4}[H^+]^{-1}) \tag{2}$$

While H^+/H_2 is the official electrochemical reference, preparing and maintaining a pristine SHE or RHE electrode can be time-consuming.[26] Instead, experimental studies almost always use more convenient reference electrodes such as saturated calomel (SCE, Cl^- (4M) | Hg_2Cl_2 | Hg (l) | Pt). Because many of the studies in the later sections use such reference electrodes, we include here a table of common aqueous reduction potentials (Table 2). In some cases, reference electrodes have been

Table 2. Reduction Reactions for Aqueous Reference Electrodes and Their Standard Potentials

half-reaction	E^a (V vs SHE)
$AgCl_{(s)} + e^- \rightleftharpoons Ag_{(s)} + Cl^-_{(sat'd)}$	0.197
$Hg_2SO_{4(s)} + 2e^- \rightleftharpoons 2Hg_{(l)} + SO_4{}^{2-}_{(sat'd)}$	0.64
$Hg_2Cl_{2(s)} + 2e^- \rightleftharpoons 2Hg_{(l)} + 2Cl^-_{(sat'd)}$	0.2412
$HgO_{(s)} + H_2O_{(l)} + 2\,e^- \rightleftharpoons Hg_{(l)} + 2OH^-_{(0.1M)}$	0.926

[a]At 298 K, ref 28.

DOI: 10.1021/acs.chemrev.7b00542
Chem. Rev. XXXX, XXX, XXX−XXX

Table 3. Recommended Standard Potentials for the ORR Half-reaction in Nonaqueous Solvents with Acid HA[a]

half-reaction	$E^\circ_{O_2/H_2O(MeCN)}$[a]	$E^\circ_{O_2/H_2O(DMF)}$[a]
$H_2O_{2(solv)} + 2HA_{(solv)} + 2e^- \rightleftharpoons 2H_2O_{(solv)} + 2A^-_{(solv)}$	[+1.74−0.0592pK_a(HA)][b]	[+1.13−0.0592pK_a(HA)][b]
$O_{2(g)} + 4HA_{(solv)} + 4e^- \rightleftharpoons 2H_2O_{(solv)} + 4A^-_{(solv)}$	+1.21−0.0592 pK_a(HA)	+0.60−0.0592pK_a(HA)
$O_{2(g)} + 2HA_{(solv)} + 2e^- \rightleftharpoons H_2O_{2(solv)} + 2A^-_{(solv)}$	[+0.68−0.0592 pK_a(HA)][b]	[+0.06−0.0592pK_a(HA)][b]
$2H^+_{(solv)} + 2e^- \rightleftharpoons H_{2(g)}$	−0.028[c]	−0.662
$O_{2(g)} + 2H_{2(g)} \rightleftharpoons 2H_2O_{(solv)}$	+1.24[d]	+1.26[d]
$O_{2(g)} + H_{2(g)} \rightleftharpoons H_2O_{2(solv)}$	+0.70[d]	+0.73[d]

[a]In V vs $Fc^{+/0}$ standard at 298 K. From ref 29 unless otherwise noted. [b]Calculated from the line above assuming that the free energy of transfer from water to the organic solvent, ΔG° (aq → org), is the same for H_2O and for H_2O_2. [c]From ref 30. [d]Cell voltage for the whole (not half) reaction: $\Delta G^\circ = -4FE^\circ$.

used where the concentrations or activities of dissolved solutes are unknown (pseudoreference electrodes) or contain different solutions in their working and reference compartments so that liquid junction potentials are present.[27] Generally speaking, such issues are more frequent and problematic for organic solvents, as pointed out for individual cases below. Readers interested in more information about the preparation and subtleties of reference electrodes are directed to ref 27.

2.2. Nonaqueous Thermochemistry of Dioxygen Reduction

Studies of the ORR by *soluble* molecular catalysts, the topic of this Review, are more often performed in nonaqueous media. This contrasts with the large majority of ORR studies performed in aqueous media using *heterogeneous* electrocatalysts, both with solid electrodes and with adsorbed molecular catalysts. This is primarily due to the molecular catalysts being only soluble in organic solvents, such as *N*,*N*′-dimethylformamide (DMF) or acetonitrile (MeCN). Until recently, one limitation of these studies was that the standard or formal potentials for the ORR were not known in these media. Later, we describe these values and discuss the complexities of using them, so we encourage readers to read past Table 3.

In 2015, Pegis, Roberts, Appel, and co-workers estimated the standard potentials for O_2/H_2O ($E^\circ_{O_2/H_2O}$) in MeCN and DMF for the first time, using the thermochemical cycle in Scheme 2.[29]

Scheme 2. Thermochemical Cycle to Estimate $E^\circ_{O_2/H_2O}$ in Nonaqueous Solvents from $E^\circ_{H^+/H_2}$ (Reprinted with Permission from Ref 29; Copyright 2015 American Chemical Society)

$$O_{2(g)} + 4H^+_{(aq)} + 4e^-_{(SHE)} \xrightleftharpoons{E^\circ_{O2/H2O(aq)}} 2H_2O_{(aq)} \quad (i)$$

$$2H_{2(g)} \xrightleftharpoons{-E^\circ_{H+(aq)/H2}} 4H^+_{(aq)} + 4e^-_{(SHE)} \quad (ii)$$

$$4H^+_{(org)} + 4e^-_{(Fc^{+/0})} \xrightleftharpoons{E^\circ_{H+(org)/H2}} 2H_{2(g)} \quad (iii)$$

$$2H_2O_{(aq)} \xrightleftharpoons{\Delta G^\circ_{H2O(aq\rightarrow org)}} 2H_2O_{(org)} \quad (iv)$$

$$O_{2(g)} + 4H^+_{(org)} + 4e^-_{(Fc^{+/0})} \xrightleftharpoons{E^\circ_{O2/H2O(org)}} 2H_2O_{(org)} \quad (v)$$

This cycle is advantageous in that it depends only on (i) the well-known ORR potential in water versus SHE, (ii) the well-known H^+/H_2 potential in water versus SHE, (iii) the standard potential for the H^+/H_2 couple in the nonaqueous conditions of study, and (iv) the relatively small free energy of H_2O transfer from water to organic solvents. The key benefit is that the H^+/H_2 couple can be measured directly using a Pt wire under almost any set of conditions.[30] The $\Delta G^\circ_{H_2O(aq\rightarrow org)}$ values for MeCN and DMF are only −0.43 and −1.47 kcal mol^{-1} (−19 and −64 meV), respectively.[29] Therefore, with the approximation that $\Delta G^\circ_{H_2O(aq\rightarrow org)} \approx 0$, the equilibrium potential for the ORR in a wide range of acids and solvents can be estimated as simply ∼1.23 V higher than the measured H^+/H_2 potential under the same conditions. Scheme 2 explicitly indicates the phase, medium, and electrochemical reference of all the species involved, and we recommend that all papers in this area do the same.

More recently, Passard and co-workers obtained quite different estimates for the ORR standard potential in MeCN and DMF using a different thermochemical cycle (Figure 1).[31] This cycle is

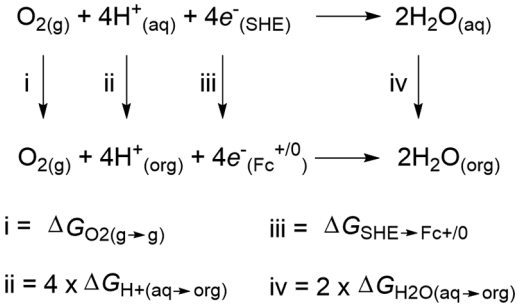

Figure 1. Thermochemical cycle to estimate O_2/H_2O in organic (org) solvents used in ref 31.

challenging because it requires free energy values for proton transfer from water to the organic solvent and requires a conversion from aqueous SHE to the $Fc^{+/0}$ electron reference (Fc = ferrocene, $Fe(C_5H_5)_2$). In our view, these values are difficult to determine, and there is disagreement in the literature values.[29] Therefore, we use here and recommend the values derived from Scheme 2, which are directly tied to the experimental H^+/H_2 potentials.

Recommended values for the ORR standard potentials in DMF and MeCN are given in Table 3. These are given as equilibrium potentials using an acid (HA), as most nonaqueous reactions are done with dilute solutions of a weak acid. The 1 M H^+ standard state can be achieved in DMF, for instance, with the convenient reagent [DMF−H^+][OTf^-], (OTf^- = triflate, $CF_3SO_3^-$),[29] which is a quite strong acid. In MeCN, however, it is difficult to achieve a solvated proton as the major species. Rather, the standard potentials in Table 3 are estimated via extrapolation of weaker acid data and knowledge of the pK_a scale in MeCN.[32]

The values in Table 3 are more complicated in practice than the aqueous values in Table 1. It should be emphasized that they apply to the standard states of *all* of the reagents, taken here as 1 M for solutes[25] and 1 atm for dissolved gases at 298 K. This means that HA and A^- *both* need to be present; in practice, this means that solutions must be buffered, with [HA] = [A^-]. This experimental condition was met only for a limited subset of the studies described later; more commonly, only the acid was

DOI: 10.1021/acs.chemrev.7b00542
Chem. Rev. XXXX, XXX, XXX−XXX

Scheme 3. Reactions Involved in Homoconjugation Equilibria Common in Nonaqueous Conditions

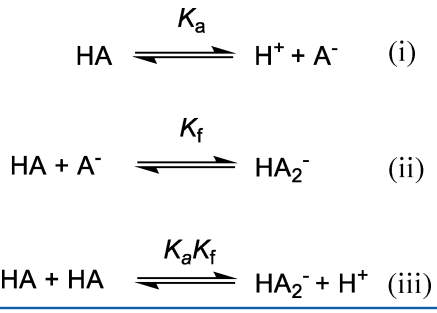

added. This can have a large effect on the ORR potential. For example, a 10^3 ratio of [HA] to [A^-] causes a 178 mV shift in the equilibrium potential (based on the Nernst equation for this process, eq 3). The thermochemistry of homogeneous experiments performed without added conjugate base is further complicated by the change in [A^-] as the reaction proceeds, which shifts the equilibrium potential. In electrochemical processes such as the ORR, A^- is formed at the electrode, causing its concentration to vary with both time and space. For these reasons, we strongly encourage that ORR studies be performed in buffered solutions, especially if the effective overpotential (η_{eff}) is reported for a particular process (see section 2.5). We advise using buffers that do not strongly homoconjugate (see later) in the solvent of interest (e.g., $[PhNH_3]^+/PhNH_2$ in MeCN). Regardless of buffer choice, however, we hope that all ORR studies will report such η_{eff} values.

$$E_{O_2/H_2O} = E^\circ_{O_2/H_2O} - \left(\frac{0.0592\ V}{4}\right)\log\frac{[H_2O]^2[A^-]^4}{P_{O_2}[HA]^4} - (0.0592\ V)pK_a(HA) \quad (3)$$

The standard potentials also refer to solutions that are 1 M in water. However, very few ORR studies in organic media have been performed in the presence of substantial amounts of added water. While the absence of water makes the equilibrium potentials more positive (by Le Chatelier's principle), it is typically a modest effect. Most organic solvents contain residual water (≥1 mM) unless substantial care is taken, and water is formed as the reaction proceeds. At [H_2O] = 10 mM, the deviation in the equilibrium potential from the 1 M value in Table 3 is only 59 mV.

Returning to the use of common acids (HA) in organic solvents, we recommend to readers the extensive data on pK_a values (reaction i, Scheme 3) in a variety of organic solvents reported by Izutsu,[32] Kütt et al.,[33] and Bordwell.[34] Readers should also be aware that acids in organic solutions often undergo homoconjugation (reactions ii and iii, Scheme 3), which can change the acidity (proton activity) of an HA solution.[30,35−37] The pK_a values and homoconjugation constants (K_f) for some common acids in MeCN and DMF are given in Table 4.

From a practical standpoint, using a 1:1 ratio of acid/conjugate base in a system that undergoes homoconjugation will decrease the amounts of available [HA] and [A^-], although this solution retains the *same* ORR equilibrium potential, per eq 3. For example, an acetonitrile solution containing added 1000 mM phenol (PhOH) and 1000 mM phenolate (PhO^-) will only contain 7.9 mM PhOH and PhO^- once the homoconjugation equilibrium defined in Table 4 has been established.[38] Readers desiring more information are recommended to see the following reference works: refs 30, 36, 37, 39, and 40.

The IUPAC recommended electrochemical reference in organic solvents is the ferrocenium/ferrocene couple ($Fc^{+/0}$),[44,45] which is used in Table 3. From a practical standpoint, electrochemical experiments typically use a pseudoreference electrode and calibrate to $Fc^{+/0}$ as an internal standard. This avoids concerns about liquid-junction potentials and changes in concentration within the aqueous or nonaqueous reference electrode, among other issues. A common nonaqueous reference electrode is the silver/silver nitrate electrode ($Ag^+ + e^- \rightarrow Ag^0$), although the aqueous electrodes are also frequently used as references for nonaqueous electrochemistry. For cautions about using aqueous electrodes as the absolute electrochemical reference in nonaqueous solvents, readers are referred to the following reference works: refs 27 and 46.

In addition to Fc, a number of substituted ferrocenes have been used as redox standards in nonaqueous solutions. They often possess rapid interfacial electron transfer kinetics and are easily referenced to $Fc^{+/0}$. Substitution on the cyclopentadienyl rings tunes the $Fc^{+/0}$ redox potential by a large range (>1 V, Table 5)[47] and can be useful for avoiding interference with electrochemical measurements. The redox potentials listed in Table 5 are values in MeCN, and similar potential differences are found in other polar organic solvents.[48] For example, decamethylferrocene ($Me_{10}Fc$) has a standard potential of −510 mV vs $Fc^{+/0}$ in MeCN and −496 mV vs $Fc^{+/0}$ in methanol.[45]

2.3. Dioxygen Solubility

The solubility of O_2 in catalytic or electrocatalytic solutions is an important parameter in the ORR. By Henry's Law, the concentration of a gas in solution is directly proportional to the

Table 4. pK_a's and Homoconjugation Constants (K_f) of Common Acids HA or BH^+ in MeCN and DMF

AH or BH^+[a]	pK_a MeCN	$\log(K_f)_{MeCN}$[b]	ref	pK_a DMF	$\log(K_f)_{DMF}$[b]	ref
$[H_3O]^+$	2.2	3.9 (B_2H^+)	35			
$[DMF-H]^+$	6.1	1.6 (B_2H^+)	30	0		32
$HCl_{(g)}$	8.1		32	3.5	2.2 (HA_2^-)	32
*p*TsOH	8.6		33	2.3		32
$PhNH_3^+$	10.6	0.6 (B_2H^+)	35	3.7		32
$[PyH]^+$	12.5	0.8 (B_2H^+)	35	3.4		32
CF_3CO_2H	12.7	3.9 (HA_2^-)	35	6		41
CH_2ClCO_2H	18.6		32	10.1		42
$PhCO_2H$	21.5	3.6 (HA_2^-)	35	12.3	1.2 (HA_2^-)	32
AcOH	23.5	3.9 (HA_2^-)	35	13		32
PhOH	29.1	4.2 (HA_2^-)	35	18.8		43

[a]For BH^+ acids, an inert counteranion is assumed. [b]K_f is defined in reaction ii, Scheme 3.

DOI: 10.1021/acs.chemrev.7b00542
Chem. Rev. XXXX, XXX, XXX−XXX

Table 5. Redox Potentials for Substituted Ferrocenes in MeCN[47]

substituent(s)	$E_{1/2}$ vs $Fc^{+/0}$
(1,1′-$(CF_3)_2$)Fc	0.64
(1,1′-diacetyl)Fc	0.49
(acetyl)Fc	0.27
Fc	0.00
MeFc	−0.06
Me_2Fc[a]	−0.10
OMeFc	−0.12
NH_2Fc	−0.37
Me_5Fc[b]	−0.27[c]
$Me_{10}Fc$	−0.51[c]

[a](1,1′-$(CH_3)_2$)Fc. [b](1,2,3,4,5-$((CH_3)_5)$)Fc. [c]Values from ref 45.

Table 6. Henry's Law Constants for O_2 in Organic Solvents at 298 K[55]

solvent	H^{cp} (mM/atm O_2) pure solvent	H^{cp} (mM/atm O_2) solvent + electrolyte	ref
acetone	11.4		55
methanol	10.3		55
2-propanol	10.2		55
ethanol	10.0		55
MeCN	8.1	6.0[a]	56
pyridine	5.7		56
DMF[e]	4.8	3.1[b]	56
DMSO[e]	2.2		55
water	1.3[c]	1.16[d]	50

[a]Electrolyte = 0.1 M $[Et_4N][ClO_4]$, from ref 50. [b]Electrolyte = 0.1 M $[Et_4N][ClO_4]$, from ref 57. [c]From ref 51. [d]Electrolyte = 0.15 M KCl, from ref 52. [e]DMF, dimethylformamide; DMSO, dimethyl sulfoxide.

partial pressure of that gas above the solution and is independent of the partial pressure of any other gases. ORR studies typically use 1 atm of O_2 or dry air (O_2 = 20.95% v/v[49]). The Henry's Law constant for O_2 dissolving in pure water is H^{cp} = 1.2 mM atm^{-1}.[48] Like most nonpolar gases, H^{cp} for O_2 decreases with the concentration of ions in the solution. For instance, the 1.2 mM atm^{-1} value drops to 0.99 mM atm^{-1} in 0.81 M KCl.[52,53] In general, O_2 is more soluble in organic solvents than in water (Table 6), but similar decreases in solubility are observed in the presence of ions. Experimentally, it is often valuable to saturate the gas (O_2 or air) with the vapor pressure of solvent, which can be done by sparging the gas through the solvent before it enters the solution of interest. This technique minimizes solvent loss and temperature decreases due to evaporation, which is especially critical for volatile solvents. The low solubility of O_2 in most solvents is often a constraint in ORR studies. For instance, with rapid electrocatalysts, the current response is affected by depletion of O_2 within the electrode reaction/diffusion layer. Attempts to avoid substrate depletion by working at higher pressures of O_2 in organic solvents should be done only with substantial caution, as such mixtures can easily be above the explosion limit.[54]

2.4. Thermochemistry and Bond Dissociation Free Energies of O_2-Derived Intermediates

The multielectron-multiproton ORR always proceeds through a variety of oxygen intermediates. Reduction potentials and pK_a values are known in water for all of the likely free intermediates and are presented in Table 7. These data can also be depicted using Frost diagrams (Figure 2), in which the relative free energy ($nE°$) of oxygen intermediates (red squares) is plotted vs the number of electrons added to O_2. In these diagrams, the solid black line represents where the oxygen intermediates would fall if each elementary ET or PCET step yielded the same free energy change; intermediates that fall above the line are unstable. The diagrams at pH 0 and pH 7 are similar except for the position and identity of the one-electron reduced species. At low pH, the one-electron reduced product is perhydroxyl ($HO_2^•$). Above pH 4.9, however, the reduced product is superoxide ($O_2^{•-}$).

For pairs of intermediates that differ by one e^- and one H^+, the free energy difference can be described by a pK_a and an outer-sphere reduction potential, by a proton coupled ($1H^+/1e^-$) reduction potential, or by a bond dissociation free energy (BDFE). The relationship between the BDFE and the pK_a and outer-sphere $E°$ is illustrated in the square scheme for the $O_2/HO_2^•$ couple in Figure 3. The mathematical relationship is given in eq 4, in which C_G is a constant that depends on the solvent and reference

Table 7. Thermochemistry of Aqueous Oxygen-Derived Intermediates[a]

ne^-	reaction	outer-sphere $E°$	proton-coupled $E°$[b]	BDFE	pK_a	ref
$1e^-$	$O_2 + e^- \rightarrow O_2^{•-}$	−0.33				58
	$O_2 + H^+ + e^- \rightarrow HO_2^•$		−0.05			59
	$O_2 + H^• \leftarrow HO_2^•$			56.7		60
	$HO_2^• \rightarrow O_2^{•-} + H^+$				4.9	59
$2e^-$	$HO_2^• + e^- \rightarrow HO_2^-$	0.76				61
	$HO_2^- \rightarrow O_2^{•-} + H^•$			81.8		a
	$HO_2^• + H^+ + e^- \rightarrow H_2O_2$		1.44			25
	$HO_2^• + H^• \leftarrow H_2O_2$			90.8		60
	$H_2O_2 \rightarrow HO_2^- + H^+$				11.6	62
$3e^-$	$H_2O_2 + H^+ + e^- \rightarrow H_2O + OH^•$		0.793			59
	$O + e^- \rightarrow O^{•-}$	1.43				59
	$O + H^+ + e^- \rightarrow OH^•$		2.14			59
	$O + H^• \leftarrow OH^•$			106.9		60
	$OH^• \rightarrow O^{•-} + H^+$				11.9	59
$4e^-$	$OH^• + e^- \rightarrow OH^-$	1.89				59
	$OH^• + H^+ + e^- \rightarrow H_2O$		2.72			59
	$OH^• + H^• \leftarrow H_2O$			122.7		60
	$H_2O \rightarrow OH^- + H^+$				15.7	59

[a]Potentials in V vs SHE at 298 K, pH 0. BDFE values in kcal mol^{-1}. [b]Calculated using the outer-sphere $E°$ values for O_2 and $HO_2^•$ and the BDFE for $HO_2^•$.

DOI: 10.1021/acs.chemrev.7b00542
Chem. Rev. XXXX, XXX, XXX−XXX

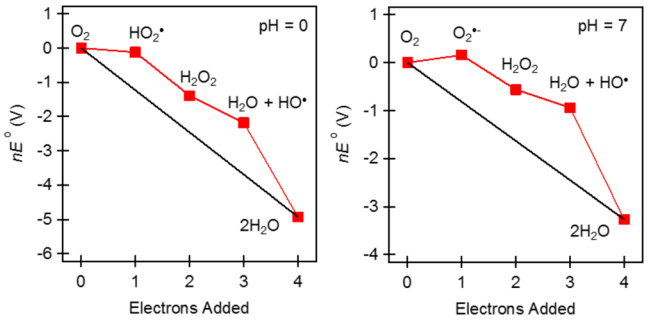

Figure 2. Frost diagrams for dioxygen at pH 0 (left) and pH 7 (right).

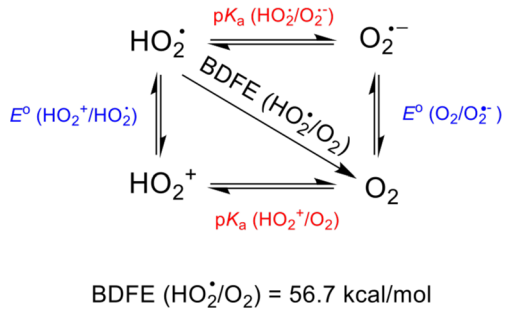

Figure 3. Square scheme for $O_2/HO_2^{\bullet}$. Vertical arrows represent electron transfers, horizontal arrows represent proton transfers, and the diagonal represents the bond dissociation free energy (BDFE).

electrode.[60] The use of BDFEs instead of E° and pK_a values brings a different perspective to the thermochemistry of the ORR. For example, homolytic bond strengths are much less dependent on the medium than E° and pK_a values (BDFE $[O_2/HO_2^{\bullet}]$ = 56.7 kcal mol^{-1} in water and ca. 58 kcal mol^{-1} in DMSO).[60] For that reason we have suggested that BDFE values are the optimal way to compare redox thermochemistry between solvents or between small-molecule and enzymatic systems.[60]

$$\text{BDFE} = 1.37(\text{p}K_a) + 23.06(E^\circ) + C_G \quad (4)$$

For homogeneous ORR reactions, the combination of a soluble reductant and an acid can be assigned an "effective BDFE" using eq 4, even though no X−H bond is being homolytically cleaved.[60,63] For instance, the combination of ferrocene (as the reductant) and pyridinium cation (as the acid) yields an effective BDFE in MeCN of 71.5 kcal mol^{-1}.[60,63] Thermochemically, this combination should be able to add H$^{\bullet}$ to $HO_2^{\bullet}$ (and yield H_2O_2) but should not be able to reduce O_2 to $HO_2^{\bullet}$ (assuming that the O−H BDFEs in MeCN are similar to the aqueous values in Table 7). While this approach has not to our knowledge previously been applied to electrochemical or electrocatalytic systems, the same approach must hold when the e^- is delivered by an electrode. These are thermodynamic calculations, so the source of the electron is not relevant, and eq 4 will calculate the $BDFE_{eff}$ when E° is replaced by the applied potential, typically the catalyst $E_{1/2}$. The relationship of this $BDFE_{eff}$ to catalysis is discussed in section 2.5.3.

2.5. ORR Efficiency and Overpotential

Identifying the overall efficiency of homogeneous ORR catalysts is critical for understanding and improving catalytic systems. Like many catalytic systems, ideal homogeneous ORR catalysts should be able to sustain fast catalytic rates near the ORR thermodynamic potential for extended periods of time. With these goals in mind, the intrinsic parameters to evaluate ORR efficiency are turnover frequency (TOF), overpotential (η), and turnover number (TON). Additionally, ideal ORR catalysts should be selective for a desired product of the ORR (H_2O vs H_2O_2). Often, ORR catalysts are studied in a variety of conditions, including different solvents and proton sources, using either electrodes or soluble reductants as electron equivalents. Below, we briefly summarize the approaches toward measuring the efficiency of the ORR when an electrode (section 2.5.1) or soluble reductant (section 2.5.2) is used. Additionally, the concept of analyzing the efficiency of homogeneous ORR using BDFEs (section 2.5.3) is discussed. These approaches enable the efficiency of homogeneous ORR catalysts to be compared, regardless of the experimental setup and conditions.

2.5.1. Electrochemical ORR with Soluble Catalysts. The thermodynamic analysis of the ORR, discussed in sections 2.1−2.4, is central to understanding the energy efficiency of a homogeneous ORR reaction because it is related to the *overpotential* (η) of the reaction. The overpotential is an experimental parameter: the difference between the applied potential (E_{appl}) and the equilibrium potential (E_{ORR}) under the experimental conditions ($\eta = E_{ORR} - E_{appl}$). For a traditional heterogeneous electrocatalyst, a larger overpotential leads to a higher turnover frequency (TOF), as described by the Tafel slope. This behavior is familiar to anyone who has seen the demonstration of water electrolysis, where the rate of bubbling is higher when the voltage is increased. In heterogeneous systems, performance metrics for efficiency typically compare the TOF or current density for ORR at a fixed η (e.g., 300 mV). The "best" catalyst will achieve the largest TOF at some defined η or the lowest η for a defined current or TOF.

For homogeneous catalysts driven electrochemically, however, the behavior is different. For cathodic processes such as the ORR, ideal cyclic voltammograms would be S-shaped waveforms that reach a limiting current at negative potentials (Figure 4, left). At

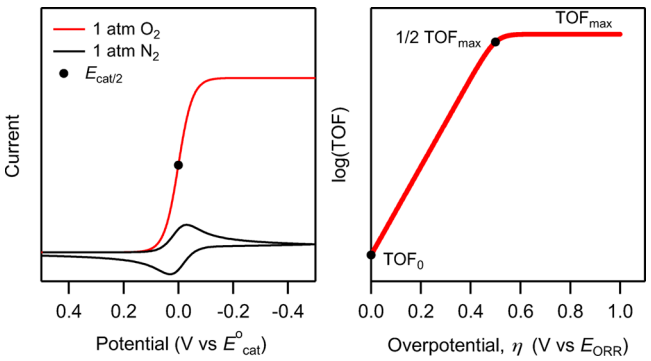

Figure 4. (Left) Simulated cyclic voltammograms for ORR driven by a molecular catalyst with a redox potential E°_{cat} in the presence of N_2 (black trace) or O_2 (red trace). The $E_{cat/2}$ value is the half-wave potential. (Right) Molecular Tafel plots for ORR by the system shown on the left. The $^1/_2TOF_{max}$ data point corresponds to the TOF that would be observed if the electrode potential were held at $E_{cat/2}$.

these potential-independent currents (<0 V, Figure 4), essentially all of the soluble catalyst has been reduced, and the current is limited by *chemical* steps in solution. At these potentials, the catalyst turnover frequency (TOF) also reaches a limiting value, referred to as TOF_{max}.[64] In the potential-dependent region, prior to the plateaued current, catalyst TOF typically responds in a Nernstian fashion to the electrode potential, which is directly related to η (see paragraph above). This has been well-illustrated by Artero and Savéant's molecular

DOI: 10.1021/acs.chemrev.7b00542
Chem. Rev. XXXX, XXX, XXX−XXX

Tafel plots, which plot log(TOF) as a function of η (Figure 4, right).[64] The relationship between log(TOF) and η is given by eq 5 for reactions that are first order in catalyst and is discussed later.[64] Equations for reactions that are second order in electrocatalyst have been derived,[65] but such cases have not yet been applied to the ORR.

$$\mathrm{TOF} = \frac{\mathrm{TOF}_{\max}}{1 + \exp\left[\frac{F}{RT}(E_{\mathrm{ORR}} - E_{\mathrm{cat}/2})\right]\exp\left[-\frac{F}{RT}\eta\right]} \quad (5)$$

The slope of the molecular Tafel plots (log(TOF) vs η) in the low-η region is 1/59 mV. Extrapolation to $\eta = 0$ gives the TOF at zero driving force (TOF_0), analogous to the "exchange current density" acquired from extrapolating Tafel plots of heterogeneous materials to $\eta = 0$. In the high-η region, the exponential terms in the denominator of eq 5 approach 0. In this region, essentially all of the catalyst has been reduced and $\mathrm{TOF} = \mathrm{TOF}_{\max}$.[64] The parallels to heterogeneous materials make molecular Tafel analysis a powerful way to benchmark catalyst performance.

An alternative approach for benchmarking catalyst performance involves examining the log(TOF) at the "effective overpotential" (η_{eff}, eq 6) for ORR catalysis.[36,66] η_{eff} is the difference between E_{ORR} and the potential at the midpoint of the catalytic wave, $E_{\mathrm{cat}/2}$, defined as the potential at which the TOF is half of the maximum TOF ($\mathrm{TOF}_{\max/2}$) (black dot in Figure 4). $E_{\mathrm{cat}/2}$ is sometimes very close to the $E_{1/2}$ of the catalyst, so eq 6 is frequently used with $E_{1/2}$ instead of $E_{\mathrm{cat}/2}$. η_{eff} corresponds to the "elbow" of the molecular Tafel plot. Effective overpotential analysis allows $\mathrm{TOF}_{\max/2}$ and η_{eff} values to be compared across multiple catalysts, which is valuable as these are two of the most critical metrics of an ORR catalyst. However, this comparison is only appropriate when the mechanisms have the same reaction order in catalyst and is only valid under a specific set of catalytic conditions. In practice, most studies report $\mathrm{TOF}_{\max}$, which comes from eqs 7 and 8, even when perhaps $\mathrm{TOF}_{\max/2}$ would be more appropriate.[66−68] Either the effective overpotential or molecular Tafel plot analysis can be used to identify catalysts and conditions that yield the largest $\mathrm{TOF}_{\max}$ at the lowest η_{eff}.

$$\eta_{\mathrm{eff}} = E_{\mathrm{ORR}} - E_{\mathrm{cat}/2} \quad (6)$$

Accurately quantifying the $\mathrm{TOF}_{\max}$ from the current obtained in an experimental cyclic voltammograms is a challenge in molecular electrocatalysis, in particular for the four-electron ORR. In traditional homogeneous catalysis, the TOF is simply the moles of product produced per mole of catalyst per unit time. For molecular electrocatalysts, the relationship between catalytic current and TOF is more complex because the reaction occurs only within a thin solution layer near the electrode surface, the reaction diffusion layer, and only catalyst molecules in this layer should be counted in calculations of $\mathrm{TOF}_{\max}$.[69] The reaction diffusion layer is inherently heterogeneous, meaning the concentration of substrate, product, and catalyst species can vary in time and space. Consequently, the current response is dependent on a multitude of factors, including the scan rate, the diffusion coefficients of substrate and catalyst, and the *ratio of substrate to catalyst*.

$$i = \frac{C^{\circ}_{\mathrm{cat}}FSD^{1/2}(k_{\mathrm{obs}})^{1/2}}{1 + \exp\left[\frac{F}{RT}(E - E^{\circ}_{\mathrm{cat}})\right]} \quad (7)$$

The simplest relationship between current (i) and potential (E) for a homogeneous catalytic process is defined in eq 7, where D is the diffusion coefficient of the catalyst, S is the electrode surface area, F is Faraday's constant, E°_{cat} is the catalyst standard potential, and C°_{cat} is the bulk concentration of catalyst.[28] This i/E relationship has a Nernstian "S" shape because it assumes that all ET steps are fast and accurately defined using the Nernst equation. When $E \ll E^{\circ}_{\mathrm{cat}}$, the catalytic current reaches a potential-independent plateau ($i = i_{\mathrm{pl}}$) because the denominator becomes insignificant (all of the catalyst at the electrode surface is reduced), leading to $i_{\mathrm{pl}} = C^{\circ}_{\mathrm{cat}}FSD^{1/2}(k_{\mathrm{obs}})^{1/2}$. This equation is valid for a $1e^{-}$ EC' mechanism, where E represents an electrochemical step involving rapid electron transfer between the electrode and homogeneous catalyst, C represents a chemical step in solution with a substrate and reduced catalyst, and the prime (′) indicates that this mechanism is catalytic, regenerating an oxidized catalyst (Scheme 4). In the EC' mechanism, k_{obs} = $\mathrm{TOF}_{\max}$. Other mechanisms may have different relationships between the current, $\mathrm{TOF}_{\max}$, and k_{obs}, and these have been well-documented by Costentin and Savéant.[70]

Scheme 4. *EC′* Mechanism for Reductive Molecular Electrocatalysts

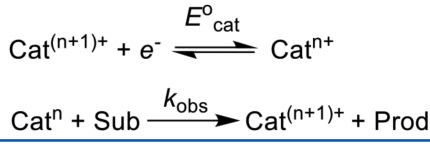

The value of k_{obs} (and thus $\mathrm{TOF}_{\max}$) for complexes that catalyze multielectron processes such as the ORR can be determined using eq 8.[66,71−73]

$$i = \frac{n^{\sigma}_{\mathrm{cat}}C^{\circ}_{\mathrm{cat}}FSD^{1/2}(k_{\mathrm{obs}})^{1/2}}{1 + \exp\left[\frac{F}{RT}(E - E^{\circ}_{\mathrm{cat}})\right]} \quad (8)$$

Equation 8 differs from eq 7 only by addition of the $n^{\sigma}_{\mathrm{cat}}$ term, where n_{cat} is the number of electrons transferred in the catalytic cycle and the exponent σ is a stoichiometric factor reflecting the nature of the elementary ET steps. The stoichiometric factor, σ, equals 1 if each ET step occurs between the electrode and the catalyst or 1/2 if each ET step occurs between catalyst species in solution.[70] If the nature of the ET steps is unknown, it seems prudent to assume that all electron transfer steps are heterogeneous (from the electrode), as this will give the lower-limit $\mathrm{TOF}_{\max}$. The use of eq 8 to calculate $\mathrm{TOF}_{\max}$ is valid provided that the turnover-limiting step occurs immediately after the $\mathrm{Cat}^{(n+1)+}/\mathrm{Cat}^{n+}$ reduction shown in Scheme 4 and that all other chemical and electrochemical steps are downhill and fast. While other more complex electrochemical mechanisms have been derived and well-studied by Costentin and Savéant, they have not been applied to the ORR at this time.[70,74]

Another significant challenge for ORR catalysis is finding conditions where the cyclic voltammograms achieve the canonical "S" shape shown in Figure 4, left. Strictly speaking, eq 8 is only valid when this shape is achieved, which often requires careful choice in the concentration of catalyst, reactants, and scan rate.[65] Often, experimental voltammograms do not resemble an "S" shape for the ORR. Rather, peak-shaped catalytic waves are commonly encountered due to substrate depletion near the electrode surface and/or catalyst deactivation. Substrate depletion is a particular challenge for the ORR because the concentration of dissolved oxygen is quite low at ambient pressure (1.2 and 3.1 mM in electrolyte-containing water and DMF in equilibrium with 1 atm O_2, respectively; see section 2.3 and Table 6). Increasing the amount of dissolved O_2 can be done with high pressures of

DOI: 10.1021/acs.chemrev.7b00542
Chem. Rev. XXXX, XXX, XXX−XXX

O_2 in special electrochemical equipment,[71,72] but we recommend first examining the safety considerations involving nonaqueous solvents and high pressures of O_2 in ref 54. Carver, Matson, and co-workers reported the first examples of using high-pressure electrochemistry for the ORR catalyzed by homogeneous iron porphyrin electrocatalysts in order to acquire the TOF_{max} for iron porphyrins in acidified MeCN[71] and H_2O.[72] Using a Parr reactor equipped with electrochemical connections, substrate depletion became minimal at 17 and 68 atm O_2 in MeCN and H_2O, respectively.

More recently, the foot-of-the-wave analysis has become commonplace for the ORR, as it allows TOF_{max} to be determined without the use of a high-pressure electrochemical cell.[66,73] Briefly, foot-of-the-wave analysis extracts kinetic information at the "foot", or onset, of the catalytic wave (e.g., when $E > 0$ V vs E°_{cat}, Figure 4, left) where substrate depletion/catalyst deactivation is minimal. Interested readers are referred to the seminal works of Costentin and Savéant regarding the extraction of TOF_{max} from catalytic waves under diverse conditions.[38,65]

2.5.2. TOF and Efficiency for ORR with Soluble Catalysts and Soluble Reductants. Molecular catalysts for the ORR have often been studied using soluble reductants in place of an electrode (section 4). The TOF/overpotential relation for these systems should be similar to the relationship found in the molecular Tafel plots above, just with an adjusted definition of the overpotential (eq 9). When a soluble reductant is used, the reducing potential of the solution (E_{red}) is set by the molecular reductant (eq 10), which, by definition, is present in excess over the catalyst. This E_{red} is determined by both the standard potential of the reductant $E^\circ_{ox/red}$ and its ratio of reduced to oxidized forms, as per the Nernst equation (eq 11, for a typical $1e^-$ redox agent). When E_{red} is more than ca. 100 mV more negative than the catalyst $E_{1/2}$, essentially all of the catalyst is present in the reduced form, and the reaction should be independent of the concentration and nature of the external reductant. This corresponds to the flat region of the molecular Tafel plot, where the rate is determined solely by chemical step(s) that do not involve electron transfer.

$$\eta_{eff} = E_{ORR} - E_{red} \tag{9}$$

$$Ox^+ + e^- \rightarrow Red \tag{10}$$

$$E_{red} = E^\circ_{ox/red} - \frac{RT}{F} \log \frac{[Red]}{[Ox]} \tag{11}$$

In the less common scenario where the reducing power of the molecular reductant is comparable to or more positive than the catalyst $E_{1/2}$, the rates are slower because the concentration of the active reduced catalyst is only a fraction of the total catalyst concentration. This situation corresponds to the sloped portion of the molecular Tafel plot above. This analysis—and all of the electrochemical analysis in the previous section—is valid only when the electron-transfer steps are fast relative to the other chemical steps. Under such conditions, it is important to note that E_{red} is the *equilibrium* potential for the reductant used, not the standard potential ($E^\circ_{ox/red}$, eq 11), and that E_{red} follows the Nernst law.

Per the Nernst equation, if $[Red] = 10 \times [Ox^+]$, then E_{red} is 59 mV more reducing than the $E^\circ_{ox/red}$ standard potential (eq 11). The arguments made here are similar to those made when using weak acids for the ORR (see section 2.2, after Table 3)—a "buffered" ratio of [Red] and $[Ox^+]$ would be required to be similar to an electrode poised at a particular potential. This is rarely, if not ever, done in practice. Typically, a large amount of reductant (with $E_{red} < E_{cat}$) is simply added to solution.[73,75−77] Conducting experiments this way is problematic for the overpotential analysis, as the ratio of [Red] to $[Ox^+]$ may change substantially during a catalytic reaction.

For example, in the ORR study described above, Wasylenko and co-workers used excess $Me_{10}Fc$ to measure a first-order rate constant (k_{obs}, TOF_{max}) for the Fe(tetraphenylporphyrin (TPP))-catalyzed ORR.[73] Under the reported conditions, k_{obs} was independent of $[Me_{10}Fc]$ and suggested that the reduction of Fe(III) and other intermediates is thermodynamically downhill. Despite this observation, the $E_{1/2}$ of $Me_{10}Fc$ was found to be less reducing than the $E_{1/2}$ of the iron porphyrin catalyst. The complete reduction of Fe(III) was observed in the presence of excess $Me_{10}Fc$ and was likely a consequence of E_{red} (with a large excess of $Me_{10}Fc$ to $Me_{10}Fc^+$; see eq 11). Estimating η_{eff} using the $E_{1/2}$ or $E^\circ_{ox/red}$ of the reductant is often imprecise and should be avoided. When the reductant $E^\circ_{ox/red}$ is greater than or equal to the catalyst $E_{1/2}$, the accurate determination of overpotential for the ORR catalysis requires the use of "buffered" reductant solutions—a mixture of Ox^+ + Red.

2.5.3. Analysis of ORR Efficiency Using Bond Dissociation Free Energies. When equal numbers of protons and electrons are added to O_2 (or any substrate), the thermochemistry and thermodynamic efficiency can be analyzed in terms of effective bond dissociation free energies (BDFEs). The top part of Figure 5 derives the ΔG° for the addition of two H atoms to O_2

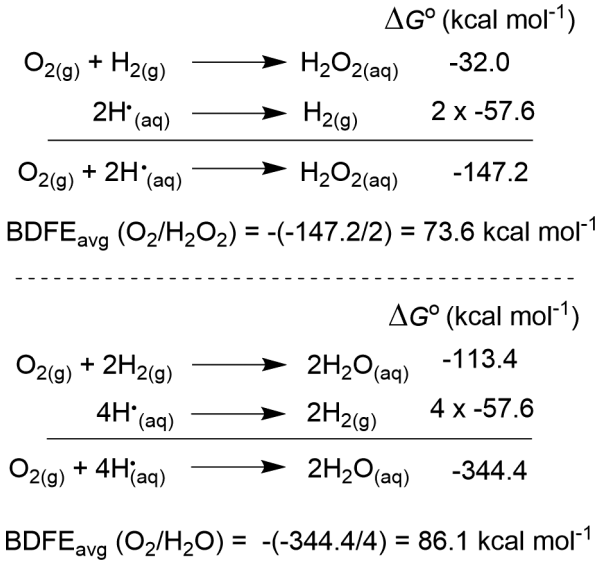

Figure 5. Average BDFE values for O_2 reduction to H_2O_2 and H_2O.

to make H_2O_2, which is the sum of the two O−H BDFEs formed in the reaction. The average BDFE in H_2O_2 is 73.6 kcal mol^{-1}. Thus, if a reagent HX is used to supply the $H^\bullet$ (forming $X^\bullet$), the BDFE of that reagent must be <73.6 kcal mol^{-1} for the reaction to be favorable. The $H^\bullet$ equivalents could also come from a reductant/acid pair with an effective BDFE (section 2.4) weaker than ~74 kcal mol^{-1}.

The reduction of O_2 to H_2O is more complicated because it requires both the formation of four O−H bonds and the cleavage of the O−O bond. The overall thermochemical cycle is similar, however, and can be described as having an average effective BDFE of 86.1 kcal mol^{-1}, which includes both the O−H bond and O−O bond energies (Figure 5, bottom). Therefore, production of H_2O from O_2 requires the addition of $H^\bullet$ equiva-

DOI: 10.1021/acs.chemrev.7b00542
Chem. Rev. XXXX, XXX, XXX−XXX

lents from reductant/acid pairs that have an effective BDFE (section 2.4) weaker than ~86 kcal mol^{-1}. The average BDFE for reduction of O_2 to H_2O_2 is smaller by ca. 12 kcal mol^{-1} or 0.53 eV (the difference between the O_2/H_2O and O_2/H_2O_2 reduction potentials, Table 1). The average BDFE values in DMF and MeCN are presented in Table 8, using data from Table 3 and the C_G term in eq 4.

Table 8. Average BDFE Values for O_2/H_2O in Aqueous and Nonaqueous Solvents

reaction	$BDFE_{avg}$[a] (kcal/mol)
$2H_2O_{(aq)} \rightarrow O_{2(g)} + 4H^{\bullet}_{(aq)}$	86.1
$2H_2O_{(MeCN)} \rightarrow O_{2(g)} + 4H^{\bullet}_{(MeCN)}$	82.7
$2H_2O_{(DMF)} \rightarrow O_{2(g)} + 4H^{\bullet}_{(DMF)}$	83.5
$H_2O_{2(aq)} \rightarrow O_{2(g)} + 2H^{\bullet}_{(aq)}$	73.6
$H_2O_{2(MeCN)} \rightarrow O_{2(g))} + 2H^{\bullet}_{(MeCN)}$	70.6
$H_2O_{2(DMF)} \rightarrow O_{2(g)} + 2H^{\bullet}_{(DMF)}$	71.1

[a]Calculated using $BDFE_{avg} = 23.06(E_{ORR}$ vs $Fc^{+/0}) + C_g$ using ref 60 and the E_{ORR} values in Table 3.

This analysis has the advantage of focusing on the more thermodynamically relevant reductant/acid pairs rather than the properties of the individual components. The most efficient catalyst would be capable of catalyzing the ORR at fast rates using the combination of an acid plus an electrode or soluble reductant with an effective BDFE slightly weaker than 86 kcal mol^{-1}. Under such conditions, the reaction could be catalyzed *selectively* with low driving force (low overpotential).

Among the challenges of the ORR is that, in the absence of catalysis, 4H$^{\bullet}$ cannot be delivered at the average BDFE. In the Frost diagrams shown earlier (Figure 2), the slope between two intermediates that differ by 1H$^+$ and 1e^- indicates how the BDFE of that elementary step differs from the average BDFE. Slopes that are shallower than the black line indicate the formation of weaker bonds, whereas slopes steeper than the black line indicate bonds that are stronger than the average BDFE. For example, the spontaneous formation of $HO_2^{\bullet}$ from O_2 requires an effective BDFE of 56.7 kcal mol^{-1}, smaller than the average BDFE by 29.7 kcal mol^{-1} or 1.25 V. If an ORR reaction proceeds by delivery of the e^- and H$^+$ together (as is often assumed in computational studies), then the small effective BDFE in $HO_2^{\bullet}$ requires a low effective BDFE in the reagents and leads to thermodynamically inefficient catalysis (high overpotentials).

The thermodynamic goal for ORR catalysis is to even out the energies of the various intermediates, making them closer to the average BDFE line in the Frost diagram (Figure 2). Even platinum, currently the best ORR catalyst in acidic solutions, only partially achieves this goal and requires overpotentials ~400 mV in 1 M $HClO_4$ (10 kcal mol^{-1} in BDFE) to achieve significant current densities.[78] For heterogeneous materials, the selective stabilization of one intermediate over another is challenging when the chemical structure differs by nH^+/ne^-. For example, the adsorption energy of the $^{\bullet}O_2H$ radical on a metal electrode ($M + {}^{\bullet}O_2H \rightarrow M{-}O_2H$) can often be directly correlated with the adsorption energy of the $^{\bullet}OH$ radical ($M + {}^{\bullet}OH \rightarrow M{-}OH$).[79] These "scaling relations" have become a very popular approach for heterogeneous ORR catalyst comparison and design in recent years, as the thermodynamics for elementary adsorption steps can often be correlated with one another and to the kinetic barriers of the global reaction.[19,80−82] Importantly, scaling relationships suggest that a single metal center will be unable to efficiently catalyze the ORR at the thermodynamic potential if each step involves addition of H$^{\bullet}$ (1e^- and 1H$^+$). With this constraint, strong H-donors will be needed (typically delivered via solution PT and a reducing electrode potential) to make some intermediates while other intermediates will be too stabilized.[83] This analysis is one view of the very popular "scaling relationship" analysis that predicts a large inherent overpotential for the ORR.[79]

The decoupling of electron transfer from proton transfer—delivering each particle at different times—could be a promising route to breaking traditional scaling relationships. This uncoupling has been proposed as one of the ways that enzymes achieve low-overpotential PCET catalytic transformations, such as the interconversions of CO_2 and CO.[83] Decoupled ET and PT refers to when the electron and proton transfer events occur in separate elementary steps, and this often leads to unique rate/driving force relationships depending on how the driving force is varied. For example, the outer-sphere reduction of O_2 to H_2O_2 typically proceeds through the one-electron reduction of O_2, forming superoxide, which rapidly disproportionates to H_2O_2 in protic media (see section 3). Despite being a net 2H$^+$/2e^- reduction event, the overpotential for this process reflects the $O_2/O_2^{\bullet-}$ potential rather than the O_2/H_2O_2 potential. The $O_2/O_2^{\bullet-}$ couple (−0.33 V vs SHE, Table 7) is considerably cathodic of the O_2/H_2O_2 couple (0.695 V vs SHE, Table 1), leading to significant overpotentials (at pH = 0, $\eta_{eff} \approx 1$ V). The differences in electron/proton stoichiometry allow the effective overpotential to be decreased by using weaker acids or a higher pH solution.[84] For example, changing the pH from 0 to 14 will shift E_{ORR} by −829 mV but leave $E^{\circ}_{O_2/O_2^{\bullet-}}$ unchanged, leading to a much smaller overpotential ($\eta_{eff} \approx 0.17$ V). This approach targets the entire catalytic *system*, which includes the catalyst, medium, and concentration of solutes and products.

A recent report from Pegis, Mayer, and co-workers established how scaling relationships can be broken in systems where ET and PT are decoupled. Using iron tetraphenylporphyrin, the authors demonstrated how the TOF_{max} for the ORR will scale with η_{eff} when the reaction conditions are varied.[85] Knowledge of the rate law and Nernst equation was shown to predict how $\log(TOF_{max})$ will scale with η_{eff}, depending on how the overpotential was varied in DMF solutions. Changing the concentration of dissolved tosic acid (*p*TsOH) by 1 order of magnitude changed the TOF_{max} by the same amount ($TOF_{max} = k_{cat}[p\text{TsOH}]^1P_{O_2}{}^1$) and increased the η_{eff} by 59 mV, per eqs 6 and 11. In contrast, different slopes ($\partial\log(TOF_{max})/\partial\eta_{eff}$) are obtained when η_{eff} is varied via changes in P_{O_2}, pK_a, and $E_{1/2}$, keeping all other variables constant. These unique slopes are illustrated in Figure 6 for changes in the partial pressure of dioxygen (m_{PO_2}), the concentration of dissolved acid in solution (m_{HA}), the pK_a of the proton source (m_{pK_a}), and the previously reported correlation of TOF_{max} with the catalyst $Fe^{III/II}$ redox potential ($m_{E_{1/2}}$). On the basis of these slopes, it was predicted and observed that the ORR driven in DMF solutions containing salicylic acid would be 10^4 faster than predicted by the previous scaling relationship based on catalyst $E_{1/2}$, as indicated by the arrow in Figure 6. Such an analysis predicts that similar relationships should exist for all molecular electrocatalysts and suggests that there is a great degree of tunability in the kinetics and thermodynamics of catalytic reactions where the ET and PT steps do not occur in concert.

2.6. Conclusions

Two of the key metrics of a molecular catalyst for the ORR are effective overpotential (η_{eff}) and turnover frequency (TOF_{max}).

DOI: 10.1021/acs.chemrev.7b00542
Chem. Rev. XXXX, XXX, XXX−XXX

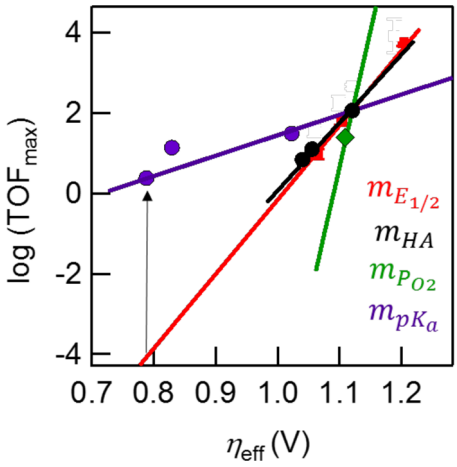

Figure 6. Correlations of log(TOF$_{max}$) with η_{eff} for iron tetraphenylporphyrin catalyzed ORR in DMF, using *p*TsOH as a proton source. The colored lines are the predicted correlations from theory, and the colored dots are experimental values. Figure adapted with permission from ref 85. Copyright 2017 American Chemical Society.

Accurate measurements of the η_{eff} for the ORR require a complete understanding of ORR thermochemistry. To the best of our knowledge, sections 2.1−2.4 contain the most up-to-date thermochemistry for the ORR in both aqueous and nonaqueous solvents, including pK_a's, dioxygen solubilities, and BDFEs. These values permit η or η_{eff} to be measured for soluble ORR catalysts in a diverse set of conditions, enabling a more facile comparison and benchmarking of catalytic systems. The TOF$_{max}$ for a catalytic system can be quantified using electrochemical methods or using soluble reductants, and using both methods can often be beneficial. Understanding how the TOF$_{max}$ and η_{eff} vary as a function of conditions (catalyst, proton source, solvent, etc.) provides insight into the current-limiting mechanism and enables further optimization of the catalytic system. Moreover, the use of buffered reductants could permit a more complementary overlap of the electrochemical (section 2.5.1) and chemical (section 2.5.2) approaches currently being used to analyze ORR catalysts discussed in sections 3 and 4. It is our hope that readers may draw inspiration from mechanistic insights to modify catalysts or solution conditions with the aim of decreasing η_{eff} without also decreasing TOF$_{max}$, or to increase TOF$_{max}$ without a large increase in η_{eff}. Using soluble catalysts and the tools of molecular chemistry, we hope that researchers continue to identify structure/activity relationships and discover general strategies for improving the energies of the ORR intermediates and the barriers between them. We believe that the insights gained from these studies will not only benefit the design of molecular catalysts but also assist in the rational design of heterogeneous materials for device fabrication.

3. OUTER-SPHERE ORR CATALYSIS

This section describes catalytic reductions of O_2 initiated via *outer-sphere* electron transfer (ET) to form dissolved superoxide ($O_2^{\bullet-}$) or—less commonly—superoxide stabilized by a proton (perhydroxyl, $HO_2^{\bullet}$) or Lewis acid ($MO_2^{\bullet}$). The formation of $HO_2^{\bullet}$ ($O_2 + H^+ + e^- \rightarrow HO_2^{\bullet}$) is a proton-coupled electron transfer (PCET) process, whereas the formation of a Lewis acid-stabilized $M^{n+}-O_2^{\bullet-}$ ($O_2 + M^+ + e^- \rightarrow MO_2^{\bullet}$) has been termed metal ion-coupled ET (MCET).[86,87] Although formations of $HO_2^{\bullet}$ and $MO_2^{\bullet}$ are not outer-sphere ET reactions, they are included in this section because they are distinct from the *inner-sphere* pathways discussed in section 4, in which O_2 reduction occurs upon direct bonding to a *redox-active* transition metal center ($M + O_2 \rightarrow MO_2^{\bullet}$).

Once formed, $O_2^{\bullet-}$ often undergoes a series of PT, ET, PCET, or disproportionation reactions, typically yielding H_2O_2. In some instances, PCET reactions occur in a single, concerted step, and these reactions are termed concerted-proton electron transfers (CPETs). This section highlights the thermochemistry and kinetics of outer-sphere O_2 reduction from a catalytic standpoint, building on the thermochemical information in section 2. The outer-sphere reactivity of O_2 is also critical in a variety of biological contexts, although these topics fall outside the scope of this Review.[15] Detection of $O_2^{\bullet-}$ is possible using a variety of methods, as discussed elsewhere.[88]

This section begins with the aqueous chemistry of outer-sphere ORR and follows with nonaqueous and biphasic studies of outer-sphere ORR mechanisms. A significant amount of outer-sphere ORR reports have been conducted in nonaqueous solvents (section 3.2), and these studies are separated into sections where reducing equivalents are supplied from an electrode (section 3.2.1) or from a homogeneous reductant in solution (section 3.2.2). Redox-mediated reactions, in which a soluble (homogeneous) reductant is regenerated at an electrode, are discussed in section 3.2.1.1. Finally, this section concludes with case studies of CPET and MCET reactions encountered in outer-sphere ORR.

3.1. Aqueous Outer-Sphere ORR

Aqueous outer-sphere ET to O_2 has been studied for decades, particularly for its relevance in biology.[15] The leaking of $O_2^{\bullet-}$ in biological systems leads to the production of free radicals and cell death and has driven the evolution of superoxide dismutase enzymes.[15,58,89] Model examples of aqueous outer-sphere ET to O_2 have origins that date (at least) to the work of Taube and co-workers in 1980.[90] The kinetics of these examples, among others, were summarized in a 1985 review that detailed all of the known rate constants for aqueous reactions of $O_2^{\bullet-}$ and $HO_2^{\bullet}$.[91]

In water, $O_2^{\bullet-}$ rapidly undergoes bimolecular self-disproportionation at neutral or acidic pHs.[91] In basic solutions (pH > 12), $O_2^{\bullet-}$ will typically persist for minutes to hours before ultimately forming HO_2^-.[88] The thermodynamics and kinetics of $O_2^{\bullet-}$ formation, as well as its resulting reactivity, have been extensively probed using pulse radiolysis,[92] photolytic methods,[93] and soluble reductants with well-characterized redox potentials and self-exchange rates.[94−96] The first measurements of the self-exchange rate constant and reorganizational energy for $O_2/O_2^{\bullet-}$ were obtained by Jonsson and co-workers (450 ± 160 M^{-1} s^{-1} and 45.5 kcal mol^{-1}, respectively) using $(^{18}O)_2$ isotopic labeling experiments.[97] The great value of $^{16}O/^{18}O$ kinetic isotope effects in O_2 chemistry has been developed by Klinman, Roth, and co-workers.[98,99] As measured by Taube and co-workers[94] and Zahir, Espenson, and Bakac,[96] the Marcus cross-relation can be readily applied for reactions that use O_2 as an oxidant and yield self-exchange rate constants ($O_2/O_2^{\bullet-}$) that are typically within 10^1-10^3 of Jonsson's reported value.[97] In contrast, when $O_2^{\bullet-}$ is used as a reductant, the reported self-exchange rate constants vary by 10^{13}, depending on the redox-accepting partner.[95,100] Weinstock has resolved this unusual disparity by considering the different effective radii of the electron donor and acceptors. With this revised version of the Marcus cross-relation, exceptional agreement was obtained for $O_2/O_2^{\bullet-}$ self-exchange rates from reactions with different redox partners.[100,101]

DOI: 10.1021/acs.chemrev.7b00542
Chem. Rev. XXXX, XXX, XXX−XXX

Once formed, $O_2^{\bullet-}$ tends to be a PCET oxidant. Superoxide is not an outer-sphere ET oxidant, and formation of the free peroxide dianion (O_2^{2-}) has never been reported in aqueous solutions. The instability of O_2^{2-} in aqueous solutions was discussed by Taube and co-workers in a study of O_2 reactivity with a binuclear Ru(II) complex.[102] O_2^{2-} is very basic and needs to be stabilized by cations in a solid or by extensive hydrogen bonding.[103−105] Superoxide is a mild PCET oxidant, forming a weak O−H bond (BDFE[H−$O_2^{\bullet}$] = 60.4 kcal mol^{-1} in water, Table 7).[60] In contrast, $HO_2^{\bullet}$, which is in equilibrium with $O_2^{\bullet-}$ near neutral pH (pK_a $HO_2^{\bullet}/O_2^{\bullet-}$ = 4.9, Table 7)[91] is a more powerful PCET oxidant (BDFE[HO_2−H] = 90.8 kcal mol^{-1}).[60] The larger BDFE reflects the higher basicity of HO_2^- than $O_2^{\bullet-}$, (pK_a[H_2O_2] = 11.6, pK_a[$HO_2^{\bullet}$] = 4.9, Table 7).[60] The reactivity of $O_2^{\bullet-}$ via hydrogen atom transfer (HAT) has also been studied by Taube and co-workers[94] and Anson and co-workers.[106,107]

In the context of ORR, outer-sphere ET to O_2 has been extensively explored in efforts to make H_2O_2 electrocatalytically.[108,109] In water, most electrodes will reduce O_2 to $O_2^{\bullet-}$, which then disproportionates to H_2O_2.[110−112] Similarly, many molecular reductants reduce O_2 to $O_2^{\bullet-}$.[113] However, we have found no examples where an aqueous, soluble molecular species acts as a catalyst for outer-sphere O_2 reduction to $O_2^{\bullet-}$. A few examples of this catalysis in organic solvents are presented in section 3.2.1.1.

3.2. Nonaqueous Outer-Sphere ORR

Superoxide ($O_2^{\bullet-}$) is much more persistent in dry aprotic solvents than in water because it requires protons to disproportionate. The kinetics of $O_2^{\bullet-}$ formation are often limited by the large reorganizational energy of $O_2/O_2^{\bullet-}$, which leads to non-Nernstian peak separations in cyclic voltammograms.[114] In nonaqueous solvents, the reactivity of $O_2^{\bullet-}$ in acidified media is particularly relevant to the ORR. Below, representative ORR examples are organized by solvent class and reagent type.

3.2.1. Electrochemical Reductions in Polar Aprotic Solutions. The superoxide radical anion is sufficiently stable in polar aprotic solvents like MeCN and DMF that a reversible $O_2/O_2^{\bullet-}$ redox couple can be identified on the CV-time scale (Figure 7). Most experimental values of $E_{1/2}(O_2/O_2^{\bullet-})$ range from −0.77 to −0.90 V vs SCE and vary somewhat with medium.[115]

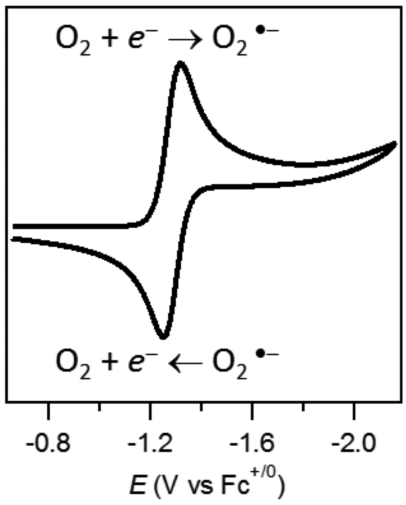

Figure 7. Cyclic voltammogram at a glassy carbon electrode of a 0.1 M [Bu_4N][PF_6] MeCN solution containing O_2. 100 mV/s.

A number of early reports examined the electrochemistry of O_2 in acidified solutions of dimethyl sulfoxide (DMSO),[56,114,116,117] pyridine,[56] DMF,[56,114,118,119] and MeCN.[56,118,119] Generally, in the presence of protons, the one-electron reduction feature ($O_2/O_2^{\bullet-}$) is replaced with an irreversible, two-electron cathodic response. The potential of the two-electron wave is sensitive to a number of experimental conditions, particularly acid identity[56,115,118] and electrode composition.[56,119] In all cases, however, catalysis requires formation of $HO_2^{\bullet}$, which can be formed through either a stepwise (ET−PT) or concerted mechanism (CPET) (Scheme 5). It has been proposed that, under some conditions, $HO_2^{\bullet}$ can be formed by reaction of O_2 with $H^{\bullet}$ adsorbed on the electrode (Ads. HAT, Scheme 5).[56,119]

Scheme 5. Mechanisms of O_2 Reduction to $HO_2^{\bullet}$

ET-PT	$O_2 + e^- \rightarrow O_2^{\bullet-}$	(i)
	$O_2^{\bullet-} + H^+ \rightarrow HO_2^{\bullet}$	(ii)
CPET	$O_2 + e^- + H^+ \rightarrow HO_2^{\bullet}$	(iii)
Ads. HAT	$O_2 + H^{\bullet}_{ads} \rightarrow HO_2^{\bullet}$	(iv)
	$O_2 + H^+ + e^- \rightarrow HO_2^{\bullet}{}_{ads}$	(v)

The stepwise ET−PT formation of $HO_2^{\bullet}$ has been shown to occur in MeCN and DMF on both platinum and glassy carbon (GC) electrodes when weak acids (e.g., PhOH, H_2O, 3,5-di-*tert*-butylcatechol, α-tocopherol, and 1-butanol) were used.[56,119] Stopped-flow kinetic studies have been used to optically monitor the disappearance of $O_2^{\bullet-}$ (dissolved tetramethylammonium superoxide) upon exposure to acid.[118] In the presence of any acid, $O_2^{\bullet-}$ was rapidly protonated to form $HO_2^{\bullet}$ before further disproportionation. However, protonation was diffusion-controlled only when strong acids were employed.[118] A similar stepwise ET−PT mechanism was recently reported in DMSO and chlorobenzene (PhCl) mixed-solvent solutions (DMSO/PhCl = 100:0, 50:50) containing NH_4^+ using glassy carbon electrodes[117] or the fullerene radical anion ($C_{60}^{\bullet-}$).[120]

With platinum electrodes, Sawyer and co-workers found that O_2 reduction in acidic MeCN (excess $HClO_4$) proceeds by reaction of adsorbed $H^{\bullet}$ via HAT (reactions iv and v, Scheme 5).[56,119] Somewhat different behavior was seen using gold and GC electrodes. Although GC does not stabilize adsorbed $H^{\bullet}$, in some cases $HO_2^{\bullet}$ adsorption is thought to occur. Specifically, the authors proposed the CPET formation of $HO_2^{\bullet}{}_{ads}$ from MeCN solutions containing O_2 and acid (reaction v, Scheme 5). This reaction appears to be complex, however, as the limiting current became independent of acid when [$HClO_4$] > 6 mM.[119]

The perhydroxyl radical $HO_2^{\bullet}$ rapidly decays in polar aprotic solvents to make O_2 and H_2O_2.[91] For many years, the mechanism of this decay was thought to be homogeneous disproportionation, $2HO_2^{\bullet} \rightarrow H_2O_2 + O_2$.[116,118,119,121] However, in 1987, Andrieux and co-workers showed that the more likely mechanism is the heterogeneous disproportionation, $HO_2^{\bullet} + O_2^{\bullet-} \rightarrow HO_2^- + O_2$.[114] Electrochemical studies in DMSO and DMF were used to consider four potential reactions of $HO_2^{\bullet}$: (i) stepwise, electrode-initiated ET−PT, (ii) disproportionation of $HO_2^{\bullet}$ and $O_2^{\bullet-}$, (iii) HAT from solvent to $HO_2^{\bullet}$, and (iv) homogeneous disproportionation of two $HO_2^{\bullet}$ molecules. Computed voltammetric responses of the four mechanisms showed that only the disproportionation of $HO_2^{\bullet}$ and $O_2^{\bullet-}$ to form HO_2^- and O_2 was viable.[114]

DOI: 10.1021/acs.chemrev.7b00542
Chem. Rev. XXXX, XXX, XXX−XXX

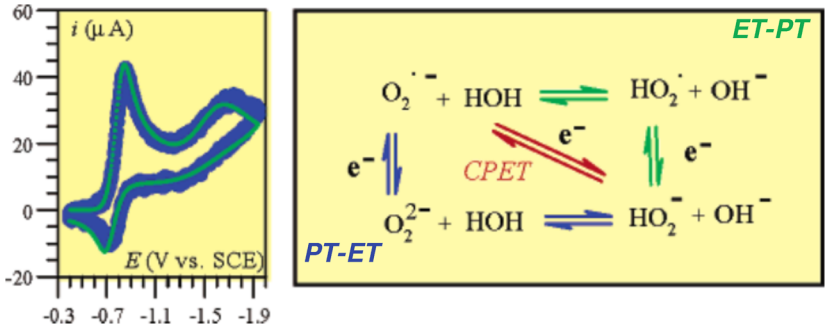

Figure 8. (Left) Cyclic voltammetry of the reduction of dioxygen in 0.1 M [^{n}Bu$_4$N][BF$_4$] DMF solution at a glassy carbon electrode in the presence of 0.55 M H_2O. Scan rate: 0.1 V/s. Green line: simulated curve. (Right) Competing PT–ET, ET–PT, and CPET mechanisms. Reproduced with permission from ref 124. Copyright 2017 American Chemical Society.

In aprotic solvents containing dissolved O_2 and weak acids (e.g., H_2O, MeOH, and ^{i}PrOH), an irreversible redox feature has been observed at potentials more negative than $E(O_2/O_2^{\bullet-})$ (Figure 8). Originally assigned as the one-electron reduction of $O_2^{\bullet-}/O_2^{2-}$,[116,122,123] this irreversible reduction has been explored extensively in the past half century. Nearly a decade after first appearing in the literature, several studies identified the reduction feature as a CPET process.[124−126]

Costentin and co-workers were the first to reach this conclusion, noting that reports of electrochemical reactions involving CPET are scarce.[124] In DMF solutions with added H_2O, the irreversible voltammetric feature was assigned to the CPET reduction of complexed water−superoxide and the formation of HO_2^- (Figure 8). The concerted process is favored because (i) the low basicity of $O_2^{\bullet-}$ disfavors initial PT from weak acids and (ii) initial ET to form the unstable intermediate O_2^{2-} is also unfavorable. The authors used this voltammetric feature to develop the theoretical and mathematical treatment of electrochemical CPET processes, and suggested that such treatment can be generally applied for other electrochemical CPET reactions.[124]

Soon thereafter, the reductions of other superoxide complexes ($[HA\cdots O_2^{\bullet-}] + e^- \rightarrow HO_2^- + A^-$, where HA = H_2O, MeOH, and ^{i}PrOH) were reported in MeCN.[125] Titrations of HA shifted the reduction potential of the $[HA\cdots O_2^{\bullet-}]$ complex positively and were ascribed to the formation of hydrogen-bonded adducts. Kinetic isotope effects (KIEs) were observed for all of the acids (k_H/k_D as large as 5.6 for MeOH/MeOD), which strongly implicates CPET.[125] Savéant later revisited the analysis of the $[HA\cdots O_2^{\bullet-}]$ complexes and highlighted the importance of the hydrogen-bonded network surrounding $O_2^{\bullet-}$. Rather than simple invocation of $O_2^{\bullet-}$ solvation by protic substrate, short hydrogen-bonded chains were proposed to account for the observed KIEs.[126]

3.2.1.1. Electrochemical ORR Catalyzed by Soluble Redox Mediators. There are several reports of catalysis that mediate ET from an electrode to O_2 by soluble molecular reductants (e.g., redox mediators). Redox mediators have often been used to shuttle reducing equivalents from electrodes to enzymatic cofactors,[127−129] although such shuttling is much less commonly employed for nonenzymatic, outer-sphere ORR reactions. This is likely because outer-sphere ET to O_2 generally proceeds quite well at electrodes, so there is little kinetic advantage to using soluble catalysts for this mechanism. However, soluble redox mediators can increase the volume of the electroactive solution beyond the standard electrochemical reaction diffusion layer.

The well-known redox agent methylviologen (MV^{2+}, **1**, Figure 9) has been reported as a catalyst for the redox-mediated $2H^+/2e^-$

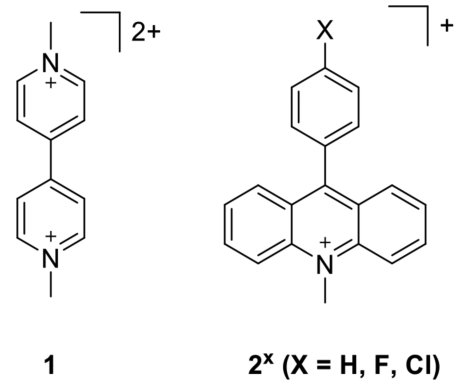

Figure 9. Organic, outer-sphere catalysts used as electrochemical redox mediators for the ORR in refs 130 and 133.

ORR in DMSO, with acids such as chloroacetic acid.[130] In DMSO, MV^{2+} is easier to reduce than O_2, so reduction of MV^{2+} is the dominant process at the electrode. Because MV^{2+} is easier to reduce, ET from $MV^{\bullet+}$ to O_2 is uphill (ca. 280 mV); nonetheless, it is still fast enough to promote catalysis. Consequently, ET from $MV^{\bullet+}$ to O_2 is the rate-determining step, with $k = 2.3 \pm 0.3 \times 10^5$ M^{-1} s^{-1}. The cyclic voltammograms evidenced "total catalysis," in which catalysis occurs so rapidly that O_2 is completely consumed within the reaction layer.[131,132] Even faster rates were later obtained in a similar study using 9-(4-X-phenyl)-*N*-methylacridinium salts, (**2^x**, Figure 9).[133]

The low number of mediated *outer-sphere* ORR examples contrasts with the volume of *inner-sphere* catalysts presented in section 4. This difference may reflect the highly aggressive reactivity of ORR intermediates (e.g., $HO_2^{\bullet}$), formed from outer-sphere mechanisms, which can oxidatively degrade most organic molecules. Lewis acids, which are often more robust to decomposition, have also been used to facilitate outer-sphere ORR and are discussed later (section 3.3).

3.2.1.2. Electrochemical Reductions in Ionic Liquids. The reduction of O_2 to $O_2^{\bullet-}$ in ionic liquids has been recently reviewed.[88] Despite a number of examples, the electrochemistry of the $O_2/O_2^{\bullet-}$ couple is rarely as well-defined in these solvents as in MeCN or DMF. This is due to the tendency for $O_2^{\bullet-}$ to react with impurities and/or with the solvent itself (e.g., with quaternary phosphonium cations).[134] Moreover, among the limited examples of well-defined O_2 electrochemistry in ionic liquids, there are even fewer examples done in the presence of exogenous acid.[134−136]

In the absence of water, solutions of O_2 in 1-ethyl-3-methylimidazolium bis(trifluoromethanesulfonyl)imide ([EMIm][TFSI])[137]

DOI: 10.1021/acs.chemrev.7b00542
Chem. Rev. XXXX, XXX, XXX−XXX

and the 1-butyl-1-methylpyrrolidinium analogue ([BMP][TFSI])[138] displayed a chemically reversible $1e^-$ wave at ca. −1 V vs $Fc^{+/0}$. The addition of water (up to 1% v/v) or phenol to these solutions increased the current and irreversibility of the $O_2/O_2^{\bullet-}$ couple (Figure 10).[138] Similar behavior was observed in

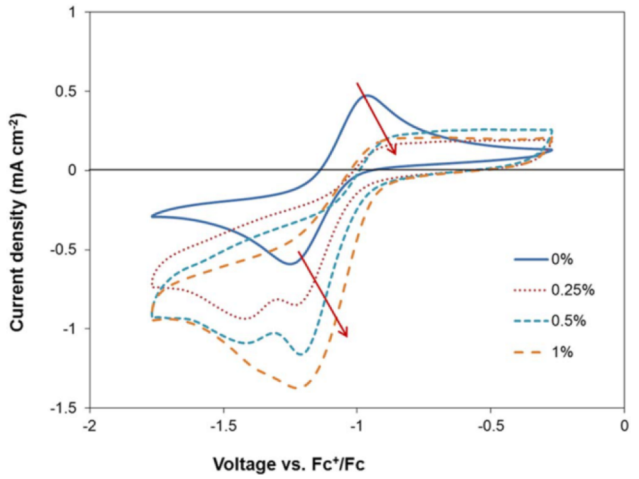

Figure 10. Effect of water addition (% v/v as noted) on cyclic voltammograms for O_2-sparged [BMP][TFSI]. Scan rate: 0.05 V/s. Reproduced with permission from ref 138. Copyright 2014 Electrochemical Society.

DMF.[135] The irreversibility of the $O_2/O_2^{\bullet-}$ couple in solutions containing water was ascribed to the reaction of $O_2^{\bullet-}$ with H_2O ($2O_2^{\bullet-} + H_2O \rightarrow O_2 + HOO^- + HO^-$).[138] The more effective solvation of $O_2^{\bullet-}$ by the protic additives was proposed to account for the positive potential shift and may be related to the solvent acceptor number (AN_{H_2O} = 54.8),[139] although this hypothesis has not been explicitly tested.[138]

Switzer and co-workers observed similar current enhancements near the $O_2/O_2^{\bullet-}$ couple on GC and platinum electrodes when a variety of acids ($\Delta pK_a \approx 30$) were added to solutions of 1-butyl-2,3-dimethylimidazolium trifluoromethanesulfonate ([BdMI][TFS]). On GC, the linear sweep voltammogram evidenced two-electron currents near $E_{1/2}(O_2/O_2^{\bullet-})$. A four-electron process occurred at more negative potentials, although this overlapped with direct proton reduction ($2e^- + 2H^+ \rightarrow H_2$). Cyclic voltammograms using platinum electrodes showed a four-electron wave at potentials positive of $E_{1/2}(O_2/O_2^{\bullet-})$, consistent with H_2O_2 formation and platinum-catalyzed disproportionation ($2H_2O_2 \rightarrow 2H_2O + O_2$).[136]

The reactivity of electrogenerated $O_2^{\bullet-}$ in ionic liquids is similar to the reactivity observed in polar aprotic solvents. Chemically reversible $O_2/O_2^{\bullet-}$ cyclic voltammograms have been reported in some ionic liquids in the absence of protons, although the peak separations remained far from Nernstian at typical scan rates and temperatures (ca. 0.1 V s^{-1}, 298 K).[137,138] The larger peak separations seen in ionic liquids are suggested to reflect, in part, the large reorganizational energy of $O_2/O_2^{\bullet-}$[28,140] and the smaller diffusion coefficients for O_2 and $O_2^{\bullet-}$ in ionic liquids.[88] The addition of protons to these solutions resulted in H_2O_2 formation, although in some instances there was evidence that H_2O was also formed from further disproportionation.[136]

3.2.2. ORR Catalysis with Homogeneous Reductants. Outer-sphere ORR can also be initiated via solution ET from a dissolved molecular reductant to O_2. The following sections describe such ORR systems, which do not involve electrochemistry or electrodes.

3.2.2.1. Homogeneous ORR Using Ferrocenes. In the absence of acidic protons, Fc and its derivatives are generally stable to O_2. This is because the $O_2/O_2^{\bullet-}$ couple is typically more than 1 V negative of the $Fc^{+/0}$ couple. In contrast, the standard potentials of O_2/H_2O_2 and O_2/H_2O in 1 M acid are anodic of $Fc^{+/0}$ (Table 3, section 2.2). Consistent with these thermodynamics, the reduction of O_2 to H_2O or H_2O_2 using Fc has been observed in acidic solutions (Scheme 6).[141]

Scheme 6. Reactions of Fc with O_2 in Acidic Organic Solutions

$$4Fc + 4H^+ + O_2 \rightarrow 2H_2O \quad \text{(i)}$$
$$2Fc + 2H^+ + O_2 \rightarrow H_2O_2 \quad \text{(ii)}$$

Fc was first reported to reduce O_2 to H_2O in the presence of trifluoroacetic acid (TFA) nearly 50 years ago.[142] It was suggested that the reaction proceeded by reaction of protonated Fc $[(C_5H_5)_2Fe{-}H]^+$ with O_2 to form $HO_2^{\bullet}$. This mechanism was much later supported by density-functional theory (DFT) calculations on the reaction of $[Me_{10}Fc{-}H]^+$ with O_2.[143−154] The reduction of H_2O_2 by Fc has also been reported in EtOH containing $HClO_4$.[155]

Extensive studies of outer-sphere ORR by ferrocenes at immiscible solution interfaces have been described by Girault and co-workers.[144−153] Their approach delivers electrons and protons to dissolved O_2 from opposite sides of a solution boundary, for instance, e^- from $Me_{10}Fc$ in a dichloroethane (DCE) layer and H^+ from an acidified water layer. In electrochemical terminology, such cells with a "soft boundary" are written as [DCE ($Me_{10}Fc$)||H_2O (H^+)]. While these reactions are not truly homogeneous, they are presented in this section because they only involve liquid phases. Typically, these biphasic reactions produce H_2O_2. In most cases, the polar product was found preferentially in the bulk aqueous phase, away from further reducing equivalents in the organic layer.

Mechanistically, the ORR was found to occur by initial reaction of O_2 with $[Me_{10}Fc{-}H]^+$ in the organic layer before H_2O_2 extraction.[143,144,147,156] The rates of the ORR are sensitive to the electrolyte[144] and to the Galvani potential,[149] a thermodynamic indicator of the effective polarization across the liquid|liquid interface.[144] Faster rates were observed for larger Galvani potentials, as more protons can be effectively "pumped" into the organic phase.[151] The fastest rates were observed for solutions containing tetrakis(pentafluorophenyl)borate ($BAr^F{}_4^-$) as a common electrolyte ion,[144] as $BAr^F{}_4^-$ can assist proton movement into the organic phase.[153] Similar base-assisted proton partitioning was also reported for 4-dodecylaniline.[146] When ClO_4^- was used as the common anion (DCE containing tetrahexylammonium perchlorate, water containing $HClO_4$), protons could not migrate into the organic phase, and the ORR occurred only at the boundary layer.[148] Related reactions were also described (i) with 1,2-diferrocenylethane,[145] (ii) with trifluorotoluene[153] or an ionic liquid[150] in place of DCE, and (iii) with aqueous LiOH instead of aqueous acid.[152]

As part of these liquid|liquid ORR studies, Girault and co-workers coupled scanning electrochemical microscopy (SECM) with enzymatic detection of H_2O_2. In experiments using horseradish peroxidase and the redox mediator 2,2′-azino-bis-3-ethylbenzothiazoline sulfonate ($ABTS^{2-}$), the H_2O_2 generated from O_2 reduction was further reduced to H_2O (Figure 11). The

DOI: 10.1021/acs.chemrev.7b00542
Chem. Rev. XXXX, XXX, XXX−XXX

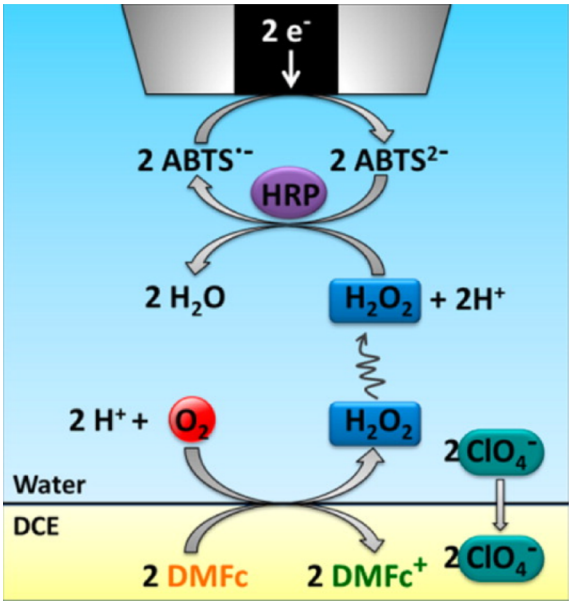

Figure 11. (A) Schematic diagram of SECM experiment for enzymatic detection of H_2O_2 generated at the liquid|liquid interface (rather than in the organic phase). Reproduced with permission from ref 148. Copyright 2013 American Chemical Society.

oxidized mediator ($ABTS^-$) was detected electrochemically and used to estimate the amount of H_2O_2 produced.[148]

3.2.2.2. Metal-free Macrocycles for Outer-Sphere ORR. In addition to the extensive literature on metal macrocycles that catalyze *inner-sphere* mechanisms for the ORR,[11] as discussed in section 4.4, metal-free macrocycles have also been studied as *outer-sphere* ORR catalysts (Table 9 and Figure 12). For example, 5,10,15,20-*meso*-tetraphenylporphyrin (H_2TPP, **3**) catalyzes the reduction of O_2 to H_2O_2 in polarized DCE|water systems containing Fc derivatives and aqueous acids.[157−160] The protonated macrocycles, H_3TPP^+ or H_4TPP^{2+}, were proposed to reversibly form unusual adducts with O_2 (Figure 13), which could then react with the reductant to form $HO_2^\bullet$. Using a number of ferrocene reductants, ET was found to be rate-determining, and the results suggest a symmetric activation barrier (transfer coefficient ~1/2).[159] The use of various tetraarylporphyrin catalysts (**4**−**6**) with different basicities implicated the diprotonated macrocycle in the O_2 adduct.[161] The reactions were inhibited by water and by the anionic conjugate base of the acid, especially smaller anions, which were thought to competitively bind the protonated macrocycle.[158,160]

The porphyrin-like macrocycle [14]triphyrin(2.1.1) (HTrip, **7**, Figure 12) was recently reported to catalyze the ORR using Me_8Fc and $HClO_4$ in benzonitrile (PhCN).[162] Mechanistic studies showed that HTrip is doubly protonated and doubly reduced (forming H_3Trip) prior to a rate-determining reaction with O_2. The reaction rates saturated at high $[O_2]$, suggesting the formation of a weak O_2 adduct ($H_3Trip\text{-}O_2$, $K_s = 8.4 \times 10^2\ M^{-1}$). The authors proposed that, upon formation of $H_3Trip\text{-}O_2$, HAT occurred to make $H_2TRip^\bullet$ and $HO_2^\bullet$. This radical pair was detected by electron paramagnetic resonance (EPR) spectroscopy in a related photochemical experiment at low temperatures.[162]

For both HTrip and the porphyrin reactions, the proposed mechanisms implicate the formation of O_2 adducts and CPET or HAT reactions to make $HO_2^\bullet$. For the porphyrin examples, the reducing equivalent to make $HO_2^\bullet$ comes from an external reductant; however, for H_3Trip, the reduced macrocycle supplies its own electrons for $HO_2^\bullet$ formation.

3.3. Lewis Acid Acceleration of Outer-Sphere ORR Systems

The outer-sphere reduction of O_2 to $O_2^{\bullet-}$ can be facilitated using Lewis acidic metal ions via MCET.[164] Fukuzumi and co-workers have used photoinduced ET from 1-benzyl-1,4-dihydronicotinamide to O_2 to generate $O_2^{\bullet-}$, which rapidly complexed M^{n+}.[165] They have used EPR spectroscopy to identify the $M^{n+}-O_2^{\bullet-}$ complexes and to quantify the strength of the interaction.[166] Unlike acidic protons, which react with $O_2^{\bullet-}$ to form unstable $HO_2^\bullet$, the $M^{n+}-O_2^{\bullet-}$ complexes are relatively stable.[166,167] Outer-sphere ET (k_{ET}) to O_2 from $Co^{II}TPP$ was reported to only occur in the presence of Lewis acids,[166,167] and the rate constant for the reaction increases with the strength of the $M^{n+}-O_2^{\bullet-}$ interaction (ΔE). The relationship between $\log(k_{ET})$ and ΔE is linear over nearly 7 orders of magnitude (Figure 14).[166,167] We note that the third-order rate law (rate = $k_{ET}[Co^{II}TPP][O_2]$-[Lewis acid]) does not uniquely implicate an *outer-sphere* ET mechanism. Rather, initial O_2 binding could be followed by Lewis acid attack (see section 4.2.2).

Although such MCET reactions for outer-sphere ORR can be used to stabilize $O_2^{\bullet-}$, a large overpotential is often required to facilitate ORR via outer-sphere pathways. Coupling MCET reactions to *inner-sphere* reactions may be more effective for improving the thermodynamic requirements of other ORR systems (a few examples are highlighted in section 4.2.2).

3.4. Conclusions and Generalizations on Outer-Sphere ORR Systems

The various reported studies show that O_2 can be reduced by an electrode or a soluble reductant in an *outer-sphere* manner—that

Table 9. Metal-free Macrocycles for Outer-Sphere ORR

catalyst	ligand scaffold	solvent(s)	proton source	reductant	product[a]	ref
3	5,10,15,20-*meso*-tetraphenylporphyrin	water/DCE	H_2SO_4	$Me_{10}Fc$		157
3	5,10,15,20-*meso*-tetraphenylporphyrin	DCE	$HBAr^F{}_4$,[b,c] TFA	Fc		158
3	5,10,15,20-*meso*-tetraphenylporphyrin	water/DCE	HCl	Fc		159
3	5,10,15,20-*meso*-tetraphenylporphyrin	water/DCE	HCl	Me_nFc (n = 2, 4, 6, 8)		159
3	5,10,15,20-*meso*-tetraphenylporphyrin	water/DCE	HCl	$Me_{10}Fc$		159
3	5,10,15,20-*meso*-tetraphenylporphyrin	DCE	$HBAr^F{}_4$[b]	Fc	H_2O_2	160
3	5,10,15,20-*meso*-tetraphenylporphyrin	water/DCE	HCl	Fc	H_2O_2	161
4	5-(*p*-aminophenyl)-10,15,20-tris(pentafluorophenyl)porphyrin	water/DCE	$HBAr^F{}_4$[b,c,d]	Fc	H_2O_2	163
5	5,10,15,20-tetrakis(4-methoxyphenyl)porphyrin	water/DCE	HCl	Fc	H_2O_2	161
6	5,10,15,20-tetra(4-nitrophenyl)porphyrin	water/DCE	HCl	Fc	H_2O_2	161
7	[14]triphyrin(2.1.1)	PhCN	$HClO_4$	Me_8Fc	H_2O_2	162

[a]Selectivities were not reported, but in some cases iodometric titrations confirmed H_2O_2 as major product. [b]$HBAr^F{}_4$ = tetrakis(pentafluorophenyl)-boric acid, $[H(Et_2O)_2][B(C_6F_5)_4]$. [c]Isolated as crystalline solid as reported in reference. [d]In situ synthesis, not isolated, as reported in reference.

DOI: 10.1021/acs.chemrev.7b00542
Chem. Rev. XXXX, XXX, XXX−XXX

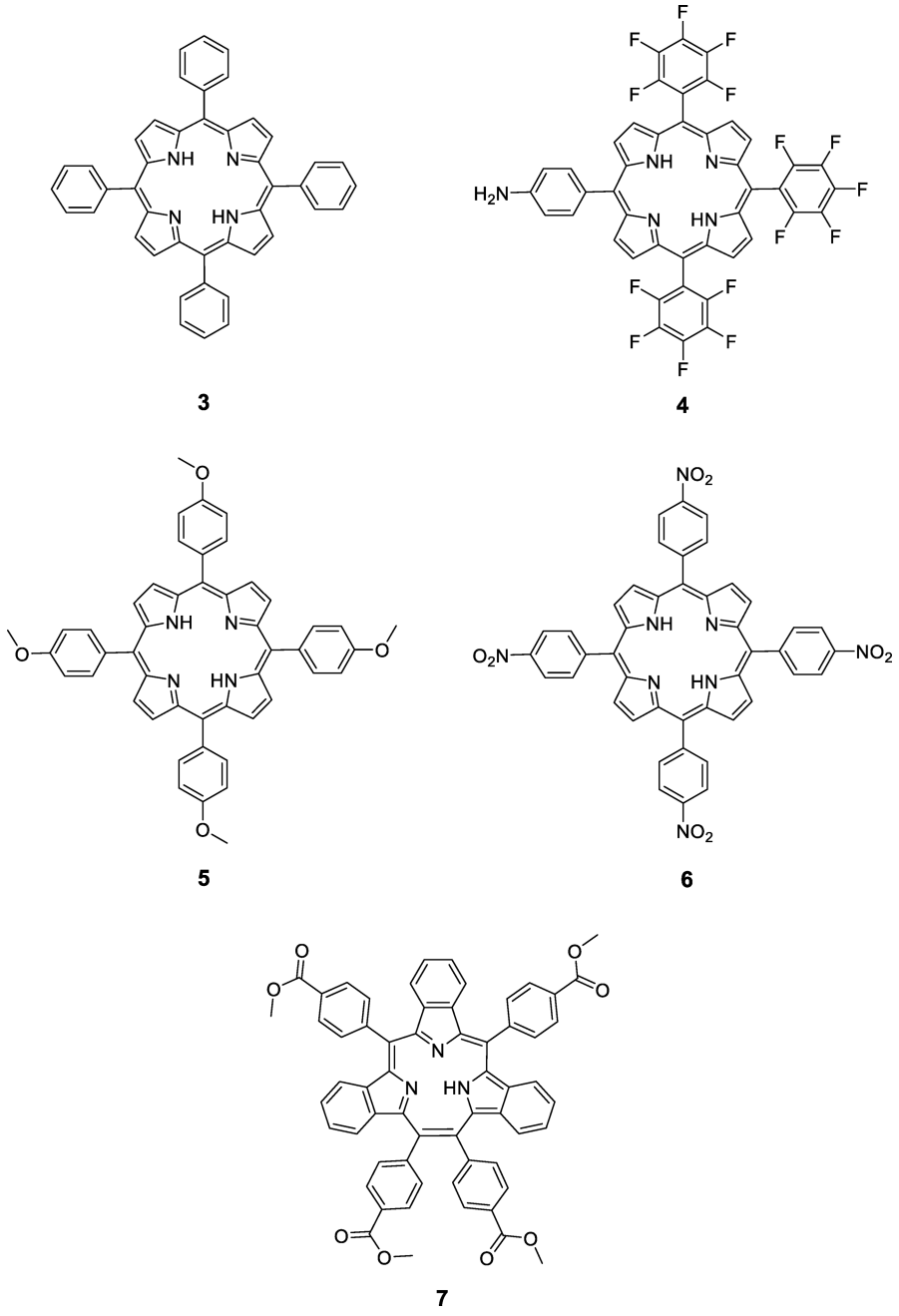

Figure 12. Macrocycles used as outer-sphere ORR catalysts in refs 157−162.

is, without substantial binding of O_2 or $O_2^{\bullet-}/HO_2^{\bullet}$ products to the chemical reductant or electrode. These reactions predominantly depend on the nature and reduction potential of electron supply (both homogeneous and heterogeneous), the solvent, the proton source, and the proton activity. Although the proposed mechanisms vary, a few general comments can be made:

(i) Typically, in solutions where an electrode supplies reducing equivalents, O_2 is first reduced to $O_2^{\bullet-}$. In the presence of a proton source, this initial ET is followed by PT to give $HO_2^{\bullet}$. The nature of these reactions is dependent on acid strength and electrode material, and, in some cases, HAT from electrode-adsorbed $H^{\bullet}$ to O_2 has been proposed to occur in place of stepwise ET−PT.

(ii) In both homogeneous and biphasic solutions containing a soluble reductant (e.g., $Me_{10}Fc$), the reaction of O_2 with reductant and acid typically forms $HO_2^{\bullet}$. Strong evidence for forming $HO_2^{\bullet}$ via CPET is present in only a few systems and may be an interesting direction for future pursuits.

(iii) $O_2^{\bullet-}$ is somewhat stable in highly aprotic media, but under no conditions has $HO_2^{\bullet}$ accumulated. Under many conditions, $HO_2^{\bullet}$ is rapidly reduced to HO_2^{-} either by reduction or disproportionation. Disproportionation is thought to most commonly occur by $HO_2^{\bullet} + O_2^{\bullet-} \rightarrow HO_2^{-} + O_2$. $HO_2^{\bullet}$ can also be reduced to H_2O_2 via CPET reactions. The reduction of $O_2^{\bullet-}$ to O_2^{2-} has not yet been definitively observed. Rather, $O_2^{\bullet-}$ has been shown to (i) protonate to $HO_2^{\bullet}$, (ii) react via CPET to form HO_2^{-}, or (iii) bind a Lewis acid.

(iv) Hydrogen bonds and Lewis acids can play a significant role in the kinetics and thermodynamics of forming O_2-derived intermediates. In such cases, the basicity of O_2-derived intermediates increases dramatically upon further reduction (e.g., O_2 to $O_2^{\bullet-}$ to O_2^{2-}). Direct implication of hydrogen bonding to

DOI: 10.1021/acs.chemrev.7b00542
Chem. Rev. XXXX, XXX, XXX−XXX

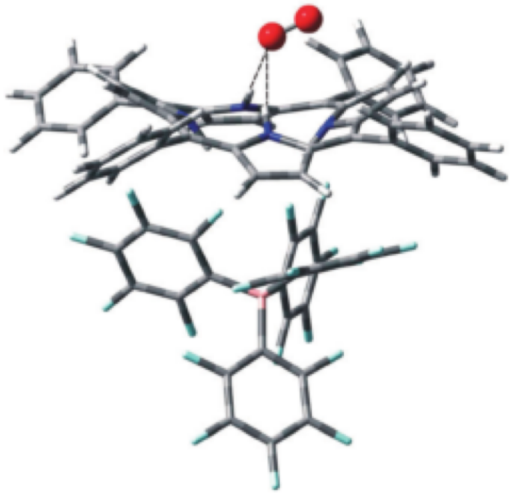

Figure 13. DFT/M05-2x optimized structure of $(H_4TPP^{2+})|O_2|(BAr^F{}_4{}^-)$ system; the averaged O−H distances were calculated to be 2.338 Å, suggestive of an interaction with O_2. Reproduced with permission from ref 158. Copyright 2011 Royal Society of Chemistry.

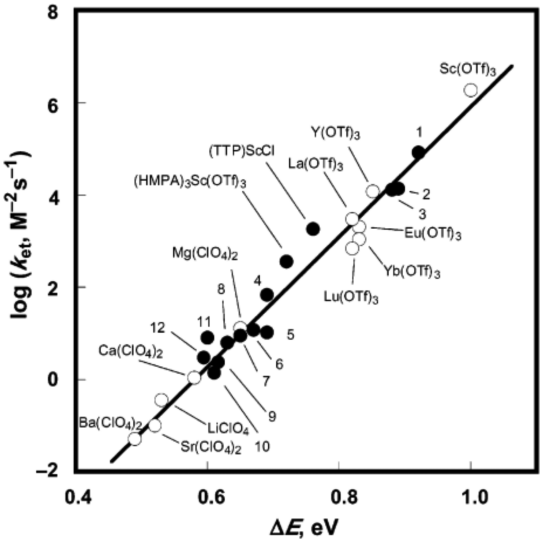

Figure 14. Plots of $\log(k_{ET})$ vs ΔE in electron transfer from $Co^{II}TPP$ to O_2 promoted by metal ions (triflate or perchlorate salts) (○) and organotin compounds and scandium complexes (●) in MeCN at 298 K. Reproduced with permission from ref 167. Copyright 2003 American Chemical Society.

O_2 has been suggested in two systems for the formation of weak O_2 adducts with organic catalysts. This seems to be an interesting area for future research given that O_2 is nonpolar and is usually considered to be unable to form significant hydrogen bonds.

(v) Outer-sphere pathways can be rapid but often require high overpotentials. In the absence of strong coordination, the intermediates derived from O_2 are high in energy and are formed only under strongly reducing conditions (see section 2). Furthermore, outer-sphere pathways predominantly form H_2O_2, as cleavage of the O−O bond is thermodynamically challenging. These are all primary reasons why *inner-sphere* catalysts play such an important role in the ORR, as described in the next section.

4. INNER-SPHERE ORR CATALYSIS

Many different transition metal complexes are capable of facilitating the oxygen reduction reaction by an inner-sphere mechanism. In this context, "inner-sphere" means that O_2 binding occurs in concert with electron transfer from a metal center, whereby O_2 is formally reduced and M is formally oxidized by one electron ($M + O_2 \rightarrow MO_2^{\bullet}$). While the primary focus of this section is the ORR catalysis (sections 4.3−4.6), we begin with a discussion of the stoichiometric steps that are often critical in ORR. As explained in section 2, a fundamental role of the catalyst is to preferentially bind and stabilize the higher-energy intermediates along the path from O_2 to H_2O or H_2O_2, shown in the Frost diagrams of Figure 2. Sections 4.1 and 4.2 are selective rather than comprehensive and lay the groundwork for the catalytic studies that follow.

4.1. Oxygen Binding to Transition Metal Complexes

Dioxygen binding[9,168−171] and the influence of the secondary coordination sphere on dioxygen activation[171−174] have been widely studied for many years, since it was discovered that O_2 binds to the iron center in hemoglobin. Similar kinds of O_2 adducts are important in O_2 transport, O_2 reduction, and O_2 activation for oxidation reactions.

4.1.1. Binding Modes of Oxygen Complexes. Dioxygen can bind to one, two, or occasionally more metal centers, yielding monometallic, bimetallic, and polymetallic complexes (c.f. refs 168, 171, and 175−179). The most common coordination geometries are drawn in Figure 15. The specific binding mode depends on the structure of the surrounding ligands, the availability of coordination sites at the metal, and the pattern and energies of the frontier metal d-orbitals.[168−170] In monometallic complexes, the accessible oxidation states of the metal also play a role in determining the dioxygen-binding mode.[9,175,176] The traditional names of η^1-superoxo and η^2-peroxo structures imply $1e^-$ and $2e^-$ oxidations of the metal center, respectively. There was, however, significant debate many years ago about the appropriate assignment of the metal and dioxygen oxidation states in these adducts.[9,170,175,176,180,181] Recently, Kennepohl and co-workers have revisited this question, using X-ray and Raman spectroscopies with DFT calculations to show that, at least in some cases, there is little charge transfer from M to O_2 in peroxo adducts.[182,183] The dioxygen-binding mode can also influence trends in dioxygen reactivity (c.f. refs 168, 178, and 179), making it an important parameter to consider when designing ORR catalysts. For example, the vast majority of *mononuclear* ORR catalysts proceed via η^1-superoxo intermediates, with only a few examples of catalysis via η^2-peroxo complexes.[184−187]

4.1.2. Thermodynamics of Oxygen Binding to Reduced Metal Complexes. The thermodynamics of O_2 binding to a metal center are of particular relevance to ORR catalysis. Experimental and calculated values of the free energy, enthalpy, entropy, and equilibrium constant for the reaction $M + O_2 \rightleftharpoons M(O_2)$ have been reported for a large number of synthetic, biomimetic, and biological metal complexes.[9,175,176,188,189] Strangely, few studies[190,191] describing either experimental or computational ORR catalysis have included the O_2-binding energetics for their catalytic system. This should be possible at least in some cases by excluding protons, and we believe such

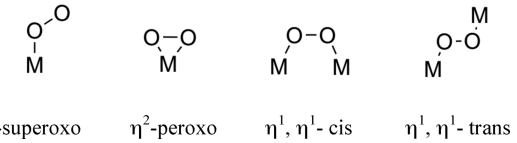

Figure 15. Common geometries of dioxygen−metal binding interactions.

DOI: 10.1021/acs.chemrev.7b00542
Chem. Rev. XXXX, XXX, XXX−XXX

measurements could enrich future ORR studies. Generally, metal−dioxygen bond formation is enthalpically driven,[9] and in the absence of secondary sphere effects, it is governed by the reducing power of the metal center and availability of an open coordination site.[66] A study by Shi and Zhang[188] calculated the energy of oxygen binding to a number of Co and Fe porphyrins (P's) and phthalocyanines (Pc's) (Table 10), finding that iron

Table 10. Computed Energies of Oxygen Binding to Select Co and Fe Macrocycles[a]

complex	E_{bO_2} (eV)
CoPc	0.43
CoMeOPc	0.47
CoF16Pc	0.27
CoTsPc	0.32
CoP	0.47
CoTPP	0.43
FePc	0.75
FeMeOPc	0.65
FeF16Pc	0.63
FeP	0.58
FeTPP	0.78

[a]Values taken from ref 188. Abbreviations: Pc = phthalocyanine, MeOPc = octamethoxy-Pc, F16Pc = hexadecafluoro-Pc, TSPc = tetrasulfonic-Pc, P = porphyrin, TPP = tetraphenyl-P.

complexes bind dioxygen more favorably than their cobalt analogues. An increase in the electron-donating nature of the ligand was found to enhance the Co−O_2 binding, but this trend was less evident for the iron complexes. The study also reported that the ORR activity scaled linearly with dioxygen-binding ability for FePc's but that the reverse was true for CoPc's. Thus, the authors proposed that, for these Pc ORR catalysts, a more appropriate activity descriptor is the ionization potential, which scales linearly with ORR activity and M(III/II) redox potential for both CoPc and FePc complexes. These analyses were performed for heterogeneous catalysts, specifically metal macrocycles adsorbed on an electrode surface. Related computational results have been recently reported for homogeneous systems of iron porphyrins in which the favorability of O_2 binding was found to linearly correlate with the catalyst reduction potential.[66]

In a related study, Baran and co-workers computationally analyzed the binding energies of the neutral O_2-derived intermediates hydroxyl ($HO^{\bullet}$), perhydroxyl ($HO_2^{\bullet}$), and oxyl ($O^{\bullet\bullet}$) radicals to a variety of metal porphyrin complexes.[192] In general, the $HO^{\bullet}$ and $HO_2^{\bullet}$ binding energies were found to decrease from left to right across the periodic table. The computed energies were used to derive scaling relationships and predict the ORR overpotentials for a range of different catalysts. Cobalt was found to be the optimal metal center, capable of forming stable $HO^{\bullet}$ and $HO_2^{\bullet}$ intermediates without binding either ligand too strongly. Formation of intermediates that are too weakly or too strongly bound may limit the catalytic ORR efficiency.

4.1.3. Axial Ligand Effects. The most common catalysts for the ORR are complexes of planar N_4-macrocycles, and a sometimes underappreciated aspect of oxygen binding to such complexes and their subsequent reactivity is the nature of the axial ligand trans to the O_2-binding site. Axial ligand effects have been widely studied in the context of heme enzyme reactivity;[193−196] however, few, if any, studies have examined their influence on the TOF_{max} and η_{eff} for homogeneous ORR catalysis. This is likely because axial ligands bind in dynamic equilibria, and it can be challenging to determine the nature of the axial ligand in each of the catalytic intermediates.

Solomon and co-workers probed axial ligand effects on the rate of reaction of $O_2^{\bullet-}$ with iron(III) tetrakis(4-*N*-methylpyridyl)-porphyrin complexes having bis(imidazole), dihistidyl, dicyano, and diaquo axial ligands.[197] The measured rate for the diaquoporphyrin exceeded all others by 2−3 orders of magnitude, indicating a different mechanism. The authors proposed that the greater lability of the water ligand allowed an inner-sphere electron-transfer path with direct formation of an $Fe^{III}TMPyP(O_2^{\bullet-})$ complex, whereas the bis(imidazole), dihistidyl, and dicyano porphyrins reacted via outer-sphere electron transfer.

Several reports have indicated that ORR catalysis can be enhanced by imidazole binding as an axial ligand.[198−200] Discussed in greater detail in section 4.4.1.2, one study observed larger reductive currents for the solutions containing iron(III) tetraphenylporphyrin and O_2 when imidazole was present.[198] Tsuda and Kasai investigated the effects of axially bound imidazole on iron and cobalt porphyrin O_2 adducts using DFT and found the O−O bond to be weaker in the species with imidazole bound, consistent with the electron-donating nature of the ligand.[199] Cleavage of the O−O bond is required for selective reduction of O_2 to H_2O. Related DFT calculations by Ohta and co-workers determined that the presence of an imidazole axial ligand increases the pK_a of Fe(III)-superoxo and Fe(III)-peroxo porphyrin species, thus promoting formation of an Fe(III)-hydroperoxo complex.[200] Fe(III)-hydroperoxo species are often considered essential for O−O bond cleavage and formation of H_2O as the major ORR product. Overall, the experimental and computational studies of ORR by N_4-macrocyclic compounds indicate that axial ligands (trans to the O_2) have a significant effect, but this has not yet been systematically explored.

4.2. Secondary Coordination-Sphere Effects on Oxygen Binding

The O_2-bound adducts of metalloenzyme cofactors are often stabilized and activated through secondary coordination-sphere interactions,[193,201−206] and they have inspired attempts to use similar effects to enhance ORR catalysis in molecular systems. Indeed, secondary coordination-sphere modifications have been shown to play an important role in facilitating O_2 binding and activation in synthetic systems.[7,8,177−179,206−208] The select examples discussed here demonstrate the effects of hydrogen-bonding functional groups and Lewis acids, with emphasis on their (potential) role in ORR catalysis.

4.2.1. Hydrogen-Bonding Motifs. An early challenge in O_2-binding research was understanding why hemoproteins, such as hemoglobin and myoglobin, have relatively similar binding strengths for O_2 and CO, while porphyrin model systems strongly favor CO.[7,8] This difference was in part attributed to the presence of hydrogen-bond donors within the active site pocket that could stabilize the bound superoxide adduct.[209,210] To model these interactions, many porphyrin complexes that incorporate hydrogen-bonding groups into the secondary coordination sphere have been prepared. These hydrogen-bonding groups can enhance the O_2 reduction activity of metalloporphyrins by increasing their O_2 binding affinity and inhibiting unwanted dimerization and the formation of μ-oxo complexes. Examples of this include Collman's picket-fence porphyrins (**8**),[8] Chang's Kemp's acid porphyrins (**9**),[23] and Nocera's hangman porphyrins (**10**)[211] (Figure 16). The more recent examples have emphasized the acidity of the secondary

DOI: 10.1021/acs.chemrev.7b00542
Chem. Rev. XXXX, XXX, XXX−XXX

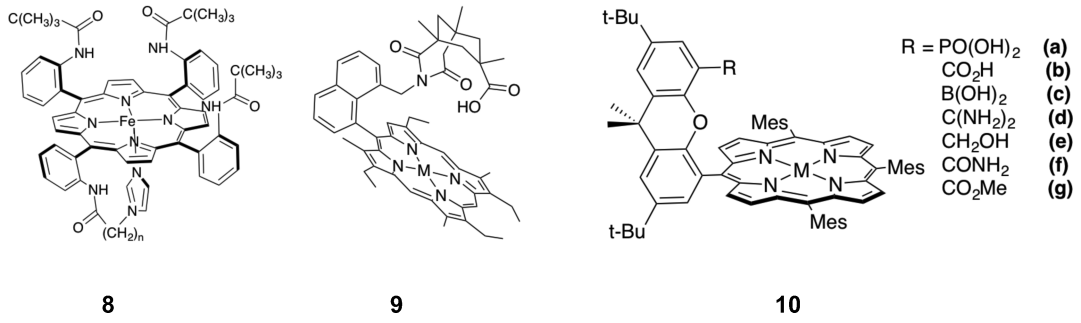

Figure 16. Collman's picket-fence porphyrin (**8**), Chang's Kemp's triacid porphyrin (**9**), and Nocera's hangman porphyrin (HPX−**10**$^{a-g}$).

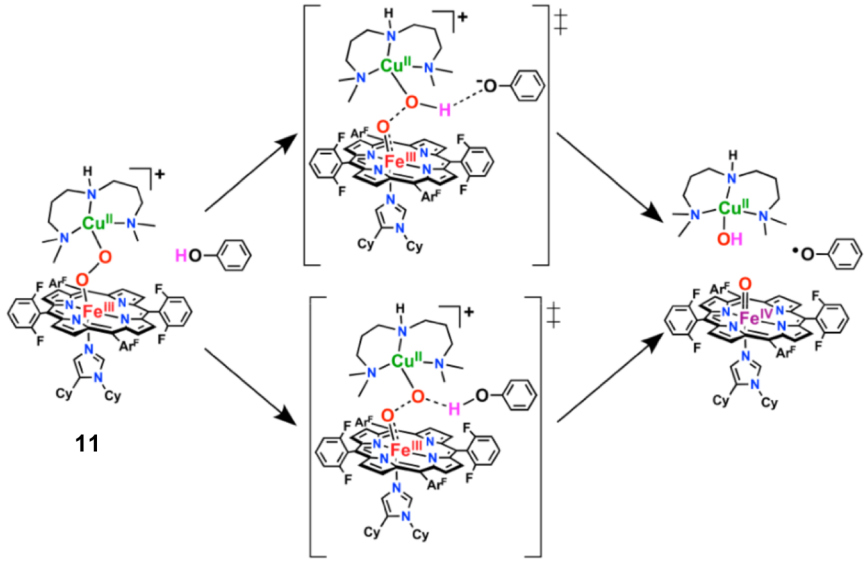

Figure 17. Potential pathways for O−O bond cleavage, proton-initiated (PI, top) and hydrogen-bond assisted (HB, bottom). Reproduced with permission from ref 219 Copyright 2017 American Chemical Society.

coordination-sphere group as well as its hydrogen-bond donor ability and the possibility of these acids serving as proton relays and participating in ORR and other PCET reactions.[11,174,192,200,212−214] In general, positioning an acidic or H-bonding functional group in close proximity to the O_2-binding site has been found to promote dioxygen activation and improve catalytic ORR activity,[213] hydrogen peroxide disproportionation,[214,215] and water oxidation.[216]

The inclusion of hydrogen-bonding motifs in the secondary coordination sphere has been employed as a method for facilitating O−O bond cleavage, a crucial mechanistic step for controlling the selectivity of ORR catalysts. In cytochrome *c* oxidase (C*c*O), this step is believed to proceed via HAT from a tyrosine residue to a peroxo intermediate, yielding Fe^{IV}═O, Cu^{II}−OH, and a tyrosyl radical.[4,202,217,218] Using a biomimetic heme-peroxo-copper complex (**11**, Figure 17), a recent study compared computational and experimental data to understand the role of secondary coordination-sphere hydrogen-bond donors in the mechanism of O−O bond cleavage.[219] Two potential pathways were proposed, proton-initiated (PI) and hydrogen-bond assisted (HB) (Figure 17), distinguishable by the degree of PT at the transition state. Agreement between experimental and computed KIEs for the reaction of **11** and *para*-methoxyphenol (4-OMePhOH) supported the HB O−O homolysis pathway. Importantly, the authors note that their calculations indicated that the presence of phenol decreases the kinetic barrier to O−O bond cleavage in both pathways, which suggests an important role for acidic or hydrogen-bonding groups in ORR catalyst design.

The ability of hydrogen-bond donors to promote O−O bond cleavage has been explored in a variety of synthetic systems, including organic peroxides[220] and hangman porphyrin and corrole complexes.[174,192,200,214] Perhaps the most dramatic example was reported by Costentin and co-workers, who showed that reductive O−O bond cleavage is nearly 700 mV more favorable for organic peroxides containing a proximal acid than for those containing a methyl ester.[220] Inclusion of a hangman motif in porphyrin and corrole complexes has been reported to play a similar role, facilitating O−O bond cleavage and leading to higher selectivity for H_2O.[174,213,221] It is worth noting, however, that these catalysts are typically studied as composite films on electrodes, making mechanistic study more difficult and placing them in the purview of a different Review in this issue.[5] Chng and co-workers measured rates of H_2O_2 disproportionation for six iron hangman porphyrin complexes containing varying pendant groups (ΔpK_a = 23, **10**$^{a-f}$).[214] More acidic pendent groups increased the rate of H_2O_2 disproportionation by promoting heterolytic cleavage of the O−O bond. Although phosphonic acid (pK_a = 2) was the most acidic group, the highest activity was measured for the carboxylic acid derivative (pK_a = 4.2). This result was attributed to the poor basicity of the phosphonate and its inability to accept protons during the catalytic cycle. Although not focused specifically on the ORR, the study demonstrated a potential method for

DOI: 10.1021/acs.chemrev.7b00542
Chem. Rev. XXXX, XXX, XXX−XXX

predictably tuning O−O activation by modifying pendant group pK_a's.

DFT has also been used to highlight the potential benefits of secondary coordination-sphere H-bonding, specifically for hangman porphyrins.[192,200] Baran and co-workers calculated binding energies of neutral perhydroxyl ($HO_2^{\bullet}$), hydroxyl ($HO^{\bullet}$), and oxygen ($O^{\bullet\bullet}$) radicals to a variety of cobalt porphyrin catalysts, including unsubstituted (**12**), phenyl-fluorinated (**13**), and hangman (**14**) porphyrins (Figure 18).[192] The binding of these radicals results in the analogous adsorbed intermediates, denoted as *OOH, *OH, and *O. The authors concluded that the presence of a hangman motif selectively stabilized the metal-bound oxo (*O) species by improving the thermodynamics of proton transfer to this otherwise too weakly bound intermediate. Still, the addition of the secondary coordination-sphere groups did not disrupt the scaling relationship between $HO^{\bullet}$ and $HO_2^{\bullet}$ binding. Ohta and co-workers performed related DFT studies on Fe(III)-superoxo and Fe(III)-hydroxo species with acid and methyl ester hangman porphyrins to investigate the effects of secondary coordination-sphere motifs on their PCET reactivity.[200] The authors examined the factors influencing ORR selectivity in these systems and found that a combination of secondary coordination sphere and axial ligand effects (see section 4.1.3) resulted in the preferential $4H^+/4e^-$ reduction via O−O bond cleavage in the Fe(III)-hydroperoxo intermediate.

The influence of intramolecular H-bonding on O_2 activation and reactivity has also been demonstrated with nonheme complexes.[173,208,222] Borovik and co-workers have developed what is likely the most convincing system for showing effects of secondary coordination-sphere hydrogen bonds on O_2 adducts

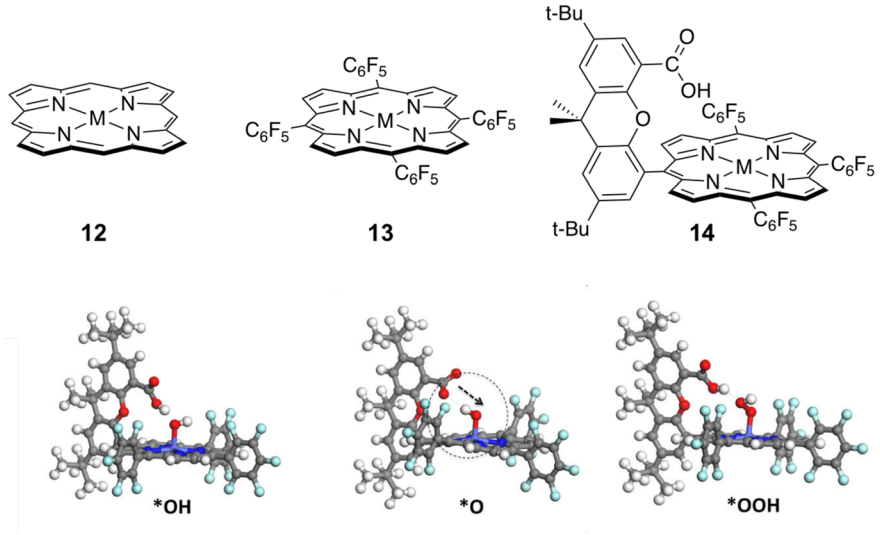

Figure 18. Porphyrin derivatives examined by DFT calculation (top). Computed intermediates for **14**, demonstrating the ease of H^+ transfer to the metal-oxo (O) intermediate that provides a stabilizing effect (bottom). Adapted with permission from ref 192 . Copyright 2014 American Chemical Society.

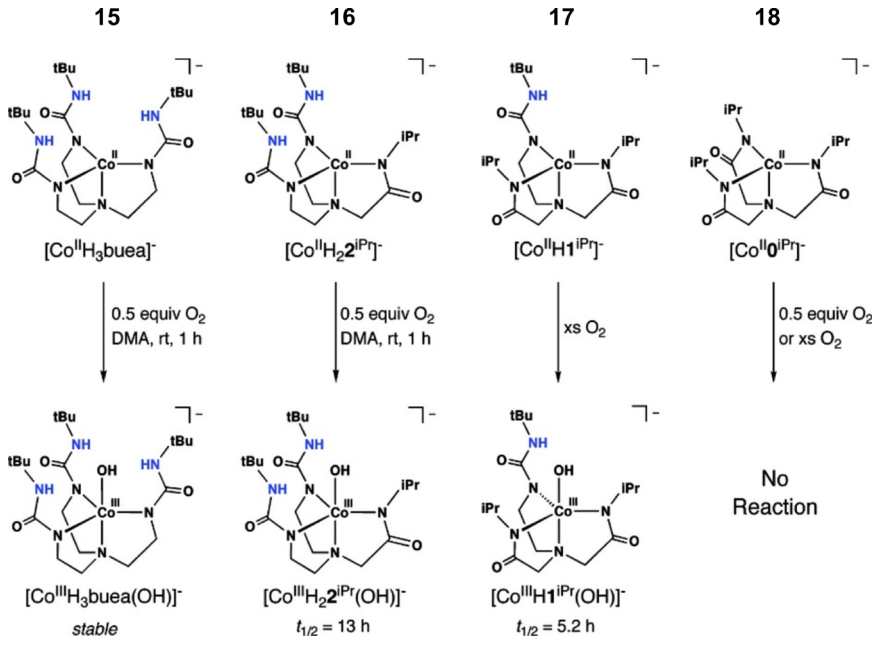

Figure 19. Dioxygen reactivity of a series of Co complexes (**15**−**18**) containing varying numbers of hydrogen-bond donor groups in the secondary coordination sphere. Reproduced with permission from ref 173. Copyright 2010 American Chemical Society.

DOI: 10.1021/acs.chemrev.7b00542
Chem. Rev. XXXX, XXX, XXX−XXX

and other ORR intermediates in a series of Mn, Fe, and Co complexes.[173,208,222] The H-bonding network located above cobalt tripodal complexes of the H_3buea ligand (**15**–**18**) promoted dioxygen activation and stabilized the resulting Co^{III}–OH species (Figure 19). On the other hand, a tripodal cobalt(II) complex prepared with an identical primary coordination sphere but lacking hydrogen bonds (**18**) was found to be insensitive to dioxygen. A similar tripodal cobalt complex with pendant amine substituents reported by Blacquiere and co-workers underwent reversible O_2 binding to the superoxo species, although the equilibrium strongly favored the unbound form.[223]

Borovik and co-workers also prepared unprecedented Mn(III) and Fe(III) terminal oxo complexes using the H_3buea ligand scaffold (ligand shown in Figure 19). The ability to form these unusually stable and low-valent metal-oxo complexes highlights the dramatic influence of the H-bonding groups. The HAT reactivity of $[Mn^{III}H_3buea(O)]$ and $[Mn^{IV}H_3buea(O)]$ has also been explored.[173] The metal-oxo basicity was found to dictate the following mechanism—the more basic $[Mn^{III}H_3buea(O)]$ proceeded via a stepwise PT-ET pathway to form Mn(II)–OH, while $[Mn^{IV}H_3buea(O)]$ underwent PCET to yield Mn(III)–OH. Metal-oxo intermediates are likely intermediates in most ORR catalytic cycles, although in most cases, are formed well after the rate- and selectivity-determining steps.

4.2.2. Lewis Acid Effects. The presence of Lewis acids in the secondary coordination sphere has also been shown to promote the stability and reactivity of O_2–transition metal adducts,[164,171,172,224–227] specifically metal-oxo,[171,227–235] -peroxo,[236–241] and -superoxo[235,239–243] complexes. Lewis acids can aid in the formation of high-valent oxo species[171,228–231] and can substantially increase their reactivity. The binding of Lewis acids to nonheme Mn(IV)- and Fe(IV)-oxo complexes enhanced OAT and electron-transfer reaction rates, with faster rates observed for stronger Lewis acids.[232–234] The rate of HAT to a vanadium(V) oxo complex also increased in the presence of a Lewis acid.[235] In nonheme Fe(III)-peroxo complexes, the rate and driving force for $1e^-$ reduction (and subsequent heterolytic O–O bond cleavage) have been found to increase in the presence of redox-inactive metal ions and scale linearly with the Lewis acidity of the cation.[236–238] On the basis of these results, Lee and co-workers offered a possible connection to biological oxygen reduction, proposing a mechanism for cytochrome *c* oxidase involving dioxygen activation at the Fe heme and O–O bond cleavage facilitated by the nearby Lewis-acidic Cu center.[236] A series of studies reported that stable Fe(III)-peroxo and Fe(II)-superoxo complexes could be formed in equilibrium from the reaction of KO_2 with a crown ether-appended Fe(II) porphyrin, because the crown ether maintained K^+ in close proximity to the Fe–O_2 adduct.[239–241] Free crown ether in solution did not provide the same stabilizing effect.[241] Several other reports have described the ability of redox-inactive metal ions to stabilize metal-superoxo complexes through electrostatic interactions;[235,242,243] however, this literature is surprisingly sparse given the likely importance of superoxo species as catalytic intermediates in synthetic ORR systems.

In summary, the introduction of Lewis acids and protic functionalities in the secondary coordination sphere of transition metal complexes can stabilize O_2 adducts and other intermediates and can influence the subsequent reactivity. Of particular relevance to the ORR, both hydrogen-bonding and Lewis-acid interactions can promote O–O bond cleavage. As a result, these features can be tuned to enable, enhance, or even suppress catalytic ORR activity and promote selectivity toward the production of H_2O_2 or H_2O.

4.3. Oxygen Reduction Catalysis by Early Transition Metal Complexes (Groups Vb and VIb)

The few reports of early metal complexes as ORR catalysts have demonstrated successful electrochemical and chemical reduction of O_2 to either H_2O_2 or H_2O. A series of studies by Anson, Tsuchida, and co-workers showed electroreduction of O_2 to H_2O by a series of vanadium-salen and -Schiff base complexes in dichloromethane (DCM) and acetonitrile (MeCN).[244–247] For example, in DCM with 5 mM triflic acid (HOTf), $[V^{IV}O(salen)]$ showed electrocatalytic O_2 reduction at −0.04 V vs $Fc^{+/0}$.[245] It was initially reported[244] that [(salen)VOV(salen)] (**19**) catalyzed the reduction of O_2 to H_2O, but further analysis[245,246] of $V^{IV}O$(salen) complexes (**20**) found $[V^{III}(salen)]^+$ to be the species involved in O_2 binding. The proposed catalytic ORR mechanism involved acid-induced disproportionation of $[V^{IV}O$-(salen)] and $[V^{IV}(salen)]^{2+}$, O_2 binding to $[V^{III}(salen)]^+$ followed by dimerization to a μ-peroxo species, and, finally, O–O bond cleavage and $1e^-$ reduction to regenerate the $[V^{IV}O(salen)]$ (Figure 20). Similar mechanistic observations

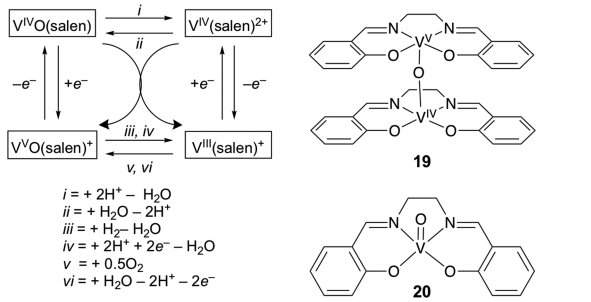

Figure 20. (Left) Proposed mechanism for ORR catalyzed by $V^{IV}O(L)$, where L = salen and Schiff base, based on ref 246. (Right) Vanadium-salen species investigated as ORR catalysts (refs 244–246).

were made in both DCM and MeCN solutions, although solvent binding slowed catalytic turnover in acetonitrile. Furthermore, acid-induced decomposition of $[V^{III}(salen)]^+$ in MeCN motivated investigation into other potential ligand scaffolds.

Of the series of vanadium-Schiff base complexes that were synthesized and examined for catalytic ORR activity (Figure 21),[247] three (**23**, **29**, and **35**) demonstrated greater acid stability than $[V^{III}(salen)]^+$. All of these complexes were proposed to proceed through the same ORR mechanism as the salen complex. In one example, electrolysis of an MeCN solution of **29** in the presence of HOTf at 0.11 V vs $Fc^{+/0}$ showed catalytic O_2 reduction with a TON > 60. The authors also report faster rates for the stoichiometric reduction of O_2 by the Schiff base complexes in DCM versus MeCN, but catalysis was not examined under these conditions. Like with the studies of $[V^{IV}O(salen)]$, the rate enhancement observed in DCM was attributed to the noncoordinating nature of the solvent.

Chromium complexes have also been shown to catalyze oxygen reduction in the presence of an acid and a chemical reductant. The chromium-oxo-corrole species **37** [(tpfc)-$Cr^V(O)$] (Figure 22) catalyzed the $2H^+/2e^-$ reduction of O_2 to H_2O_2 with trifluoroacetic acid (TFA) and Me_8Fc as sources of protons and electrons, respectively.[248] The reduction was first order in **37** and in O_2, with the second-order rate constant k_{cat} = 1.4 ± 0.1 × 10^2 M^{-1} s^{-1}. Interestingly, mechanistic analysis

DOI: 10.1021/acs.chemrev.7b00542
Chem. Rev. XXXX, XXX, XXX–XXX

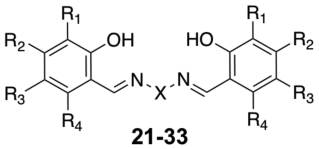

21-33

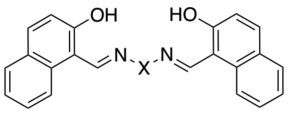

34-36

	R_1	R_2	R_3	R_4	X
21	H	H	H	H	CH_2CH_2
22	t-Bu	H	t-Bu	H	CH_2CH_2
23	H	H	H	H	*a*
24	H	H	H	H	$CH_2CH_2CH_2$
25	H	H	NO_2	H	CH_2CH_2
26	H	H	H	H	$CH_2C(CH_3)_2CH_2$
27	H	H	H	H	*b*
28	t-Bu	H	t-Bu	H	*b*
29	t-Bu	H	t-Bu	H	*a*
30	H	H	NO_2	H	$CH_2C(CH_3)_2CH_2$
31	H	H	NO_2	H	*c*
32	H	H	MeO	H	CH_2CH_2
33	H	MeO	H	MeO	CH_2CH_2
34	--	--	--	--	CH_2CH_2
35	--	--	--	--	*a*
36	--	--	--	--	*b*

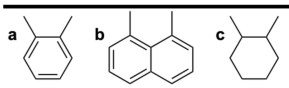

Figure 21. Vanadium-Schiff base complexes investigated as ORR catalysts in ref 247.

revealed that [(tpfc)$Cr^{V}O$] is only a catalyst precursor and is not regenerated after the first equivalent of O_2 is reduced. Rather, the catalyst resting state is [(tpfc)$Cr^{III}(OH_2)$], which reacts with O_2 to form [(tpfc)$Cr^{IV}(O_2^{\bullet-})$]. Selectivity for H_2O_2 production was thought to reflect the kinetically facile protonation of a [(tpfc)Cr^{IV}(OOH)] intermediate in the presence of excess acid.

Studies of oxygen reduction with early metal complexes have demonstrated that ligand scaffolds containing redox-active groups can be used to facilitate the desired reactivity. For example, Lu and co-workers reported that exposing a Zr complex containing an azacatecholate ligand (**38**) to O_2 resulted in the $2H^+/4e^-$ reduction of O_2 to form the hydroxide-bridged dimer $\mathbf{38}^{O_2}$ (Figure 23, top).[249] While not catalytic, this result demonstrated that noninnocent ligands can store proton and

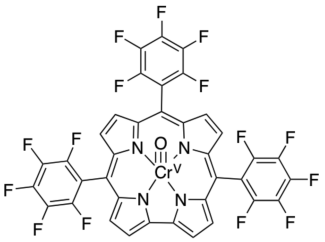

37

Figure 22. Cr(V)-oxo corrole used as an ORR precatalyst in ref 248.

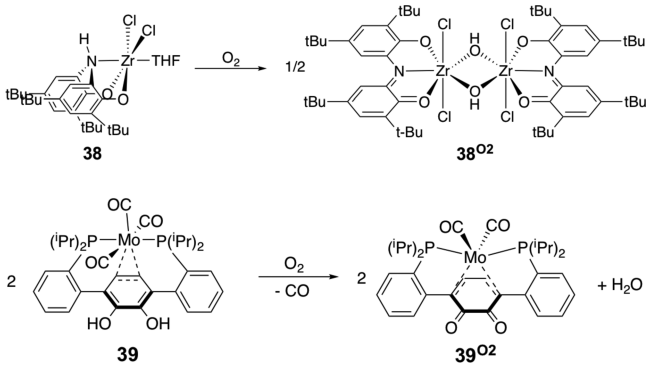

Figure 23. Zirconium (**38**, top) and molybdenum (**39**, bottom) reagents for ORR featuring redox-active ligands, and their oxygenated products $\mathbf{38}^{O_2}$ and $\mathbf{39}^{O_2}$, based on refs 249 and 250, respectively.

electron equivalents, thereby allowing oxygen reduction to occur at d^0 metal centers.

The direct involvement of a redox-active ligand in ORR was also demonstrated by Henthorn and co-workers, who reported a Mo-catechol complex (**39**) that reacts with O_2 to yield the corresponding Mo-quinone complex ($\mathbf{39}^{O_2}$) and H_2O (Figure 23, bottom).[250] This transformation is proposed to occur via initial production of H_2O_2, which then can rapidly react with the second equivalent of Mo-catechol to form H_2O and another equivalent of Mo-quinone. This reaction is reminiscent of the very extensive studies of aerobic oxidations of organic materials such as hydroquinones, catalyzed by palladium and other metals, discussed in section 4.6.

In summary, ORR catalysis by complexes of early transition metals is a relatively undeveloped field. Of the early metal catalysts, vanadium complexes have been the most widely explored and perform selective oxygen reduction to water, albeit at slow rates. The single example of a chromium ORR catalyst reports more rapid ORR activity but shows selectivity for H_2O_2 rather than H_2O. Several early metal complexes achieve stoichiometric oxygen reduction using redox-active ligands to store proton and electron equivalents, an innovative strategy despite the lack of catalysis.

4.4. Oxygen Reduction by Iron, Cobalt, Manganese, and Copper Macrocycles

The majority of molecular catalysts for inner-sphere ORR are complexes of iron, cobalt, manganese, or copper with macrocyclic ligands. Much of the interest in these macrocycle catalysts stems from efforts to mimic the biological active sites for O_2 storage, transport, and activation.[7,11,175,176,207] The most widely studied ligands are N_4-macrocycles such as porphyrins, corroles, and phthalocyanines. These can now be synthesized with many different substitution patterns and therefore can be designed to possess diverse steric and electronic properties and to have specific

DOI: 10.1021/acs.chemrev.7b00542
Chem. Rev. XXXX, XXX, XXX−XXX

structures in the secondary coordination sphere.[11,251−254] Such metal−macrocycle complexes have been employed as homogeneous ORR catalysts in both electrocatalytic systems and systems that use chemical reductants. Many of these compounds have also been used as heterogeneous ORR catalysts, adsorbed on electrodes, and are covered in a parallel Review in this issue.[5]

Table 11. Iron Phthalocyanine ORR Catalysts

catalyst	ligand scaffold	solvent	proton source	$E_{1/2}$/reductant	rate constant	%H_2O_2	ref
45	4,4′,4″,4‴-tetracarboxy phthalocyanine	aqueous	0.1 N HCO_3^- (pH 9.0)	0 V vs SCE[a]	not reported	11[b]	262
46	phthalocyanine	aqueous	1 M H_2SO_4	Fe^{2+}	not reported	not reported	263

[a]Onset potential of catalysis observed by RRDE; a CV of an air-saturated solution with [**45**] = 2×10^{-5} M showed a reduction peak at −0.39 V vs SCE. [b]Majority H_2O production via a 2 + 2 mechanism.

Table 12. Iron Porphyrin ORR Catalysts

catalyst	ligand scaffold	solvent	proton source	$E_{1/2}$/reductant	rate constant[a]	%H_2O_2	ref
40	5,10,15,20-tetrakis(4-*N*-methylpyridyl)porphyrin	aqueous	H_2SO_4	−0.11 V vs SCE	1.2×10^8 M^{-1} s^{-1}	major product[b]	255
40	5,10,15,20-tetrakis(4-*N*-methylpyridyl)porphyrin	aqueous	H_2SO_4	∼ −0.1 V vs Ag/AgCl	10^7−10^8 M^{-1} s^{-1}	95	256
40	5,10,15,20-tetrakis(4-*N*-methylpyridyl)porphyrin	aqueous	H_2SO_4	0.15 V vs NHE	not reported	0[c]	257
40	5,10,15,20-tetrakis(4-*N*-methylpyridyl)porphyrin	aqueous	H_2SO_4	−0.06 V vs Ag/AgCl	not reported	0[c]	258
40	5,10,15,20-tetrakis(4-*N*-methylpyridyl)porphyrin	aqueous	pH 3.8 Britton−Robinson buffer	0.18 V vs SHE	3.0×10^1 s^{-1}	n/a[d]	259
40	5,10,15,20-tetrakis(4-*N*-methylpyridyl)porphyrin	aqueous	HOTf (0.1 M)	−0.065 V vs Ag/AgCl	6.04×10^4 M^{-1} s^{-1}	0[c]	260
41	5,10,15,20-tetrakis(2-*N*-methylpyridyl)porphyrin	aqueous	H_2SO_4	0.13 V vs Ag/AgCl	not reported	0[c]	258
42	5,10,15,20-tetrakis(3-*N*-methylpyridyl)porphyrin	aqueous	H_2SO_4	−0.02 V vs Ag/AgCl	not reported	0[c]	258
43	5,10,15,20-tetrakis(2-pyridyl)porphyrin	aqueous	HOTf (pH 0.3)	0.250 V vs NHE	6.0×10^2 s^{-1}	5	72
43	5,10,15,20-tetrakis(2-pyridyl)porphyrin	DMF	[DMF−H^+]OTf^-	−0.362 V vs $Fc^{+/0}$	3.0×10^0 s^{-1}	<15	66
44	5,10,15,20-tetrakis(4-pyridyl)porphyrin	aqueous	HOTf (pH 0.3)	0.150 V vs NHE	not reported	11−15	72
47	5,10,15,20-tetraphenylporphyrin	DMF	$HClO_4$	−0.650 V vs $Fc^{+/0}$	$(1.1 \pm 0.1) \times 10^6$ M^{-2} s^{-1}	10−20	73
47	5,10,15,20-tetraphenylporphyrin	DMF	[DMF−H^+]OTf^-	−0.530 V vs $Fc^{+/0}$	2.7×10^1 s^{-1}	<15	66
48	5,10,15,20-tetrakis(2-carboxyphenyl)porphyrin	MeCN	[DMF−H^+]OTf^-	−0.4 V vs $Fc^{+/0}$	2.0×10^2 s^{-1}	9	71
48	5,10,15,20-tetrakis(2-carboxyphenyl)porphyrin	MeCN	[DMF−H^+]OTf^-	−0.375 V vs $Fc^{+/0}$	2.2×10^6 s^{-1}	<15	66
48	5,10,15,20-tetrakis(2-carboxyphenyl)porphyrin	DMF	[DMF−H^+]OTf^-	−0.630 V vs $Fc^{+/0}$	2.0×10^3 s^{-1}	<15	66
49	5,10,15,20-tetrakis(4-carboxyphenyl)porphyrin	DMF	[DMF−H^+]OTf^-	−0.486 V vs $Fc^{+/0}$	1.5×10^1 s^{-1}	<15	66
51	5,10,15,20-tetrakis(2-carboxy-methylesterphenyl) porphyrin	MeCN	[DMF−H^+]OTf^-	−0.390 V vs $Fc^{+/0}$	2.2×10^6 s^{-1}	<15	66
51	5,10,15,20-tetrakis(2-carboxymethylesterphenyl) porphyrin	DMF	[DMF−H^+]OTf^-	−0.611 V vs $Fc^{+/0}$	2.5×10^3 s^{-1}	<15	66
52	5,10,15,20-tetrakis(4-methoxyphenyl)porphyrin	DMF	[DMF−H^+]OTf^-	−0.547 V vs $Fc^{+/0}$	1.6×10^2 s^{-1}	<15	66
53	5,10,15,20-tetrakis(4-benzenesulfonic acid)porphyrin	DMF	[DMF−H^+]OTf^-	−0.536 V vs $Fc^{+/0}$	1.8×10^2 s^{-1}	<15	66
54	5,10,15,20-tetrakis(4-bromophenyl)porphyrin	DMF	[DMF−H^+]OTf^-	−0.491 V vs $Fc^{+/0}$	5.0×10^0 s^{-1}	<15	66
55	5,15-bis(2,6-diacetamide)-10,20-bis(4-methoxyphenyl) porphyrin	MeCN	[DMF−H^+]OTf^-	−0.326 V vs $Fc^{+/0}$	6.5×10^4 s^{-1}	<15	66
56	5,15-bis(2,6-diacetamide)-10,20-bis(phenyl) porphyrin	MeCN	[DMF−H^+]OTf^-	−0.296 V vs $Fc^{+/0}$	2.2×10^4 s^{-1}	<15	66
57	5,15-bis(2,6-diacetamide)-10,20-bis(4-trifluorophenyl) porphyrin	MeCN	[DMF−H^+]OTf^-	−0.280 V vs $Fc^{+/0}$	2.2×10^2 s^{-1}	<15	66
40	5,10,15,20-tetrakis(4-*N*-methylpyridyl)porphyrin	water/DCE	HCl	Fc, Me_2Fc	not reported	2.6	261
47	5,10,15,20-tetraphenylporphyrin	DMF	$HClO_4$	$Me_{10}Fc$	$(3.4 \pm 0.5) \times 10^6$ M^{-2} s^{-1}	10−20	73
47	5,10,15,20-tetraphenylporphyrin	MeCN	$HClO_4$	Fc	2.9×10^6 M^{-1} s^{-1}	not reported	106, 107
				Me_2Fc	1.2×10^7 M^{-1} s^{-1}		
50	α_4-$FeFc_4$ porphyrin	THF	HOTf	Fc (appended)	not reported	0 or ∼50%[e]	267
58	Fe/Cu[f]	1:1 pH 7 buffer/MeCN	pH 7, phosphate buffer	Cyt *c*	$(3.9 \pm 0.2) \times 10^3$ M^{-1} s^{-1}	5	270
59	Fe/Cu[f]	acetone	TFA	$Me_{10}Fc$	4.1×10^1 s^{-1}	minor product[g]	271
60	Fe[f]	acetone	TFA	$Me_{10}Fc$	2.4×10^1 s^{-1}	minor product[g]	271

[a]Reported rate constants include turnover frequencies under the particular experimental conditions to *k* values for second- or third-order rate laws (M^{-1} s^{-1} or M^{-2} s^{-1}, respectively). [b]H_2O_2 reported as major product but selectivity not quantified. [c]H_2O produced via a 2 + 2 mechanism. [d]Percent H_2O_2 could not be accurately determined because Fe^{II}TMPyP can reduce H_2O_2 both in bulk solution and at the electrode; however, the value is predicted to be less than the 60% H_2O_2 measured for heterogeneous ORR electrocatalysis with FeTMPyP. [e]Zero % H_2O_2 with 2−3 equiv of HOTf; ∼50% H_2O_2 with excess HOTf. [f]See Figure 33 or refs 270 and 271 for ligand scaffold. [g]H_2O reported as major product but selectivity not quantified.

DOI: 10.1021/acs.chemrev.7b00542
Chem. Rev. XXXX, XXX, XXX−XXX

4.4.1. Iron Macrocycles. Iron macrocycles, particularly porphyrin complexes, have long been used as homogeneous (and heterogeneous) ORR catalysts. Initial studies of iron macrocycles as homogeneous catalysts were performed in aqueous solutions, although more recent work has tended toward catalysis in organic solvents (DMF, MeCN) due to increased solubility. The experimental conditions, rate constants, and selectivities of iron phthalocyanine and porphyrin ORR catalysts are summarized in Tables 11 and 12, respectively.

4.4.1.1. Iron Macrocycles in Aqueous Solution. The water-soluble iron(III) 5,10,15,20-tetrakis(*N*-methylpyridyl)porphyrins (**40**–**42**, Figure 24), extensively studied by Kuwana

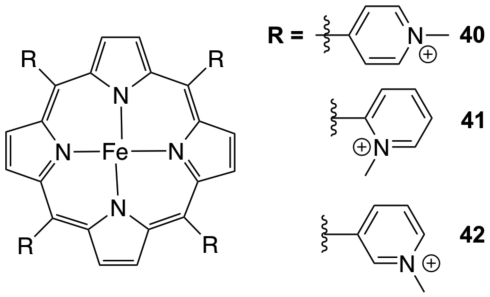

Figure 24. Iron porphyrin ORR catalysts used in refs 255–261.

and co-workers,[255−258] selectively reduce O_2 to H_2O_2 in acidic water.[255−258] The para-derivative, **40**, was shown to catalyze the ORR via an *EC′* mechanism in which electrogenerated Fe^{II} reacts rapidly with O_2 (10^7–10^8 M^{-1} s^{-1}).[256] Further reduction of H_2O_2 to H_2O (e.g., a 2 + 2 mechanism, $O_2 \rightarrow H_2O_2 \rightarrow 2H_2O$) was observed at higher catalyst/dioxygen ratios and was attributed to the rapid reduction of H_2O_2 via **40**.[257] Complexes **42** and **40** have similar voltammetric responses, in both the absence and the presence of O_2, but the ortho-substituted derivative (**41**) behaves differently.[258] The E°_{cat} of **41** is ca. 150 mV more positive, and the reduced catalyst reacts with O_2 at somewhat slower rates. In all cases, ORR catalysis was thought to occur primarily from the dissolved catalyst, with negligible catalyst adsorption to the electrode surface.

Nonetheless, Costentin and co-workers later revisited the homogeneous and heterogeneous behavior of **40** using rotating-ring disc voltammetry (RRDV).[259] The authors found that adsorption of **40** onto the GC working electrode, although minimal, contributes *significantly* to the overall ORR activity (k_1^{het} = 780 s^{-1} and k_1^{hom} = 30 s^{-1} under their conditions). It was speculated that strong interactions of **40** with ligands on the GC surface facilitated O_2 binding, thereby enhancing catalysis. When adsorbed, **40** produced H_2O_2 with 60% selectivity. The selectivity of the homogeneous catalyst could not be calculated for comparison, because the generated H_2O_2 was further reduced to H_2O.

Nyokong, Su, and co-workers have also studied the water-soluble cationic iron tetra-*N*-methylpyridinium porphyrins.[260,261] In aqueous solutions of 0.1 M HOTf, the $4H^+/4e^-$ reduction of O_2 to H_2O was reported for **40**.[260] The study was unable to conclusively distinguish between inner- vs outer-sphere mechanisms of catalysis but did report a catalytic rate constant for an *EC′* process, k_{cat} = 6.04 × 10^4 M^{-1} s^{-1}. Similar $4H^+/4e^-$ ORR activity was observed using **40** in biphasic solutions of acidic H_2O/DCE with Fc and 1,1′-dimethylferrocene (Me_2Fc) as chemical reductants.[261] This approach demonstrated the feasibility of mimicking the water/lipid environment of biological ORR systems and showed that such biphasic systems can facilitate ORR catalysis. Similar biphasic approaches are discussed in section 3.2 for outer-sphere ORR catalysis and section 4.4.2.3 for ORR catalysis with macrocyclic cobalt complexes.

Matson and co-workers examined the ORR selectivity for the related 2-pyridyl (**43**) and 4-pyridyl (**44**) derivatives (Figure 25)

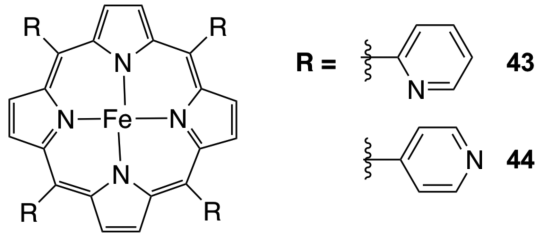

Figure 25. Iron porphyrin ORR catalysts used in ref 72.

in acidic water (pH = 0.3).[72] In contrast to **40**–**42**, **43** and **44** are much more selective for the $4H^+/4e^-$ reaction (<5% and <15% H_2O_2, respectively). The rates of catalysis were faster for **44** than for **43**, likely reflecting the 100 mV higher overpotential for **44** based upon its E°_{cat}. Contrary to the initial design strategy, DFT calculations indicated that the pyridinium cations on **43** were located too far from bound O_2 to act as proton relays. Rather, differences in solvent organization above the active sites of **43** and **44** were suggested to play a role in modulating product selectivity.[72]

Iron phthalocyanines have also been examined as aqueous ORR catalysts (Table 11).[251,262,263] Kobayashi and co-workers reported that iron 4,4′,4″,4‴-tetracarboxyphthalocyanine (**45**) catalyzes the reduction of O_2 to H_2O in aqueous solutions (Figure 26).[262] Further analysis revealed H_2O_2 as the initial

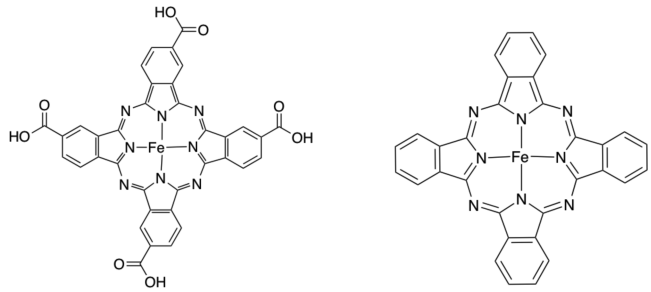

Figure 26. Iron phthalocyanine ORR catalysts used in refs 262 and 263.

product, which is further reduced to H_2O via a 2 + 2 mechanism. In contrast to the high-spin intermediates previously observed with adsorbed iron phthalocyanine ORR catalysts, a low-spin Fe(II) intermediate was identified by UV−visible absorption spectroscopy and magnetic circular dichroism (MCD).

More recently, Han et al.[263] reported that iron phthalocyanine (**46**) could be used as an effective cocatalyst in a chemically regenerative redox fuel cell (CRRFC, Figure 27). In this system, soluble aqueous Fe^{3+} is reduced to Fe^{2+} at a carbon felt electrode. Reoxidation of Fe^{2+} to Fe^{3+} by O_2 was catalyzed by **46**, with reduction of O_2 to H_2O. The authors proposed a mechanism involving (i) O_2 binding to $(Pc)Fe^{II}$, (ii) reduction of the O_2 adduct by Fe^{2+}, and (iii) protonation to yield Fe^{3+} and a $(Pc)Fe^{III}(O_2H)$ species. Further reduction of the hydroperoxide and subsequent intermediates by Fe^{2+} eventually results in H_2O

DOI: 10.1021/acs.chemrev.7b00542
Chem. Rev. XXXX, XXX, XXX−XXX

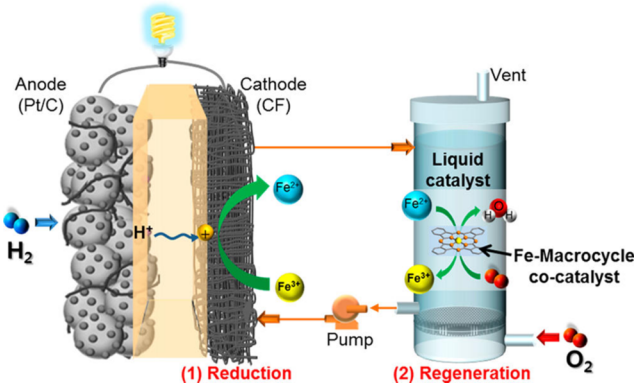

Figure 27. Depiction of a chemically regenerative redox fuel cell utilizing **46** as a cocatalyst for mediator regeneration. Reproduced with permission from ref 263. Copyright 2016 American Chemical Society.

formation and regeneration of $(Pc)Fe^{II}$. By incorporating (Pc)Fe as a redox mediator, the maximum power density of the CRRFC increased from about 170 to 249 mW cm^{-2}. Such enhancement suggests promising future directions for using macrocyclic iron catalysts to improve CRRFC performance.

4.4.1.2. Iron Macrocycles in Organic Solutions. Nonaqueous studies of iron macrocycles as homogeneous ORR catalysts have all involved porphyrin complexes. Organic solvents, such as DMF and MeCN, solubilize a wide variety of porphyrin ligands, which permits a detailed analysis of electronic and secondary coordination-sphere effects on ORR activity.

Fukuzumi and co-workers examined $Fe^{III}(TPP)ClO_4$ (**47**, Figure 28) as an ORR catalyst almost three decades ago.[264,265]

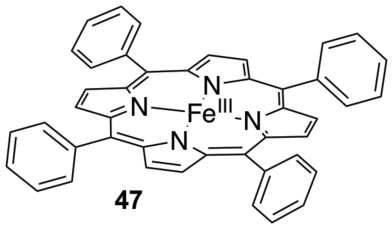

Figure 28. Iron tetraphenyl porphyrin ($Fe^{III}(TPP)$) used as an ORR catalyst in refs 73, 264, and 265.

In MeCN with $HClO_4$ and Fc derivatives as the proton source and reductant, respectively, the rate was zero-order in $[HClO_4]$ and $[O_2]$ and first-order in [reductant], $k = 2.9 \times 10^6$ M^{-1} s^{-1} with Fc and 1.2×10^7 M^{-1} s^{-1} with Me_2Fc. These results implicated electron transfer from Fc or Me_2Fc to $Fe(TPP)^+$ as the rate-limiting step. In the presence of excess O_2, H_2O_2 was the predominant product.

Much more recently, Wasylenko, Rodríguez, and co-workers studied the ORR catalyzed by the closely related Fe(TPP)Cl, in DMF with $HClO_4$ as the acid and $Me_{10}Fc$ as the reductant.[73] Under these conditions, **47** was selective for the $4H^+/4e^-$ reduction (<15% H_2O_2), and the rate was independent of the concentration of $Me_{10}Fc$. The difference between this system and Fukuzumi's is very likely due to the much higher reducing power of $Me_{10}Fc$. The rate of the ORR under these conditions was examined by cyclic voltammetry and stopped-flow kinetics (Figure 29), and both techniques showed an overall third-order rate constant, Rate = $k_{cat}[Fe(TPP)^+][O_2][HClO_4]$. The value from electrochemical measurements, $k_{cat} = (1.1 \pm 0.1) \times 10^6$ M^{-2} s^{-1}, agreed closely with the homogeneous rate constant measured spectroscopically, $k_{cat} = (3.4 \pm 0.5) \times 10^6$ M^{-2} s^{-1}, with $Me_{10}Fc$ as the reductant. These rate constants could be compared because the homogeneous reaction was independent of $Me_{10}Fc$, and the rate constant from electrochemistry refers to the region where the rate is independent of applied potential. The consistencies in the rates and selectivities calculated by the two methods revealed the potential benefits of using these techniques in parallel to better understand the properties of molecular ORR catalysts.

A study by Chlistunoff and Sansiñena demonstrated that the reactivity of **47** toward O_2 can be enhanced in the presence of electron-donating axial ligands, as the reductive current for a solution of **47** in O_2-saturated DCM increased upon addition of imidazole.[198] The result was attributed to the increased electron density on the iron center and the preference of the ligand to coordinate at both axial sites. The authors report no homogeneous ORR catalysis, but studies of Fe(TPP)Cl as a heterogeneous ORR electrocatalyst revealed higher ORR activity and selectivity for H_2O production with the inclusion of imidazole in the catalyst inks used in the preparation of catalyst thin films on the electrode.

Reminiscent of studies on the *ortho*- and *para*-pyridyl catalysts, Carver and co-workers examined the ORR selectivity of both ortho- and para-substituted iron(III) 5,10,15,20-tetrakis-(carboxyphenyl)porphyrin chloride (**48** and **49**, Figure 30).[71] Higher selectivity for H_2O was achieved with **49** and was believed to reflect the participation of the local proton source in the secondary coordination sphere. At high P_{O_2} (ca. 17 atm), the authors were able to access electrochemical responses limited only by catalyst turnover, reporting a TOF for **49** of 200 s^{-1}.

Dey and co-workers used secondary coordination-sphere effects to facilitate ORR catalysis by incorporating redox-active

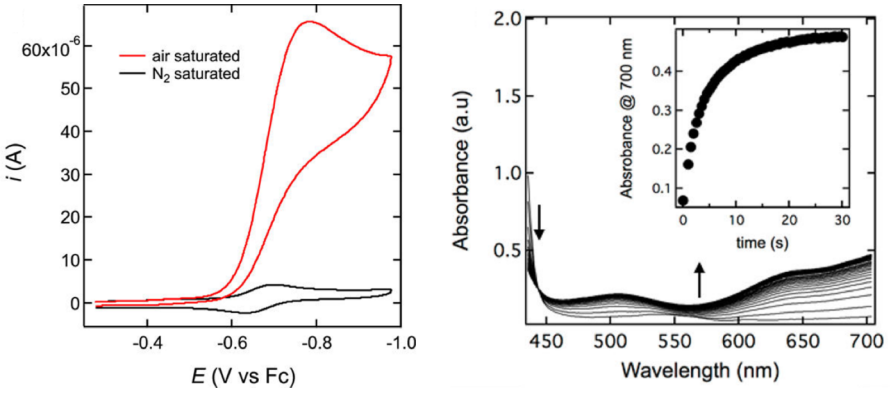

Figure 29. (Left) Cyclic voltammograms of **47** in the presence of $[DMF-H]ClO_4$ and 1 atm N_2 (black) or air (red). (Right) Spectrochemical kinetics of ORR using **47** in the presence of $Me_{10}Fc$ as a soluble reductant. Reproduced with permission from ref 73. Copyright 2014 American Chemical Society.

DOI: 10.1021/acs.chemrev.7b00542
Chem. Rev. XXXX, XXX, XXX−XXX

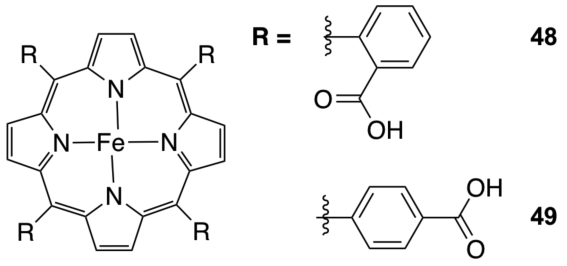

Figure 30. Iron porphyrin ORR catalysts used in ref 71.

ferrocene moieties on an iron porphyrin species.[266,267] A closely related cobalt porphyrin with appended $Ru(NH_3)_5$ moieties as intramolecular electron donors was previously reported by Anson and co-workers (see section 4.4.2.1).[268] In the absence of external acid, the α_4-$FeFc_4$ complex (**50**, Figure 31) was reported

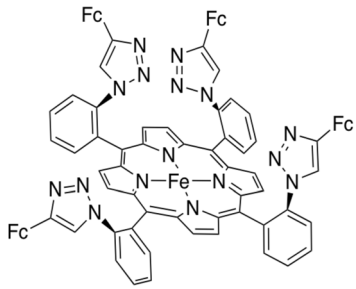

50

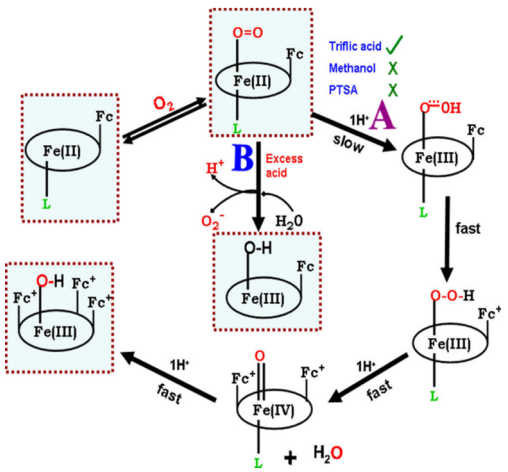

Figure 31. (Top) Iron porphyrin catalyst used in refs 266 and 267, and (Bottom) mechanism of ORR catalyzed by **50** in organic solvents Reproduced with permission from ref 267. Copyright 2013 American Chemical Society.

to facilitate the $1e^-$ reduction of $O_2/O_2^{\bullet-}$ in THF.[266] Upon addition of 2−3 equiv of HOTf, H_2O was the sole ORR product; however, significant H_2O_2 production (~50%) was observed using a larger excess of acid, suggesting hydrolysis of the Fe−$O_2^{\bullet-}$ intermediate (Figure 31, bottom).[267] Other acids such as MeOH and *p*TsOH were unable to protonate Fe−$O_2^{\bullet-}$ and also showed 50% H_2O_2 production, which was attributed to the disproportionation of $O_2^{\bullet-}$. Compound **50** also catalyzes the reduction of O_2 to H_2O when used as a heterogeneous catalyst, adsorbed on an electrode, in acidic aqueous solutions.[266,267] The mechanisms for H_2O production are thought to differ between the homogeneous and heterogeneous cases, with O−O bond cleavage proceeding by stepwise PT−ET in the former and PCET in the latter.[267] A recently published account details rate- and selectivity-determining factors for this and similar iron porphyrin complexes, both as homogeneous and heterogeneous ORR catalysts.[269]

Recently, Pegis and co-workers analyzed ORR catalysis by 11 soluble iron porphyrin complexes in DMF and MeCN.[66] For all of the catalysts, the proposed mechanism involves reduction of Fe(III) to Fe(II) followed by pre-equilibrium O_2 binding and rate-limiting protonation of the $Fe^{III}(O_2^{\bullet-})$ species. A large range in TOF (10^0−10^6 s^{-1}) was observed and found to scale linearly with the effective overpotential (η_{eff}, Figure 32) of the catalysts. Computationally, these scaling relationships reflect linear correlations between the catalyst redox potential ($E_{Fe(III/II)}$), O_2-binding affinity, and basicity of electrogenerated $Fe^{III}(O_2^{\bullet-})$. In other words, as $E_{Fe(III/II)}$ decreases, O_2-binding and $Fe^{III}(O_2^{\bullet-})$ basicity both increase, resulting in higher TOFs. Of particular importance, the authors found that **48** and **51** lie along the same scaling relationship and conclude that, at least under these conditions, the carboxylic acid groups of **48** do not act as proton relays. This fundamental analysis of molecular iron porphyrin ORR catalysts shows how catalysts studied under different experimental conditions can be directly compared.

Biomimetic models of the iron-porphyrin/copper active site of C*c*O have also been studied as homogeneous ORR catalysts.[7,207] A full discussion of these systems is beyond the scope of this Review; here, we highlight two archetypal examples of such chemistry.

Collman and co-workers reported that the C*c*O model complex **58** (Figure 33) produced H_2O with ca. 95% selectivity in a 1:1 pH 7 buffer/MeCN solution. Cytochrome *c*, the physiological electron source, was used as the reductant.[270] Mechanistic studies identified O_2 binding as the rate-determining step.

Karlin and co-workers have explored the role of Cu in the enzymatic ORR catalysis, comparing the activity of C*c*O model complex **59** with its Cu-free analogue **60** (Figure 33). Air-saturated acetone solutions containing TFA and $Me_{10}Fc$ were used.[271] (As an aside, we advise caution if acetone is used for ORR studies due to the possibility of forming explosive triacetone triperoxide.[272]) At low temperatures (−60 °C < *T* < −5 °C), kinetic studies with both **59** and **60** showed zero-order dependences on [$Me_{10}Fc$], [O_2], and [TFA], which suggested O−O bond cleavage as the rate-determining step. At higher temperatures, both catalysts had a first-order dependence on [O_2], and the Fe(II) form of the catalysts was observed as a steady-state intermediate. These observations implicated O_2 binding as the rate-limiting step. The rate constants for the two catalysts were found to be identical at low temperatures but differed by a factor of 2 at 25 °C (41 and 24 s^{-1} for **59** and **60**, respectively). The authors attributed this difference to Cu-facilitated O_2 binding in **59**.

4.4.2. Cobalt Macrocycles. Like iron macrocycles, many early studies of macrocyclic cobalt ORR catalysts were of water-soluble cobalt porphyrins, and the results of these studies are summarized in Table 13. In contrast to their iron analogues, which mainly produce H_2O, monomeric cobalt macrocycles typically produce H_2O_2 (see Tables 13 and 15).[273] This contrast in selectivity instigated the synthesis and preparation of complexes that contain two cobalt redox centers in close proximity, most commonly cofacial macrocycles. In many instances, the use of cofacial dicobalt macrocycles does indeed promote $4H^+/4e^-$ selectivity in both homogeneous solutions and liquid−liquid

DOI: 10.1021/acs.chemrev.7b00542
Chem. Rev. XXXX, XXX, XXX−XXX

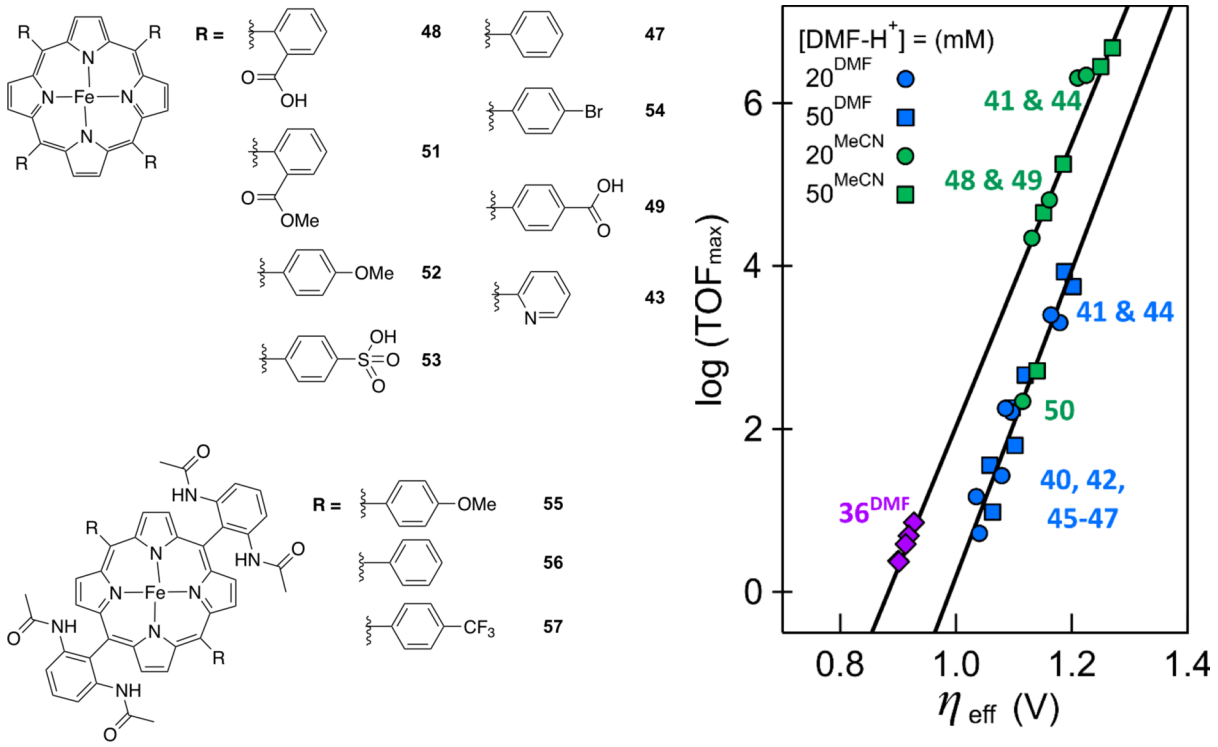

Figure 32. (Left) Iron porphyrin complexes used as ORR catalysts in ref 66 and (right) correlation of log(TOF_{max}) and effective overpotential (defined at catalyst $E_{1/2}$) for these catalysts. The points on the plot are labeled with the catalyst numbers to which they correspond. The color and shape of the points indicate the acid concentration and solvent, as noted in the figure legend. The purple diamonds correspond, from left to right, to 50, 20, 10, and 5 mM [DMF−H^+]OTf in DMF. Adapted with permission from ref 66. Copyright 2016 American Chemical Society.

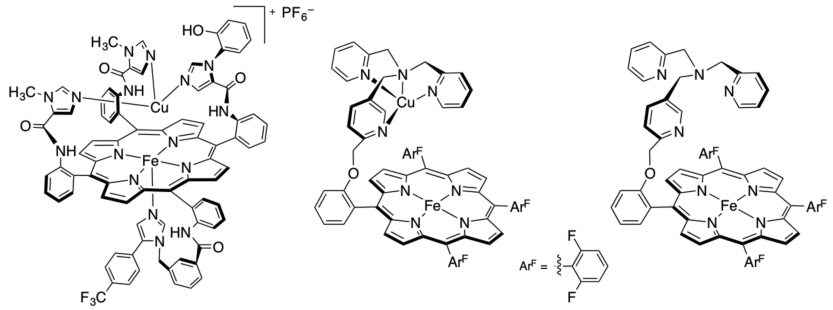

58 **59** **60**

Figure 33. C*c*O model complexes used as ORR catalysts in refs 270 and 271.

interfaces, and these results are summarized in Tables 14 and 15, respectively.

4.4.2.1. Monomeric Cobalt Macrocycles. Chan and co-workers first investigated cobalt(III) 5,10,15,20-tetrakis(4-*N*-methylpyridyl)porphyrin (**61**, Figure 34) in aqueous solutions of 0.1 N H_2SO_4.[274] Despite its solubility in water, **61** readily adsorbed to GC electrodes. Like the iron complexes of this ligand described earlier, such adsorption prompted the comparison of its homogeneous and heterogeneous behavior. In solution, **61** catalyzed the $2H^+/2e^-$ reduction of O_2 to H_2O_2 with ∼90% selectivity. A similar result was later observed in aqueous solutions of 0.1 M HOTf.[260] As with the iron porphyrins, catalysis was proposed to occur via an *EC′* mechanism, where O_2 binding and protonation follows initial electron transfer to Co(III).[260] Interestingly, the same complex in DMF was reported to bind O_2 at Co(I) rather than Co(II),[275] as described later with the cobalt nonaqueous studies. Furthermore, the adsorbed and solution behavior of **61** showed different pH dependences for ORR catalysis.[274] Such behavior was attributed to a pK_a shift for the adsorbed species resulting from interactions of the Co metal center with carbon/oxygen functionalities on the electrode surface.

The water-soluble cobalt porphyrin complexes **62** and **63** were also reported to be aqueous ORR catalysts, with H_2O_2 as the major product (Figure 35).[276,277] For both complexes, the non-planarity of the macrocycles was suggested to prevent adsorption onto GC. Under N_2, the Co(II/I) reduction potential ($E_{Co(II/I)}$) was ca. 0.32 V more positive for **62** vs **63**, consistent with the electronic effects of ligand substituents. This difference in $E_{Co(II/I)}$ was suggested to impact the ORR mechanism. For **62**, the onset of catalysis occurred near $E_{Co(II/I)}$, while catalysis via **63** was observed more positive of $E_{Co(II/I)}$, which suggested O_2 binding to Co(II) prior to reduction.

DOI: 10.1021/acs.chemrev.7b00542
Chem. Rev. XXXX, XXX, XXX−XXX

Table 13. Monomeric Cobalt Macrocycles Used As ORR Catalysts

catalyst	ligand scaffold	solvent	proton source	$E_{1/2}$/reductant	rate constant[a]	product	ref
61	5,10,15,20-tetrakis(4-*N*-methylpyridyl)porphyrin	aqueous	H_2SO_4	0.41 V vs NHE	not reported	H_2O_2[b]	274
61	5,10,15,20-tetrakis(4-*N*-methylpyridyl)porphyrin	DMF	none	−0.49 V vs SCE	not reported	n/a[c]	275
61	5,10,15,20-tetrakis(4-*N*-methylpyridyl)porphyrin	aqueous	HOTf (0.1 M)	0.150 V vs Ag/AgCl	1.44×10^4 M^{-1} s^{-1}	H_2O_2 (90%)	260
62	tetrakis(4-*N*-methylpyridyl)- *β*-octabromo-porphyrin	aqueous	pH 7, phosphate buffer	−0.31 V vs SCE	not reported	H_2O_2[d]	276
62	tetrakis(4-*N*-methylpyridyl)- *β*-octabromo-porphyrin	aqueous	0.5 M H_2SO_4	−0.30 V vs SCE	not reported	not reported	276
63	tetrakis(4-sulfonatophenyl)-*β*-octabromo-porphyrin	aqueous	pH 8.9, NaB_4O_7 buffer	−0.590 V vs Ag/AgCl	not reported	H_2O_2[d]	277
66	1,4,8,1 l-tetraazacyclotetradecane	aqueous	0.5 M $HClO_4$	−0.2 V vs SSCE	not reported	H_2O_2[d]	190
67	*meso*-5,7,7,12,14,14- hexamethyl-1,4,8,11-tetraazacy-clotetradecane	aqueous	0.1 M TFA	−0.15 V vs Ag/AgCl	not reported	H_2O_2[d]	191
70	4,4′,4″,4‴-tetracarboxyphthalocyanine	aqueous	pH 9.0, 0.1 N HCO_3^-	−0.2 V vs SCE[e]	not reported	H_2O_2 (96%)	262
64	5,10,15,20-tetrakis(4-pyridyl-Ru$(NH_3)_5$)porphyrin	aqueous	not reported	$Ru(NH_3)_6^{2+}$	not reported	H_2O_2[d]	268
65	5,10,15,20-tetraphenylporphyrin	MeCN	$HClO_4$	Fc	4.2×10^4 M^{-1} s^{-1}	H_2O_2[f]	264, 265
				Me_2Fc	1.0×10^5 M^{-1} s^{-1}		
				$Me_{10}Fc$	1.1×10^6 M^{-1} s^{-1}		
65	5,10,15,20-tetraphenylporphyrin	DCE	$[(Et_2O)_2H^+]BAr^F_4$	Fc	not reported	H_2O_2[d]	278
68	2,3,9,10-tetra methyl-1,4,8,11-tetraazacyclotetradeca-l,3,8,10-tetraene	MeCN	$HClO_4$	$Me_{10}Fc$	2.4×10^4 M^{-1} s^{-1}	not reported	264
				Me_2Fc	1×10^1 M^{-1} s^{-1}		
				$FeCp(C_5H_4$-*n*-Bu)	6.5×10^0 M^{-1} s^{-1}		
				$FeCp(C_5H_4$-*n*-Amyl)	6.0×10^0 M^{-1} s^{-1}		
				Fc	2.1×10^0 M^{-1} s^{-1}		
71	*α*-octaphenylphthalocyanine	PhCN	0.50 M HCO_2H	Me_2Fc	$(1.4 \pm 0.1) \times 10^2$ M^{-1} s^{-1}	H_2O_2 (97%)	76
				$Me_{10}Fc$	$(1.6 \pm 0.1) \times 10^5$ M^{-1} s^{-1}	H_2O_2 (74%)	
72	5,10,15-trismesitylcorrole	PhCN	0.02 M $HClO_4$	Me_2Fc	not reported	H_2O_2[d]	286
73	10-pentafluorophenyl-5,15-dimesitylcorrole	PhCN	0.02 M $HClO_4$	Me_2Fc	not reported	H_2O_2[d]	286
74	5,10,15-tris(pentafluorophenyl)corrole	PhCN	0.02 M $HClO_4$	Me_2Fc	not reported	H_2O_2[d]	286
75a	Chlorin (Ch1)[g]	PhCN	$HClO_4$	Me_2Fc	$k_{cat(1)} = (1.2 \pm 0.2) \times 10^3$ M^{-1} s^{-1}[h]	H_2O_2[d]	287
				Br_2Fc	$k_{cat(2)} = (1.9 \pm 0.3) \times 10^5$ M^{-2} s^{-1}[h]		
75a	Chlorin (Ch1)[g]	PhCN	$HClO_4$	Me_2Fc	not reported	H_2O_2[d]	288
75b	Chlorin (Ch2)[g]	PhCN	$HClO_4$	Me_2Fc	9.6×10^6 M^{-2} s^{-1}	H_2O_2[d]	288
75c	Chlorin (Ch3)[g]	PhCN	$HClO_4$	Me_2Fc	2.2×10^7 M^{-2} s^{-1}	H_2O_2[d]	288
77	2,3,7,8,12,13,17,18-octaethylporphyrin	PhCN	$HClO_4$	Fc	9.8×10^4 M^{-1} s^{-1}	H_2O_2 (94%)[i]	75
				Me_2Fc	2.1×10^5 M^{-1} s^{-1}		
82	5,10,15,20-tetrakis(4-*N*-methylpyridyl)porphyrin (**TPyP**)	PhCN	TFA	Fc	6×10^0 h^{-1}	H_2O_2 (70%)	289

[a]Reported rate constants include turnover frequencies under the particular experimental conditions to *k* values for second- or third-order rate laws (M^{-1} s^{-1} or M^{-2} s^{-1}, respectively). [b]Number of electrons = 1.97 ± 0.15 [c]Reaction product is $O_2{\cdot}^-$. [d]H_2O_2 reported as major product but selectivity not quantified. [e]More negative potentials (<−0.5 V vs SCE) promoted the reduction of H_2O_2 to H_2O. [f]Initial reduction of O_2 to H_2O_2 by $Co(TPP)^+$ was followed by slower reduction of H_2O_2 to H_2O by the Fc derivative. [g]See Figure 42 or refs 287 and 288 for ligand. [h]On the basis of the rate law, $R = (k_{cat(1)} + k_{cat(2)}[HClO_4])[\{CoII(ChH)\}^+][O_2]$. [i]Produced was 1.6×10^{-3} M H_2O_2 (calculated via iodometric titration) from a solution of 1.7×10^{-3} M O_2.

A cobalt porphyrin containing appended ruthenium moieties (**64**, Figure 36) was reported to reduce O_2 to H_2O_2 in acidic aqueous solution with free $Ru(NH_3)_6^{2+}$ as a chemical reductant.[268] No ORR catalysis was observed in the absence of added $Ru(NH_3)_6^{2+}$, in contrast to the initial hypothesis that the bound Ru-moieties could serve as local electron reservoirs for rapid intramolecular reduction after O_2 binding. The authors attribute the exclusive production of H_2O_2 under these conditions to a faster rate for H_2O_2 dissociation than for delivery of the additional electrons required for H_2O formation.

Most studies of cobalt macrocycle-catalyzed ORR have been performed under nonaqueous conditions, and Table 13 provides a summary of these results. Among the first of these studies was Sazou and co-workers' analysis of **61** in DMF.[275] The electrogenerated Co^I ($E_{Co(II/I)} = -0.49$ V vs SCE) reacted with dissolved O_2 and showed a catalytic current for the formation of $O_2^{\bullet-}$ with TON = 15. Production of $O_2^{\bullet-}$ was indirectly measured using benzoic anhydride as a scavenger, as depicted in Figure 37. This was, to our knowledge, the first reported instance of O_2 binding to a Co(I) porphyrin.

Cobalt 5,10,15,20-*meso*-tetraphenylporphyrin ($Co(TPP)^+$, **65**, Figure 38) has been studied under a variety of nonaqueous conditions using chemical reductants.[264,265] In MeCN, **65** catalyzed the $2H^+/2e^-$ reduction of O_2 to H_2O_2 with $HClO_4$ and a variety of Fc derivatives. Further reduction of H_2O_2 to H_2O just by the Fc derivative was observed on a longer time scale. The measured rate constant for ET from the external reductant to **65** agreed with the k_{ET} predicted by Marcus theory, suggesting rate-limiting outer-sphere ET. After reduction, the subsequent ET from Co^{II} to O_2 was indicated to occur via an inner-sphere pathway, before PT and further reduction. The proposed mechanism for this process is depicted in Figure 38.

$Co^{II}(TPP)$ is an active ORR catalyst in DCE with Fc and the strong acid $[(Et_2O)_2H^+]BAr^F_4{}^-$ ($HBAr^F_4$; $BAr^F_4{}^-$ = tetrakis-

DOI: 10.1021/acs.chemrev.7b00542
Chem. Rev. XXXX, XXX, XXX−XXX

Table 14. Cofacial Dicobalt Macrocycles Used As ORR Catalysts

catalyst	ligand scaffold	solvent	proton source	$E_{1/2}$/reductant	rate constant[a]	product	ref
76a	1,8-bis[5-(2,8,13,17-tetraethyl-3,7,12,18-tetramethylporphyrinyl)] anthracene	PhCN	$HClO_4$	Me_2Fc	not reported	H_2O_2 (~50%)[b]	75
76b	1,8-bis(2,8,13,17-tetraethyl-3,7,12,18-tetramethylporphyrinyl)]biphenylene	PhCN	$HClO_4$	Me_2Fc	not reported	H_2O_2 (~50%)[b]	75
76c	4,5-bis[(2,3,13,17-tetraethyl-3,7,12,18-tetramethyl-5-porphyrinyl)-9,9-dimethylxanthene	PhCN	$HClO_4$	Fc	3.6×10^5 M^{-1} s^{-1}	H_2O[c]	75
				Me_2Fc	8.0×10^5 M^{-1} s^{-1}	H_2O[c]	
76d	4,6-bis[5-(2,3,13,17-tetraethyl-3,7,12,18-tetramethylporphyrinyl)] dibenzofuran	PhCN	$HClO_4$	Me_2Fc	not reported	H_2O_2 (100%)[b]	75
78a	PCX[d]	PhCN	$HClO_4$	Me_2Fc	not reported	H_2O[c]	294
78b	PCOx[d]	PhCN	$HClO_4$	Me_2Fc	not reported	H_2O_2[e]	294
78c	PCO[d]	PhCN	$HClO_4$	Me_2Fc	not reported	H_2O_2[e]	294
79a	$PMes_2CX$[d]	PhCN	$HClO_4$	Me_2Fc	not reported	H_2O[c]	294
79b	$PMes_2Cox$[d]	PhCN	$HClO_4$	Me_2Fc	not reported	H_2O_2[e]	294
79c	$PMes_2CO$[d]	PhCN	$HClO_4$	Me_2Fc	not reported	H_2O_2[e]	294
81	$[Ru_8(\eta^6\text{-}iPrC_6H_4Me)_8(dhbq)_4(Co\mathbf{TPyP})_2][OTf]_8$	PhCN	TFA	Fc	6.6×10^1 h^{-1}	H_2O_2 (90)	289
83	methylcalixpyrrole[f]	PhCN	TFA	Fc	$3.8(2) \times 10^{-3}$ s^{-1}	H_2O (85–95%)	298
84	fluorenylcalixpyrrole[f]	PhCN	TFA	Me_2Fc	6.1×10^2 M^{-1} s^{-1}	H_2O (88%)	299
85	anthracene calixpyrrole[f]	PhCN	TFA	Fc	not reported	H_2O (70%)	300

[a]Reported rate constants include turnover frequencies under the particular experimental conditions and k values for second- or third-order rate laws (M^{-1} s^{-1} or M^{-2} s^{-1}, respectively). [b]Percentages estimated from Figure 2 of ref 75. [c]H_2O reported as major product but selectivity not quantified. [d]See Figure 44 or ref 294 for ligand. [e]H_2O_2 reported as major product but selectivity not quantified. [f]See Figure 47 or refs 298–300 for ligand.

Table 15. Cobalt Macrocycles Used As ORR Catalysts in Biphasic Media

catalyst	ligand scaffold	solvent mixture	proton source	$E_{1/2}$/reductant	$\%H_2O_2$	ref
65	5,10,15,20-tetraphenylporphyrin	water/PhCN	$HClO_4$	0.2 V vs SCE	35	301
65	5,10,15,20-tetraphenylporphyrin	water/DCE	HCl, H_2SO_4	$Me_{10}Fc$	not reported	157
65	5,10,15,20-tetraphenylporphyrin	water/DCE	HCl	Fc, Me_2Fc, $Me_{10}Fc$	major product[a]	303
65	5,10,15,20-tetraphenylporphyrin	water/DCB	HCl	Fc	11[b] mg/L	304
				Me_2Fc	not reported	
				$Me_{10}Fc$	not reported	
				TTF	not reported	
77	2,3,7,8,12,13,17,18-octaethylporphyrin	water/DCE	HCl	Fc, Co^{II}(OEP)	major product[a]	305
86a	4,5-bis[5-(2,8,13,17-tetraethyl-3,7,12,18-tetramethylporphyrinyl)]-9,9-dimethylxanthene	water/DCB	HCl	Me_2Fc	7	306
86b	2,2′-bis[5-(2,8,13,17- tetraethyl-3,7,12,18-tetramethylporphyrinyl)] diphenylether	water/DCB	HCl	Me_2Fc	12	306
				TTF	41	
86c	4,6-bis[5-(2,8,13,17-tetraethyl-3,7,12,18-tetramethylporphyrinyl)] dibenzofuran	water/DCB	HCl	Me_2Fc	15	306
69	phthalocyanine	water/DCE	H_2SO_4	Fc, Me_2Fc, $Me_{10}Fc$	major product[a]	307
87	hexadecafluorophthalocyanine	water/DCE	HCl	TTF	65	308

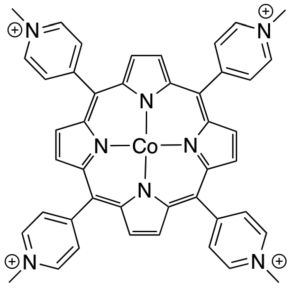

61

Figure 34. Cobalt porphyrin ORR catalyst used in refs 260, 274, and 275.

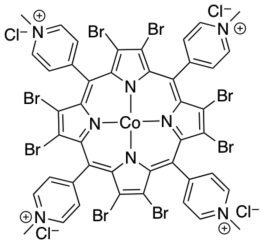

62

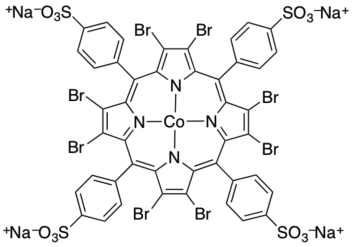

63

Figure 35. Cobalt porphyrins used as ORR catalysts in refs 276 and 277.

(pentafluorophenyl)borate).[278] In contrast to the studies described earlier using $HClO_4$ and Fc in MeCN,[264,265] the rates of ORR measured here were independent of [Fc]. Rather, the first-order dependences on both [$HBAr^F_4$] and [Co^{II}(TPP)] led the authors to conclude that "proton-assisted coordination of O_2 to Co^{II}TPP" was rate-limiting under these conditions. Interestingly, the ORR activity decreased significantly upon addition of H_2O, and computations supported the inhibitory effect of competitive H_2O binding. Evidence for this inhibitory effect was also observed for ORR catalyzed by H_2TPP,[160] where H_2O engages in hydrogen bonding with the doubly protonated (H_4TPP^{2+}) species, as described in section 3.2.2.2. Additionally, studies of hemoprotein models have reported slower rates of O_2

DOI: 10.1021/acs.chemrev.7b00542
Chem. Rev. XXXX, XXX, XXX–XXX

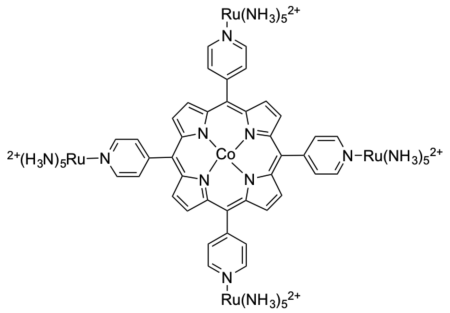

64

Figure 36. Cobalt porphyrin with ruthenium penta-amine $(Ru(NH_3)_5)^{2+}$ moieties used as an ORR catalyst in ref 268.

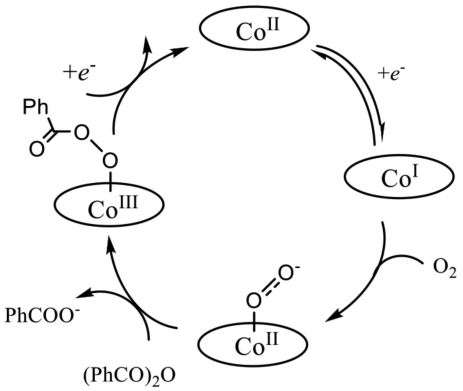

Figure 37. Proposed mechanism of superoxide insertion into benzoic anhydride using **61**. Adapted with permission from ref 275. Copyright 1990 American Chemical Society.

binding in the presence of H_2O.[279] Taken together, these results suggest that interference from H_2O may be a common feature of metalloporphyrin and porphyrin ORR catalysts.

A number of nonporphyrin cobalt macrocycles have also been reported to be ORR catalysts, and they all yield primarily H_2O_2. Some of the earliest examples were the Co(II) cyclam complexes **66**–**68** (Figure 39). Endicott and co-workers first reported **66** to react with O_2 in a two-step equilibrium process involving the formation of a 1:1 Co/O_2 adduct followed by reaction with another equivalent of **66** to yield a μ-peroxo species (reactions i and ii, Scheme 7).[280]

A subsequent study of the decomposition of the μ-peroxo species $[\{(H_2O)Co([n]aneN_4)\}_2(\mu\text{-}O_2)]^{4+}$, by both oxidizing and reducing agents in acidic solutions, suggested that the reactivity involved cleavage of the μ-peroxo by the reverse of reactions i–ii in Scheme 7.[281] Additionally, the reactivity of the related monomeric superoxide complex $[(H_2O)Co([n]aneN_4)(O_2)]^{2+}$ was examined with a variety of inner- and outer-sphere ET reagents.[282] Increased rates for both inner- and outer-sphere ET were observed with $[(H_2O)Co([n]aneN_4)(O_2)]^{2+}$ as compared to those with aqueous O_2. This was largely attributed to driving force effects because the measured equilibrium constants for the reactions were significantly more favorable in the case where O_2 was bound to Co.

Following these reports, Anson and co-workers examined **66** and the related Co(cyclam) **67** as homogeneous ORR catalysts.[190,191] Reduction in the presence of O_2 formed the μ-peroxo bridged dimer, $[LCo^{III}–O–O–Co^{III}L]^{4+}$. At more reducing potentials, the dimer was further reduced by $2H^+/2e^-$ to produce H_2O_2 and reform two Co^{2+} complexes that could bind another molecule of O_2. Formation of H_2O_2 as the sole ORR product contrasts with the $4H^+/4e^-$ ORR observed for similar macrocycles adsorbed to GC.[283] The more-crowded derivative, **67**, had a significantly smaller equilibrium constant for μ-peroxo dimerization[284] and also catalyzed the $2H^+/2e^-$ reduction of O_2 to H_2O_2.[191] Appearance of two successive waves by RRDV indicated that reduction of **67** to the relatively stable hydroperoxyl adduct ($\mathbf{67}^{O_2H}$) occurred at less reducing potentials than required for catalysis.

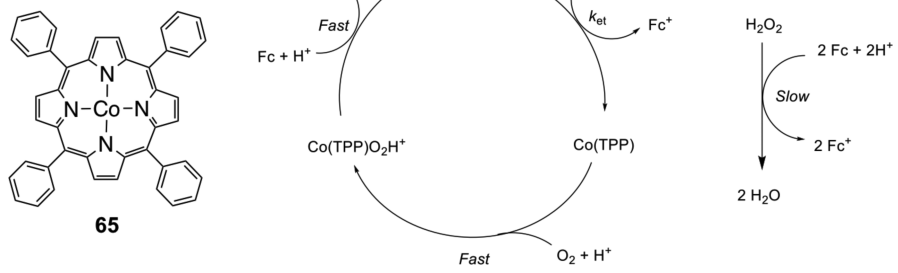

65

Figure 38. (Left) Co(TPP) and (Right) proposed mechanism of Co(TPP) as an ORR catalyst, based on refs 264 and 265.

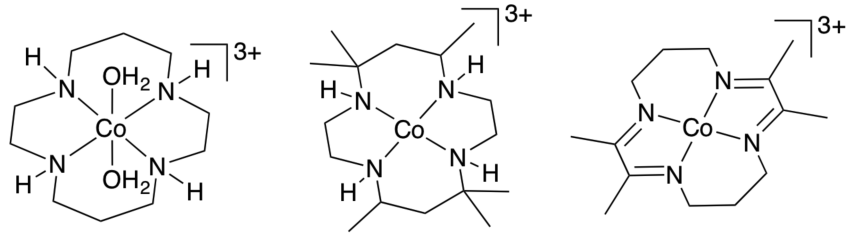

66 67 68

Figure 39. Cobalt cyclam complexes used in refs 190, 191, 264, and 280–282.

DOI: 10.1021/acs.chemrev.7b00542
Chem. Rev. XXXX, XXX, XXX–XXX

Scheme 7. Formation of a μ-Peroxo Species $[\{(H_2O)Co([n]aneN_4)\}_2O_2]^{4+}$ from O_2 Binding to $[Co([n]aneN_4)(OH_2)_2]^{2+}$ (Reaction i) Followed by Heterolytic Dimerization (Reaction ii)

$$[Co([n]aneN_4)(OH_2)_2]^{2+} + O_2 \rightleftharpoons [Co([n]aneN_4)(OH_2)(O_2)]^{2+} + H_2O \quad \text{(i)}$$

$$[Co([n]aneN_4)(OH_2)(O_2)]^{2+} + [Co([n]aneN_4)(OH_2)_2]^{2+} \rightleftharpoons [\{(H_2O)Co([n]aneN_4)\}_2O_2]^{4+} \quad \text{(ii)}$$

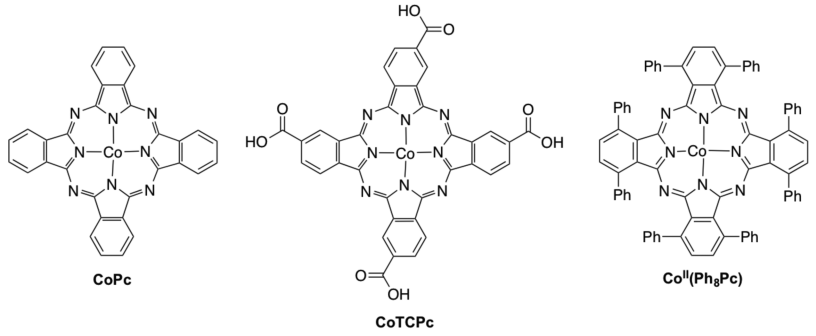

69 **70** **71**

Figure 40. Cobalt phthalocyanine complexes used as ORR catalysts in refs 76, 251, 262, and 285.

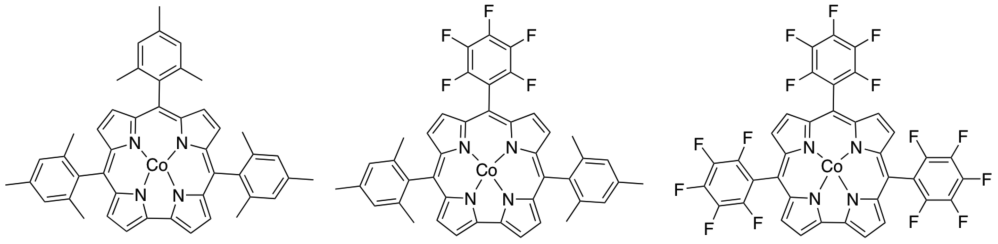

72 **73** **74**

Figure 41. Cobalt corrole complexes used as ORR catalysts in ref 286.

The related complex $Co(TIM)^{3+}$ (**68**, Figure 39) was studied in MeCN with $HClO_4$ and a variety of Fc derivatives.[264] Catalysis was found to be first order in $[HClO_4]$, $[O_2]$, and [reductant], as well as in $[Co(TIM)^{3+}]$. Under catalytic conditions, the ratio of $[O_2]$ to [reductant] consumed was 1:4, indicating formation of H_2O as the ORR product.

The reactivity of several cobalt phthalocyanine complexes (**69**–**71**, Figure 40) with O_2 has been reported.[76,251,262,285] Both **69** and **70** catalyzed the ORR via an *EC′* mechanism. Surprisingly, O_2 binding to **69** and **70** occurred only upon formation of Co^I.[251,262,285] For most of the Co complexes discussed in this Review, dioxygen binds to Co(II) and does not require reduction to Co(I) (contributions by Sazou and co-workers in 1990 and 1996 are exceptions to this generalization). **70** reduced O_2 to H_2O_2 with an onset potential of −0.2 V vs SCE, and further reduction of H_2O_2 to H_2O was observed at more reducing potentials.[251,262]

ORR catalysis by **71** was examined using a variety of chemical reductants in PhCN with formic acid, and the catalytic mechanism was found to depend on the reductant strength.[76] Using Me_2Fc, the rate-limiting step was found to be a PCET reaction between **71**, H^+, and O_2 to form the $HO_2^{\bullet}$-bound complex $[Co^{III}(Ph_8Pc)^+](HO_2^{\bullet})$. With the more-reducing $Me_{10}Fc$, the turnover-limiting step did not involve O_2 but rather was a multiple-site PCET with reduction of the cobalt center and protonation of an outward-pointing *meso*-nitrogen, forming $Co^I(Ph_8PcH)$ or $[Co^I(Ph_8PcH_2)]^+$. Whether $Co^I(Ph_8PcH)$ or $[Co^I(Ph_8PcH_2)]^+$ was formed depended on the strength of the acid used for catalysis, but both of these species reacted rapidly with O_2. H_2O_2 was produced with high selectivity (>74%) with both Me_2Fc and $Me_{10}Fc$, although more rapidly with $Me_{10}Fc$.

Cobalt corroles (**72**–**74**, Figure 41)[286] were also shown to catalyze the $2H^+/2e^-$ ORR in PhCN solutions containing $HClO_4$ and Me_2Fc. Selectivity for H_2O_2 was indicated by the generation of exactly 2 equiv of $[Me_2Fc]^+$ per $[O_2]$ in these reactions. Under similar conditions, cobalt chlorins **75a**–**c** (Figure 42) were reported to be extremely active catalysts for H_2O_2 production (TONs > 6×10^4, 7.9×10^4, and 8.3×10^4, respectively).[287,288]

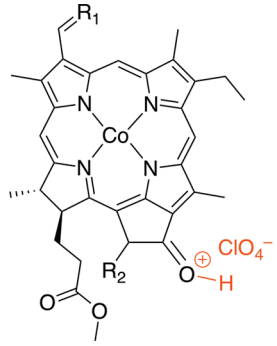

75a $R_1 = CH_2$, $R_2 = H$

75b $R_1 = O$, $R_2 = COOCH_3$

75c $R_1 = CH_2$, $R_2 = COOCH_3$

[75a-c(H)]$^+$

Figure 42. Cobalt chlorin complexes used as ORR catalysts in refs 287 and 288. Site of protonation denoted in red.

DOI: 10.1021/acs.chemrev.7b00542
Chem. Rev. XXXX, XXX, XXX−XXX

Electrochemical ORR by **75a** had an onset potential of 0.6 V vs SCE. In contrast, the related cobalt(II) octaethylporphyrin decomposed through demetalation and protonation of the free porphyrin ligand. This was taken as evidence that the lower nucleophilicity, larger N-atom core, and increased flexibility of the chlorin ligand as compared to the porphyrin ligand provided greater stability under the acidic conditions required for ORR with these cobalt catalysts.[287]

The resting state of **75a** under catalytic conditions was the protonated form, $[\mathbf{75a}(H)]^+$ (Figure 42). The turnover-limiting step was thought to be addition of O_2 and H^+ to yield the protonated superoxo adduct $[\{\mathbf{75a}(H)^{2+}\}(HO_2^{\bullet})]$.[287] However, ET to $[\mathbf{75a}(H)]^{2+}$ became rate-limiting when 1,1′-dibromoferrocene was used. Catalysts **75b,c** were reported to react via the deprotonated rather than protonated catalyst, due to the decreased basicity of the chlorin ligand.[288] This preference for the deprotonated species was used to explain the faster rates of ORR catalysis for **75b,c** as compared to **75a**.

4.4.2.2. Cofacial Dicobalt Macrocycles. Beyond monomeric cobalt macrocycles, there is extensive literature on covalently linked cofacial dicobalt ORR catalysts, which is summarized in Table 14. The initial motivations for synthesizing these cofacial structures included the idea that two $Co^{III/II}$ couples would stabilize a μ-peroxide intermediate and would then favor the $4H^+/4e^-$ ORR, as most monomeric cobalt catalysts produced primarily H_2O_2.[273] Early examples of dicobalt cofacial macrocycles were used as heterogeneous ORR catalysts adsorbed to an electrode,[290−292] but more recent studies have examined homogeneous ORR catalysis with similar systems. Much of this work involves porphyrin macrocycles, although several examples of calixpyrroles have also been reported. For all of the cofacial systems, the distance and angle between the two metal centers significantly affects the observed catalysis.

A number of cofacial dicobalt macrocycles with a single bridging linker have been studied as ORR catalysts.[75,293,294] For example, cofacial porphyrins **76a−d** (Figure 43) reduce O_2 in PhCN with $HClO_4$ and Fc or Me_2Fc; however, only **76c** was selective for the $4H^+/4e^-$ ORR.[75] The strongest O_2 binding was observed for **76c** and was thought to reflect an optimized Co−Co distance and explain the difference in selectivity. For **76c**, the rate-determining step was dependent on reductant identity. When using Fc and Me_2Fc, the reaction was indicated to be first-order in $[HClO_4]$, $[O_2]$, and [reductant]. However, when $Me_{10}Fc$ was used, the reaction became zero-order in $[HClO_4]$, $[O_2]$, and [reductant]. The experimental rate laws implicated (i) rate-limiting PCET from $Co^{III}Co^{II}$ to O_2 when Fc or Me_2Fc was used or (ii) rate-limiting intramolecular O−O bond cleavage with $Me_{10}Fc$. Additionally, because only the $2H^+/2e^-$ ORR was observed with the monomeric cobalt octaethylporphyrin (Co(OEP), **77**, Figure 43) under the same conditions, the authors concluded that the cofacial structure is important for the $4H^+/4e^-$ ORR. Compounds **76a−d** and **77** were also reported as ORR catalysts in the context of the aerobic oxidation of 9-alkyl-10-methyl-9,10-dihydroacridines.[293] In PhCN containing $HClO_4$, the highest selectivity for the $4H^+/4e^-$ ORR was observed with **76a**, and increasing amounts of H_2O_2 were produced with **76c**, **76b**, **76d**, and **77**, in that order.

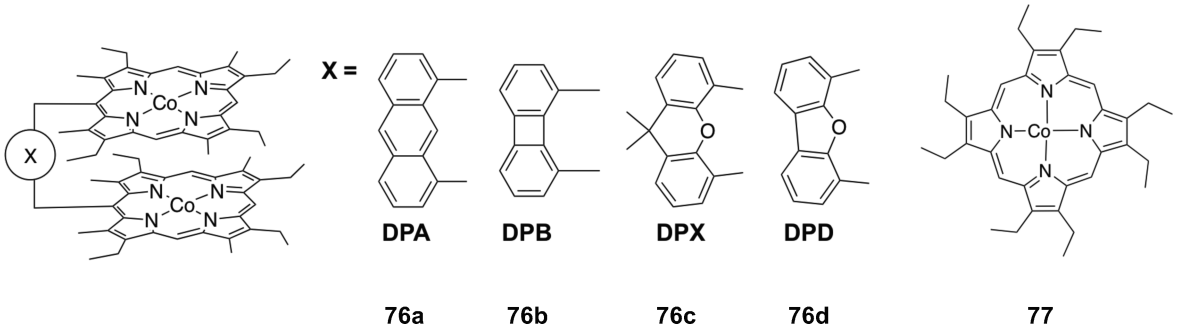

Figure 43. Cofacial cobalt porphyrin complexes and monomeric cobalt porphyrin used as ORR catalysts in refs 75 and 293.

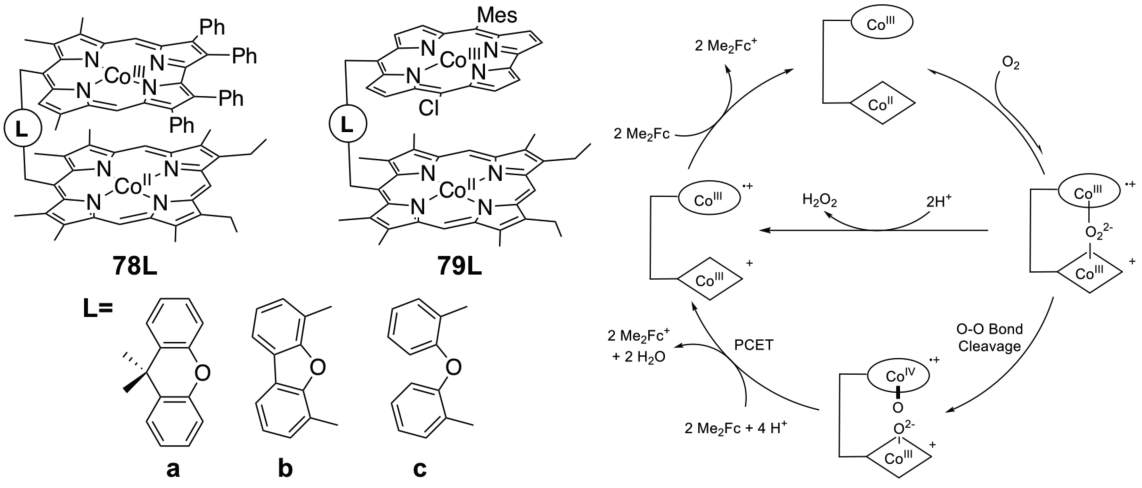

Figure 44. (Left) Cofacial porphyrin-corrole dyads used as ORR catalysts in ref 294. (Right) Proposed mechanism of ORR showing the selectivity-determining step, based on ref 294.

DOI: 10.1021/acs.chemrev.7b00542
Chem. Rev. XXXX, XXX, XXX−XXX

The cofacial porphyrin-corrole dyads **78a–c** and **79a–c** (Figure 44) were reported to catalyze the ORR.[294] In PhCN containing Me_2Fc and $HClO_4$, **78a** and **79a** were selective for the $4H^+/4e^-$ ORR, while **78b,c** and **79b,c** produced primarily H_2O_2. The observed selectivity differences were thought to reflect competition between O–O bond cleavage and protonation of a peroxo intermediate (Figure 44, right). Overall, the linker had greater influence over selectivity than did corrole derivatization. The authors suggested that the linkers in **78a**, **79a**, and **76c** induced a geometry that favored O–O bond cleavage and, as a result, the $4H^+/4e^-$ ORR.

Cofacial cobalt macrocycles have also been synthesized with multiple bridging linkers.[289,295–300] The equilibrium constant for O_2 binding to the mixed-valent $Co^{III}Co^{II}$FTF4 porphyrin (**80**$^+$, Figure 45) was measured under a variety of conditions.[295] This

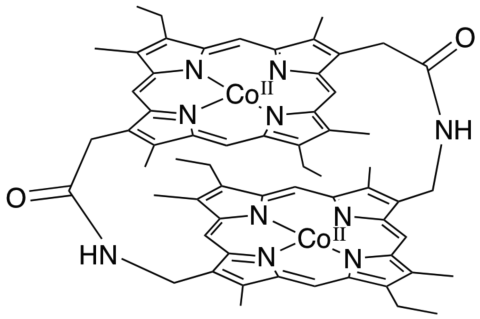

80

Figure 45. Cobalt cofacial porphyrin examined in refs 295 and 296.

K_{O_2} was the same in the presence and absence of *N*-methylimidazole, $K_{O_2} = 10^{3.0\pm0.1}$ atm^{-1}. However, water was found to competitively bind the catalyst ($K'_{O_2} = K_{O_2}/K_{H_2O} = 10^{1.3\pm0.4}$ mol atm^{-1}). A subsequent report, starting with the neutral $Co^{II}Co^{II}$FTF4 porphyrin (**80**), demonstrated that the $1e^-$ and $2e^-$ oxidized species (**80**$^+$ and **80**$^{2+}$, respectively) formed different O_2 adducts.[296] These adducts were identified by Hückel molecular orbital calculations as "hyperoxo" (defined as a $1e^-$-reduced peroxo species with each oxygen bearing a formal −1.5 charge) and bridged μ-η^2:η^2-peroxo complexes for **80**$^+$ and **80**$^{2+}$, respectively. Although both **80**$^+$ and **80**$^{2+}$ showed high affinities for O_2, only the O_2 adduct of **80**$^+$ reacted with acid. While these studies did not directly investigate homogeneous ORR catalysis with **80**, the influence of axial ligand environment and cobalt oxidation state were found to significantly impact O_2 reactivity. Such observations could be used to identify target properties of future ORR catalysts.

One tetrabridged cofacial cobalt porphyrin prism (**81**, Figure 46) has been reported as a homogeneous ORR catalyst. It was found to reduce O_2 faster (ca. 10-fold) than the related monomer **82** (Figure 46).[289] In O_2-saturated PhCN containing TFA and Fc, both **81** and **82** largely made H_2O_2 (90% and 70% H_2O_2, respectively). Under similar conditions with an electrode as the reductant, the Faradaic efficiencies for H_2O_2 production were 39% for **81** and 44% for **82**.

In air-saturated PhCN containing TFA and Fc or Me_2Fc, cofacial dicobalt Schiff base calixpyrrole complexes **83–85** (Figure 47) were selective for the $4H^+/4e^-$ ORR.[297–300] Catalyst

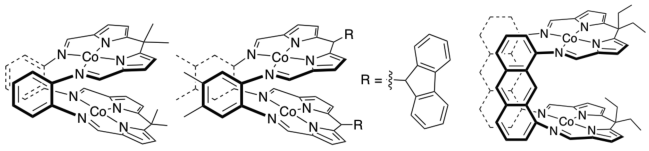

83 **84** **85**

Figure 47. Cofacial dicobalt Schiff base calixpyrrole complexes used as ORR catalysts in refs 297–300.

83 was slow ($k_{obs} = 3.8(2) \times 10^{-3}$ s^{-1}) and decomposed, yielding a low TON (ca. 16).[298] To circumvent decomposition, **84** and **85** were designed with increased steric bulk and elongated linkers, respectively.[299] Catalysis was faster for **84**, and this was ascribed to a more favorable formation of the $Co^{III}Co^{III}(O_2^{\bullet-})$ intermediate. The incorporation of anthracene linkers in **85** increased the distance between the Co centers and inhibited formation of inactive peroxide and hydroxy-bridged complexes, further enhancing the rates of catalysis.[300] Notably, use of acids stronger than TFA limited ORR catalysis, likely due to competitive decomposition of **85** via loss of Co^{2+}. Despite differences in rate, **83–85** all showed high selectivity for the $4H^+/4e^-$ ORR (<30% H_2O_2).[298–300]

4.4.2.3. Cobalt Macrocycle ORR at Liquid/Liquid Interfaces. Using cobalt macrocycles, a number of studies have examined ORR at aqueous/organic interfaces, and the results are summarized in Table 15.[301–308] An early report by Chung and Anson

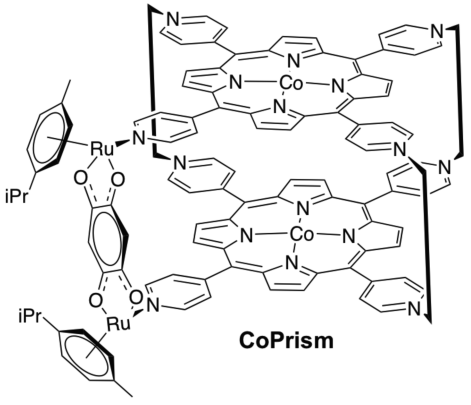

CoPrism

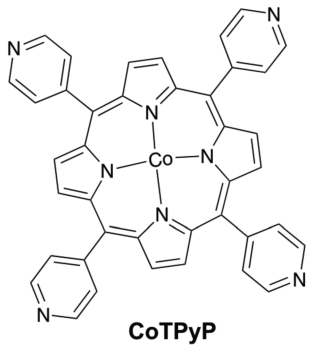

CoTPyP

81 **82**

Figure 46. Cobalt porphyrin complexes used as ORR catalysts in ref 289.

DOI: 10.1021/acs.chemrev.7b00542
Chem. Rev. XXXX, XXX, XXX–XXX

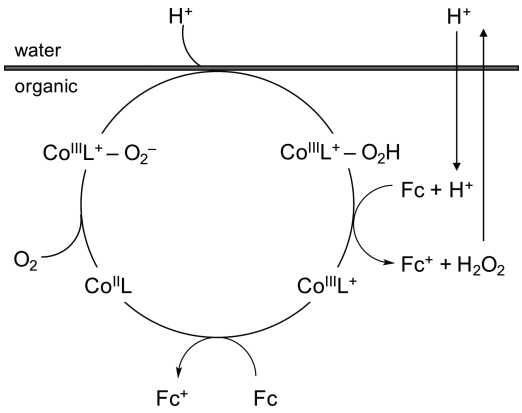

Figure 48. General mechanism of ORR at the interface of a water layer and an organic layer, as described in ref 303.

examined ORR with $Co^{II}(TPP)$ (**65**) dissolved in a thin (~30 μm) layer of PhCN that was positioned between a graphite electrode and air-saturated aqueous solution of 2 M $HClO_4$.[301] Reduction of O_2 was observed around 0.2 V vs SCE, and chronocoulometry measurements indicated formation of H_2O with ~65% selectivity, an unusually high value for a monomeric cobalt macrocycle catalyst. Compared to ORR catalysis with $Co^{II}(TPP)$ adsorbed directly onto an EPG electrode, this biphasic system exhibited larger reductive currents and higher selectivity for H_2O at the same $[Co^{II}(TPP)]$.

The ORR catalyzed by $Co^{II}(TPP)$ has also been examined in biphasic systems such as those described in section 3.2.2.1 (Figure 48).[302,303] The acid was primarily present in the aqueous phase while the reductant and the catalyst were in the organic phase. A Galvani potential difference, induced at the liquid–liquid interface, controlled proton movement from the aqueous to the organic phase, which could be facilitated by the presence of $Co^{II}(TPP)$ in the organic layer. At the aqueous/organic interface, $Co^{II}(TPP)$ was suggested to form $CoTPPH^+$ and $CoTPPH_2^{2+}$ (protonation site not reported), both of which could facilitate the $2H^+/2e^-$ ORR using $Me_{10}Fc$.[302] The amount of H_2O_2 produced was sensitive to reductant identity over the series Fc, Me_2Fc, and $Me_{10}Fc$, which suggested either (i) rate-limiting reduction of $Co^{III}(TPP)^+$ or (ii) significant differences in Galvani potentials and $[H^+]_{org}$.[303] The $2H^+/2e^-$ ORR was also observed with Co(OEP) (**77**, Figure 43) in a water/DCE solution containing Fc.[305] The authors note that **77** can also act as the reductant in this system, although the absence of Fc slowed H_2O_2 formation.

$Co^{II}(TPP)$-catalyzed ORR at liquid/liquid interfaces has been incorporated into a fuel cell.[304] Using protons generated at the anode ($H_2 \rightarrow 2H^+ + 2e^-$) in aqueous solution, $Co^{II}(TPP)$ facilitated PT into 1,2-dichlorobenzene before further reacting with O_2 and $Me_{10}Fc$. The open-circuit potential was measured to be 0.50–0.66 V and indicated formation of H_2O_2. Despite modest current efficiencies, the authors highlight the potential for promising future developments in this field.

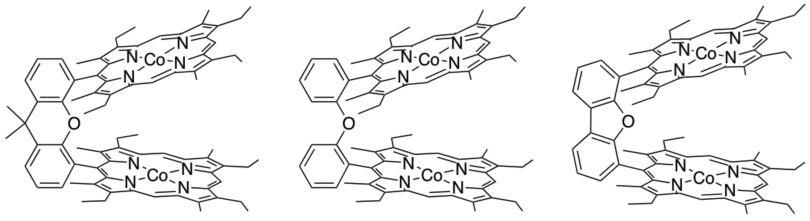

Figure 49. Cofacial cobalt porphyrins used as ORR catalysts in the biphasic system described in ref 306.

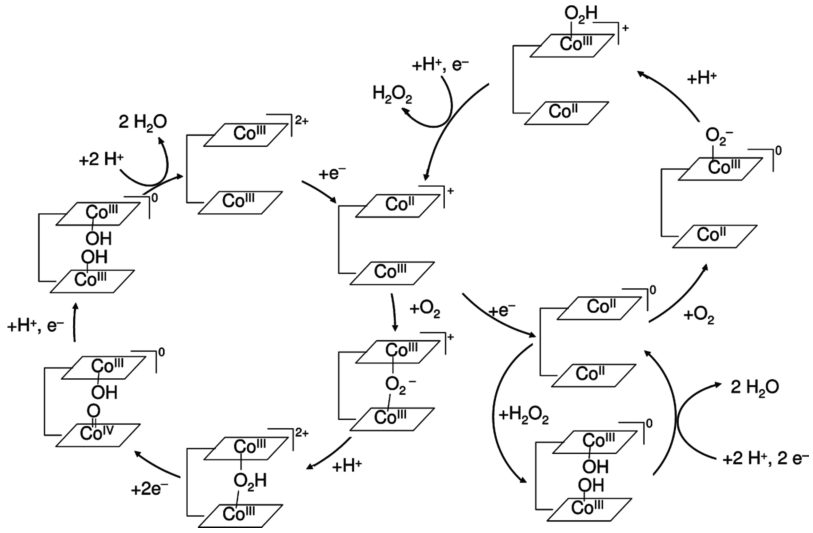

Figure 50. Proposed mechanism of dioxygen reduction using catalysts **86a–c** at the aqueous/organic interface. Two mechanisms are shown, one for the dock-in binding inside the cofacial assembly (left) and one for the dock-on binding above the cofacial assembly (right). Reproduced with permission from ref 306. Copyright 2012 American Chemical Society.

DOI: 10.1021/acs.chemrev.7b00542
Chem. Rev. XXXX, XXX, XXX–XXX

Cofacial cobalt porphyrins (**86a–c**, Figure 49) were found to be more effective ORR catalysts than Co(TPP) at the interface of acidic water and DCE containing Me_2Fc or tetrathiafulvalene (TTF).[306] Of the catalyst series, **86a** was the most selective for the $4H^+/4e^-$ ORR; however, accurate selectivity measurements were limited by the ability of both the catalyst and Me_2Fc to dismutate H_2O_2. Using DFT calculations, the authors concluded that the inherent selectivity of the catalyst depends on whether O_2 binds outside or inside of the cofacial porphyrin pocket ("dock-on" or "dock-in", respectively). Dock-in was thought to promote H_2O production, while dock-on resulted in H_2O_2 formation (Figure 50).

Under similar experimental conditions, several cobalt phthalocyanines perform the $2H^+/2e^-$ ORR at liquid/liquid interfaces.[307,308] The parent complex, CoPc (**69**), was shown to (i) bind O_2 in the organic phase, (ii) undergo a PCET reaction at the solution boundary to form H_2O_2, and (iii) return to the organic phase for reduction to **69**. Similar results were obtained for a fluorinated cobalt phthalocyanine (**87**, Figure 51).[308] In this

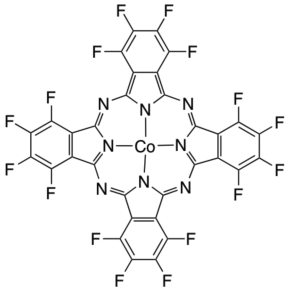

87

Figure 51. Cobalt phthalocyanine used as an ORR catalyst in ref 308.

study, TTF replaced Fc as the external reductant, allowing for more accurate selectivity measurements, as TTF does not independently catalyze H_2O_2 decomposition. Under pseudo-first-order conditions at low pH, the reaction was complete within minutes and primarily formed H_2O_2 (ca. 65%).

4.4.3. Manganese and Copper Macrocycles. There are few examples of manganese and copper macrocycles as molecular ORR catalysts (Table 16). The manganese(V) corrole complex **88** (Figure 52) was found to be a precatalyst for the selective reduction of O_2 to H_2O_2 using TFA and Me_8Fc (TON ca. 150).[309] Catalysis was first-order in [**88**] and [O_2] (k_{cat} = 2.7 ± 0.1 M^{-1} s^{-1}). The authors proposed that catalyst activation involves $2e^-$ reduction, protonation, and dissociation of aniline to form the O_2-sensitive complex $\mathbf{88}_{red}$ (Figure 52). Upon O_2 binding, several protonation and reduction steps occurred to catalytically yield H_2O_2.

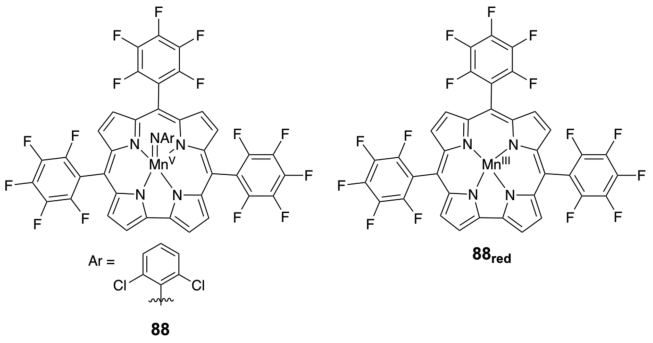

88 **88_{red}**

Figure 52. Mn-corrole complex used as an ORR catalyst in ref 309.

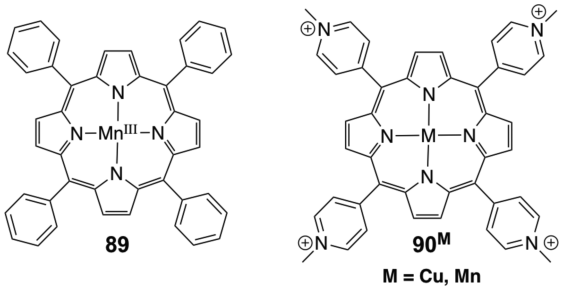

89 **90^M** **M = Cu, Mn**

Figure 53. Metalloporphyrin ORR catalysts used in refs 260, 264, 265, and 310.

$Mn(TPP)^+$ (**89**, Figure 53) has been reported as an ORR catalyst in MeCN containing $HClO_4$ and Fc derivatives.[264,265] The reaction was zero-order in [$HClO_4$] and [O_2] and first-order in [reductant], with k_{obs} = 2.6 × 10^2 M^{-1} s^{-1} and 1.4 × 10^5 M^{-1} s^{-1} using Me_2Fc and $Me_{10}Fc$, respectively. As with ORR via $Fe(TPP)^+$ and $Co(TPP)^+$ under the same conditions (discussed in sections 4.4.1 and 4.4.2.1), the authors proposed initial ET to $Mn(TPP)^+$ as the rate-determining step for catalysis.

The water-soluble $MnTMPyP^{5+}$ and $CuTMPyP^{4+}$ complexes ($\mathbf{90}^{Mn,Cu}$, Figure 53) have been reported to catalyze the $2H^+/2e^-$ ORR.[260,310] For $\mathbf{90}^{Mn}$, catalysis occurred around $E_{Mn(III/II)}$ = −0.190 V vs SCE in pH 7.0 phosphate buffer. MCD spectra indicated that the active species was a high-spin Mn^{II} complex and supported the proposed *EC′* mechanism.[310] In aqueous 0.1 M HOTf, $\mathbf{90}^{Mn}$ and $\mathbf{90}^{Cu}$ produced H_2O_2 with 76% and 69% selectivity, respectively.[260] Comparison of these catalysts with their iron and cobalt analogues revealed a linear relationship between catalytic rate and $E_{1/2}$. The correlation slope of 1 decade in TOF per 120 mV change in $E_{1/2}$ was viewed as evidence for outer-sphere ET from the reduced metal to O_2; however, the authors could not preclude the possibility of inner-sphere ET to form a M–O_2 bond. Still, this observation contrasts with

Table 16. Manganese and Copper Macrocycle ORR Catalysts

catalyst	ligand scaffold	solvent	proton source	$E_{1/2}$/reductant	rate constant[a]	%H_2O_2	ref
$\mathbf{90}^{Mn}$	5,10,15,20-tetrakis(4-*N*-methylpyridyl)porphyrin	aqueous	pH 7.0, 0.1 M KH_2PO_4 buffer	−0.190 V vs SCE	not reported	95[b]	310
$\mathbf{90}^{Mn}$	5,10,15,20-tetrakis(4-*N*-methylpyridyl)porphyrin	aqueous	HOTf (0.1 M)	−0.049 V vs Ag/AgCl	4.81 × 10^4 M^{-1} s^{-1}	76	260
$\mathbf{90}^{Cu}$	5,10,15,20-tetrakis(4-*N*-methylpyridyl)porphyrin	aqueous	HOTf (0.1 M)	−0.122 V vs Ag/AgCl	1.32 × 10^5 M^{-1} s^{-1}	69	260
88	5,10,15-tris(pentafluorophenyl)corrole	MeCN	0.01 M TFA	Me_8Fc	(2.7 ± 0.1) M^{-1} s^{-1}	major product[c]	309
89	5,10,15,20-tetraphenylporphyrin	MeCN	$HClO_4$	Me_2Fc	2.6 × 10^2 M^{-1} s^{-1}	not reported	264, 265
				$Me_{10}Fc$	1.4 × 10^5 M^{-1} s^{-1}		

[a]Reported rate constants include turnover frequencies under the particular experimental conditions to *k* values for second- or third-order rate laws (M^{-1} s^{-1} or M^{-2} s^{-1}, respectively). [b]Number of electrons = 1.9 ± 0.1. [c]H_2O_2 reported as major product but selectivity not quantified.

DOI: 10.1021/acs.chemrev.7b00542
Chem. Rev. XXXX, XXX, XXX–XXX

Table 17. Nonmacrocylic Complexes Used As ORR Catalysts

catalyst	metal	ligand scaffold	solvent	proton source	$E_{1/2}$/reductant	rate constant[a]	product	ref
91	Mn	4,5-dihydroxybenzene-1,3-disulfonic acid (Tiron)	aqueous	pH 8.0, Hepes buffer	NH_2OH or N_2H_4	2.59×10^{1}[b]	H_2O_2[c]	312
92	Mn	3,4,5,6-tetrachloro catechol	aqueous	pH 8.0, Hepes buffer	NH_2OH or N_2H_4	not reported	H_2O_2[c]	312
93	Mn	4-chlorocatechol	aqueous	pH 8.0, Hepes buffer	NH_2OH or N_2H_4	1.04×10^{1}[b]	H_2O_2[c]	312
94	Mn	2-chlorocatechol	aqueous	pH 8.0, Hepes buffer	NH_2OH or N_2H_4	not reported	H_2O_2[c]	312
95	Mn	catechol	aqueous	pH 8.0, Hepes buffer	NH_2OH or N_2H_4	1.6×10^{0}[b]	H_2O_2[c]	312
96	Mn	2-methylcatechol	aqueous	pH 8.0, Hepes buffer	NH_2OH or N_2H_4	3×10^{-1}[b]	H_2O_2[c]	312
97	Mn	2-nitrocatechol	aqueous	pH 8.0, Hepes buffer	NH_2OH or N_2H_4	1.79×10^{1}[b]	H_2O_2[c]	312
98	Mn	1,2-dinitrocatechol	aqueous	pH 8.0, Hepes buffer	NH_2OH or N_2H_4	3.5×10^{0}[b]	H_2O_2[c]	312
99	Mn	1,3-dinitrocatechol	aqueous	pH 8.0, Hepes buffer	NH_2OH or N_2H_4	2.1×10^{0}[b]	H_2O_2[c]	312
100	Mn	HmBupa	DMA	1,2-diphenylhydrazine	1,2-diphenylhydrazine	not reported	H_2O (99%)	184
101	Mn	2,2′-(2,2′-bipyridine-6,6′-diyl)-bis(1,1-diphenylethanethiolate)	MeCN	2,6-lutidinium tetrafluoroborate	Me_8Fc or $Me_{10}Fc$	not reported	H_2O_2 (80−84%)	313
102	Fe	N4Py1	MeCN	HOTf or ascorbic acid	$CoCp_2$ or ascorbic acid	not reported	not reported	314
103	Fe	N4Py2	MeCN	HOTf or ascorbic acid	$CoCp_2$ orascorbic acid	not reported	not reported	314
105	Cu	TMPA	acetone	$HClO_4$	$Me_{10}Fc$	TOF = 1.7×10^{1} s^{-1}	H_2O[i]	315
105	Cu	TMPA	acetone	TFA	$Me_{10}Fc$	2.3×10^{2} M^{-1} s^{-1}	H_2O[i]	316
105	Cu	TMPA	aqueous	pH 7 Britton−Robinson	−0.34 V vs Ag/AgCl	not reported	H_2O[i]	318
105	Cu	TMPA	acetone	HOTf	Me_2Fc	not reported	H_2O[i]	77
106	Cu	pivalato-TMPA	acetone	TFA	$Me_{10}Fc$	8.6×10^{2} M^{-1} s^{-1}	H_2O[i]	316
107	Cu	BZQ	acetone	HOTF	Me_2Fc	not reported	H_2O_2	77
108	Cu	TEPA	aqueous	pH 7 Britton−Robinson	0.17 V vs Ag/AgCl	not reported	not reported	318
108	Cu	TEPA	acetone	$HClO_4$	Me_2Fc	1.8×10^{1} M^{-1} s^{-1}	H_2O_2[c]	77
109	Cu	BMPA	aqueous	pH 7 Britton−Robinson	−0.25 V vs Ag/AgCl	not reported	not reported	318
110	Cu	*m*-xylene-linked bis[(2-(2-pyridyl)ethyl) amine	acetone	TFA	$Me_{10}Fc$	3×10^{-3} s^{-1}[d]	H_2O_2[c]	319
111	Cu	$-(CH_2)_3$-linked bis[2-(2- pyridyl)ethyl]amine	acetone	TFA	$Me_{10}Fc$	1.8×10^{-2} s^{-1}[e]	H_2O[i]	320
112	Cu	pyridine-modified polyamidoamine (G2−G6)	aqueous	pH 7.3, tris(hydroxymethy) aminomethane buffer	dithiothreitol	G2:$(7.3 \pm 0.6) \times 10^{-2}$ min^{-1}; G3: $(8.8 \pm 0.4) \times 10^{-2}$ min^{-1}; G4: $(1.13 \pm 0.12) \times 10^{-1}$ min^{-1}; G5:	not reported	321

DOI: 10.1021/acs.chemrev.7b00542
Chem. Rev. XXXX, XXX, XXX−XXX

Table 17. continued

catalyst	metal	ligand scaffold	solvent	proton source	$E_{1/2}$/reductant	rate constant[a]	product	ref
						$(1.09 \pm 0.03) \times 10^{-1}$ min^{-1}; G6: $(1.13 \pm 0.03) \times 10^{-1}$ min^{-1}		
113	Co	bis(pyridyl)pyrazolate; terpyridine	MeCN	TFA	Me_8Fc	1×10^{-1} s^{-1}[f]	H_2O[i]	322
114a	Co	1,8-bis(2,2′:6′,2″-terpyrid-4′-yl)-anthracene and phenanthroline	PhCN	$HClO_4$	Fc	not reported	H_2O (85%)	323
14b	Co	1,8-bis(2,2′:6′,2″-terpyrid-4′-yl)anthracene and bipyridine	PhCN	$HClO_4$	Fc	not reported	H_2O (65%)	323
115	Ni/Ru	*N,N′*-dimethyl-*N,N′*-bis(2-mercaptoethyl)-1,3- propanediamine and hexamethylbenzene	aqueous	H_2 gas/acetic acid	H_2	not reported	H_2O[i]	185
116	Ni/Ru	*N,N′*-dimethyl-*N,N′*-bis(2-mercaptoethyl)-1,3- propanediamine and pentamethylcyclopentadiene	aqueous	pH 2 buffer, hydroquinone, $NaBH_4$	hydroquinone, $NaBH_4$	2.4×10^{-3} s^{-1}	not reported	186
117/118	Ir	Cp*, Ts-DPEN	CH_2Cl_2	H_2, H $(OEt_2)_2BAr^F{}_4$	H_2, H $(OEt_2)_2BAr^F{}_4$	1.42×10^{-2} h^{-1}[g]	H_2O[i]	324
119[O$_2$]	Rh	2,3,5,6-tetrafluoropyridine; pivalonitrile; triethylphosphine	7:1 THF/H_2O	$[NH_4][HCO_2]$	$[NH_4][HCO_2]$	5×10^{-1} day^{-1}[h]	H_2O_2[c]	187

[a]Reported rate constants include turnover frequencies under the particular experimental conditions to *k* values for second- or third-order rate laws (M^{-1} s^{-1} or M^{-2} s^{-1}, respectively). [b]Units for rate constant = $(mol/(dm^3\ s) \times 10^6)$. [c]$H_2O_2$ reported as major product but selectivity not quantified. [d]Estimated from Figure 2a of ref 319 (1.0 mM $Me_{10}Fc$, 3 mM TFA, and 100 M catalyst). [e]Estimated from Figure 7 of ref 320 with 1.0 mM $Me_{10}Fc$ at 193 K. [f]Estimated from Figure 4b of ref 322 (1.5 mM Me_8Fc, 50 mM TFA, 25 M catalyst). [g]Turnovers in 300 h = 4.26. [h]Turnovers in 7 days = 3.6. [i]H_2O reported as major product but selectivity not quantified

the inner-sphere mechanisms and linear free-energy relationships observed for related Fe and Co porphyrins (sections 4.4.1 and 4.4.2).

4.4.4. Conclusions. Iron and cobalt complexes are by far the most widely studied homogeneous ORR catalysts with macrocyclic ligands. Only a few examples have been reported that use manganese or copper. Generally, iron macrocycles produce H_2O with higher selectivity than do their cobalt, manganese, and copper analogues. This might result from iron's ability to provide greater relative stability to the likely terminal-oxo intermediate, M═O, as compared with the other metals. Several additional factors influence the $2H^+/2e^-$ vs $4H^+/4e^-$ selectivity, including (i) acid strength and concentration, (ii) second sphere ligand effects (e.g., pendent proton donors), and (iii) the M−M distance for cofacial molecules.

4.5. Oxygen Reduction Catalyzed by Transition Metal Complexes with Nonmacrocyclic Ligands

Homogeneous ORR catalysis has also been studied with complexes of nonmacrocyclic ligands, with a number of different metals. A variety of ligand scaffolds have been examined, although most examples involve multidentate N-donor ligands. A comparison of the experimental conditions, rates, and selectivities for these catalysts can be found in Table 17.

4.5.1. Manganese Complexes. Among the first examples of manganese ORR catalysts were a series of catechol complexes (**91**−**99**, Figure 54).[311,312] Initially, **91** was identified as a

$R_1 = R_3 = SO_3H$, $R_2 = R_4 = H$; **91**

$R_1 = R_2 = R_3 = R_4 = Cl$; **92**

$R_1 = R_4 = H$, $R_3 = R_4 = Cl$; **93**

$R_1 = R_3 = R_4 = H$, $R_2 = Cl$; **94**

$R_1 = R_2 = R_3 = R_4 = H$; **95**

$R_1 = R_4 = R_3 = H$, $R_2 = CH_3$; **96**

$R_1 = R_3 = R_4 = H$, $R_2 = NO_2$; **97**

$R_1 = R_2 = NO_2$, $R_3 = R_4 = H$; **98**

$R_1 = R_3 = NO_2$, $R_2 = R_4 = H$; **99**

Figure 54. Manganese(II) complexes used as ORR catalysts in refs 311 and 312. The most active complex, $Mn(Tiron)_2$, is **91**.

selective catalyst for the $2H^+/2e^-$ ORR catalyst in pH 8 solutions containing hydroxylamine as an electron and proton source.[311] Under these conditions, **91** produced ~200 mM H_2O_2, corresponding to a TON > 10^4, within 400 min. When Mn(II) was replaced with Fe(II), Cu(II), or Co(II), insignificant amounts of H_2O_2 were generated, indicating the critical role of the manganese ion. In later work, the catalyst library was expanded to complexes of substituted catecholates, **92**−**99**.[312] More electron-withdrawing complexes exhibited greater activity for H_2O_2 production (**91** > **92** > **93** ≈ **94** > **95**). Similar yields of H_2O_2 were

DOI: 10.1021/acs.chemrev.7b00542
Chem. Rev. XXXX, XXX, XXX−XXX

achieved using hydrazine as the chemical reductant, although catalysis was ~5 times slower than with hydroxylamine. Both reductants made N_2 as a byproduct. The authors propose that the hydroxylamine anion (H_2NO^-) or hydrazine must coordinate the metal before the complex is capable of reducing O_2 (Figure 55).

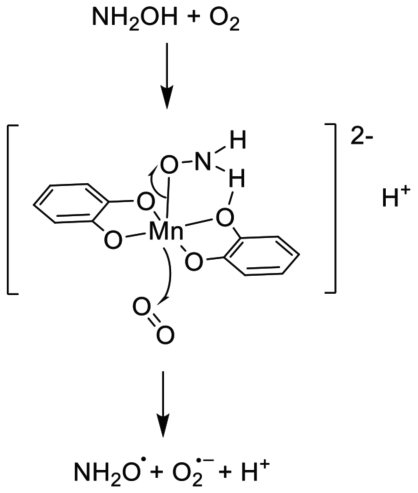

Figure 55. Proposed rate-determining step for ORR using manganese(II) catecholate complexes, as described in ref 312.

This pathway was supported by the first-order dependence on P_{O_2} and the absence of an H_2O/D_2O kinetic isotope effect.[312]

More recently, Borovik and co-workers reported a tripodal manganese(II) complex (**100**, Figure 56) that catalyzed the

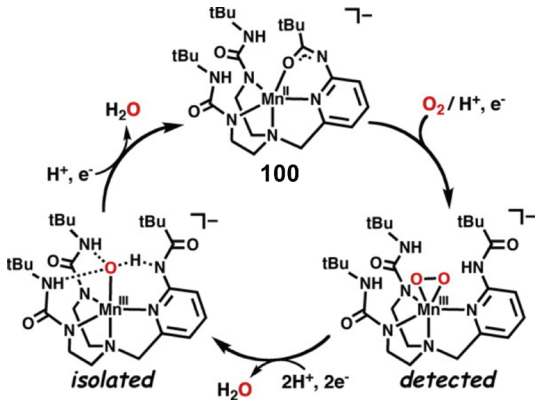

Figure 56. Tripodal manganese(II) complexes and intermediates. The e^- and H^+ are delivered from a hydrazine in the catalysis. Reproduced with permission from ref 184. Copyright 2011 American Chemical Society.

$4H^+/4e^-$ ORR in both DMSO and dimethylacetamide (DMA) solutions containing 1,2-diphenylhydrazine (DPH).[184] In the presence of excess DPH or hydrazine, catalysis was observed with TONs ≈ 200. The authors assigned an observed intermediate to a manganese(III)-peroxo complex with a protonated ligand, based on its ESI-MS spectra and reactivity. This species decayed to an isolable Mn(III)−OH complex, which then formed a Mn(II)−OH_2 complex upon addition of 0.5 equiv of DPH. Loss of water closed the catalytic cycle. Consistent with the proposed mechanism (Figure 56), catalysis was inhibited by H_2O in solution.

We have found only one report of a dinuclear manganese ORR catalyst (**101**, Figure 57).[313] In MeCN solutions containing

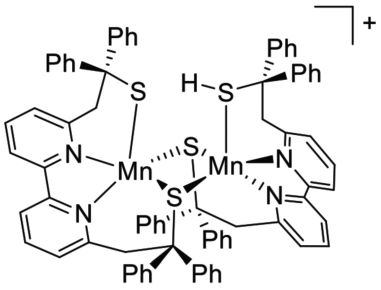

Figure 57. Bimetallic manganese thiolate complex used as an ORR catalyst in ref 313.

lutidinium and Me_8Fc or $Me_{10}Fc$, **101** performed the $2H^+/2e^-$ ORR with 80% selectivity. Interestingly, stepwise stoichiometric additions of O_2 and H^+ yielded production of water via protonation of a mono-μ-hydroxo dinuclear Mn(III) complex. However, under the acidic conditions required for ORR catalysis, M−O bond cleavage was favored over O−O bond cleavage, and thus H_2O_2 production predominated.

4.5.2. Iron Complexes. In 2009, Soo and co-workers reported several tetrapyridyl iron complexes containing potential phenylamine proton relays in the secondary coordination sphere (**102**−**104**, Figure 58).[314] Although these compounds were not

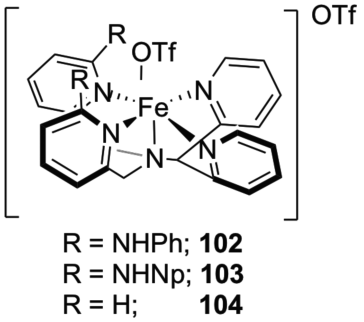

Figure 58. Iron N4Py complexes **102** and **103** used for dioxygen reduction in ref 314.

used under catalytic conditions, the reported reactivity is relevant to ORR examples. Similar to that of Borovik's manganese complex (**100**, Figure 56),[184] this ligand scaffold has a protic environment above the active site but provides the added benefit of acid and base stability due to the neutral donating amine ligands. Addition of O_2 to **102** or **103** resulted in the quantitative formation of a Fe(III)−OH product, as confirmed by $(^{18}O)_2$-labeling experiments. Using decamethylcobaltocene and triflic acid, the Fe(III)−OH complex could be reduced to Fe(II)−OH and protonated to yield H_2O and the starting Fe(II) species (**102** or **103**). Reaction of the Fe(III)−OH complex with ascorbic acid also regenerated **102** or **103**. Notably, **104**, containing an identical primary coordination sphere but no secondary coordination-sphere motifs, did not react with O_2.

4.5.3. Copper Complexes. In 2010, Fukuzumi and co-workers reported the first monomeric copper(II) ORR catalyst (**105**, Figure 59).[315] In acetone containing $Me_{10}Fc$ and $HClO_4$, **105** was selective for the $4H^+/4e^-$ ORR. The authors proposed a catalytic mechanism initiated by rate-determining reduction of Cu^{II} by $Me_{10}Fc$. They suggested that O_2 binding to give a dimeric

DOI: 10.1021/acs.chemrev.7b00542
Chem. Rev. XXXX, XXX, XXX−XXX

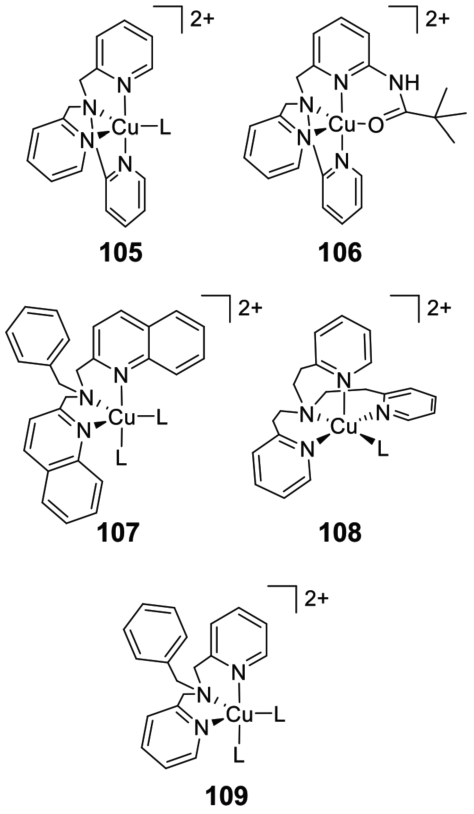

Figure 59. Copper complexes used as ORR catalysts in refs 315−318. The counteranions were ClO_4^-, and L = H_2O.

copper-peroxo complex was followed by acid-catalyzed O−O bond cleavage (Figure 60) to form H_2O. Under catalytic conditions, the authors report a TOF of ∼17 s^{-1} and a TON of 5.

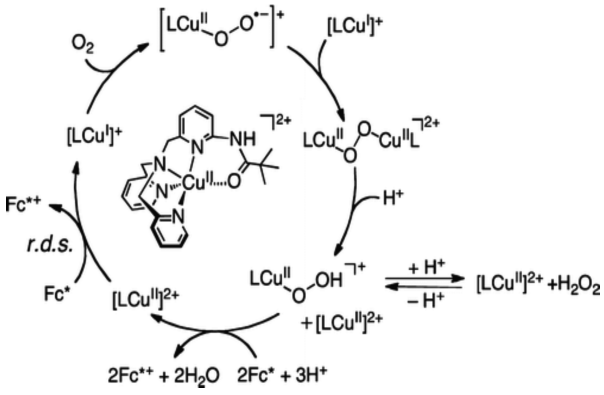

Figure 60. Mechanism of H_2O formation using copper complexes. Reproduced with permission from ref 317. Copyright 2013 American Chemical Society.

The ORR activity of **105** was later compared to that of the structurally similar catalyst **106** (Figure 59) in acetone containing $Me_{10}Fc$ and TFA.[316] Catalysis by **105** was inhibited by binding of the conjugate base, CF_3COO^-, to Cu(II), which shifted the Cu(II/I) redox couple 300 mV negative. Improved rates of catalysis were observed with **106**, in part because the carbonyl of the pivalamide substituent prevented conjugate base binding. Spectroscopic evidence of hydroperoxo and μ-peroxo intermediates was observed for **105** and **106**, suggesting that the two catalysts follow the same mechanism (Figure 60).[315,316] For **106**, the rate of H_2O_2 reduction was much faster than the rate of O_2 reduction, which indicated that the selectivity- and rate-determining steps occur in different parts of the catalytic cycle.

In the presence of $Me_{10}Fc$ and $Sc(OTf)_3$, **105** catalyzed the $2e^-$ reduction of O_2 to form scandium(III) peroxide $[Sc(O_2)^+]$ (Figure 61).[317] This contrasts with the $4e^-$ reactivity observed in

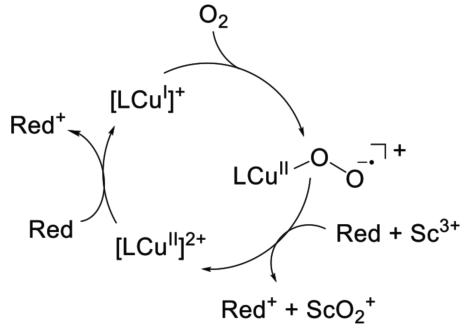

Figure 61. Proposed mechanism for $2e^-$ reduction of O_2 promoted by scandium(III) as a Lewis acid, based on ref 317. Red is $Me_{10}Fc$ for **105** and Me_2Fc for **107**.

the presence of HOTf. Similar selectivity changes were also observed for Y^{3+}, Mg^{2+}, Ca^{2+}, Yb^{3+}, and Lu^{3+}, although the fastest rates were recorded with Sc^{3+}. For both Lewis and Brønsted acids, the rate-determining step was assigned as ET to $[LCu^{II}]^{2+}$. Complex **107** (Figure 59) also catalyzed the $2e^-$ reduction of O_2 in the presence of Sc^{3+}, although the rate-determining step in this case was O_2 binding. This mechanistic difference was ascribed to the difference in Cu(II)/Cu(I) reduction potential between **107** (0.44 V vs SCE) and **105** (−0.05 V vs SCE).

A related study evaluated **105**, **108**, and **109** (Figure 59) as ORR catalysts in pH 7 buffered aqueous solutions.[318] The Cu(II/I) reduction potentials of these complexes spanned ∼500 mV. A comparison of **105** ($E_{1/2}$ = −0.34 V vs Ag/AgCl) and **109** ($E_{1/2}$ = −0.25 V vs Ag/AgCl) demonstrated that the catalyst with the more-negative $E_{1/2}$ value produced a larger catalytic current for the ORR. Compound **108**, having the most positive $E_{1/2}$ of the series at 0.17 V vs Ag/AgCl, did not display ORR activity on the CV time scale. When adsorbed onto a glassy carbon disc electrode, **105** was highly selective for H_2O production, but a 2 + 2 mechanism could not be ruled out because **105** can also reduce H_2O_2.

In acetone containing $HClO_4$ and Fc or Me_2Fc, **108** (Figure 59) was selective for the $2H^+/2e^-$ ORR.[77] The reaction was first-order in $[HClO_4]$, $[O_2]$, and [**108**] but zero-order in [reductant]. This observation contrasts with the conclusions reached for **105**, in which catalysis is gated by initial ET and the product was H_2O. For **108**, the rate-determining step was thought to involve the formation a LCu(II)−O_2H intermediate, which could be observed spectroscopically at low temperature. Acid addition to LCu(II)−O_2H formed H_2O_2 quantitatively. The rate of formation of LCu(II)−O_2H was independent of temperature in both stoichiometric and catalytic reactions, which was proposed to arise from a balance of the exothermic pre-equilibrium O_2 binding and the $\Delta H^{\ddagger}$ for the subsequent PCET step (Figure 62). The authors speculated that the selectivity differences observed between **105** and **108** reflected the Cu−O bond lengths of reduced intermediates, with longer bonds favoring the $2H^+/2e^-$ ORR.

Dinuclear copper complexes have also been used for homogeneous ORR (**110** and **111**, Figure 63). The phenolate-bridged catalyst, **110**, was reported to selectively reduce O_2 to H_2O_2 in acetone containing $Me_{10}Fc$ and TFA.[319] The authors

DOI: 10.1021/acs.chemrev.7b00542
Chem. Rev. XXXX, XXX, XXX−XXX

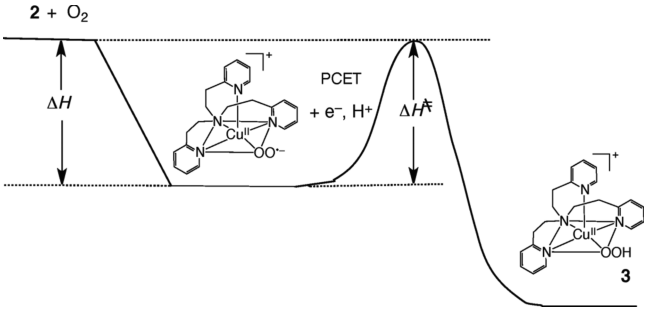

Figure 62. Origin of temperature-independent rate constant for ORR using catalyst **108** (labeled **2** in the figure). Reproduced with permission from ref 77. Copyright 2013 American Chemical Society.

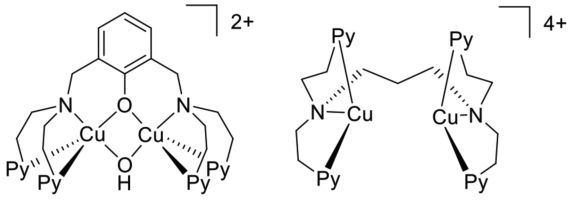

110 **111**

Figure 63. Bimetallic copper complexes **110** and **111** used as ORR catalysts in refs 319 and 320, respectively.

identified two operative mechanisms, each initiated by protonation and loss of the bridging hydroxide, followed by reduction to either $Cu^{I}Cu^{II}$ or $Cu^{I}Cu^{I}$. Both reduced forms further reacted with O_2 and acid to form a hydroperoxo complex, which released H_2O_2 upon protonation. In contrast, **111** was selective for the $4H^{+}/4e^{-}$ ORR under the same conditions.[320] The reduced catalyst, $\mathbf{111}^{2-}$, bound O_2 to form an equilibrium mixture of $Cu^{II}Cu^{II}$ $\eta^2{:}\eta^2$-peroxo and $Cu^{III}Cu^{III}$ bis-μ-oxo complexes. ET to the O_2 adduct was found to be rate-determining, and subsequent protonation steps yielded H_2O and completed the catalytic cycle (Figure 64).

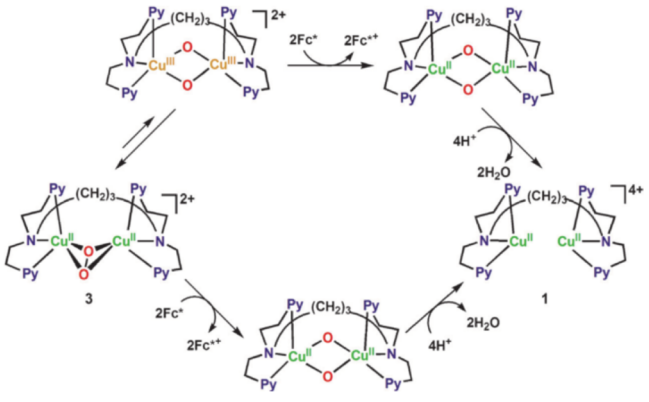

Figure 64. Potential catalytic pathways for O_2 reduction using catalyst **111**. Reproduced with permission from ref 320. Copyright 2012 John Wiley and Sons.

A unique example of copper-catalyzed ORR used a series of polyamidoamine dendrimer generations (**112**, Figure 65) to reduce O_2 to H_2O_2 in pH 7.3 buffered water containing dithiothreitol and catechol.[321] The reaction rate was monitored optically by following the formation of *ortho*-benzoquinone ($k_{obs} \approx 5 \times 10^{-5}$ s^{-1}). The authors highlighted the difference in

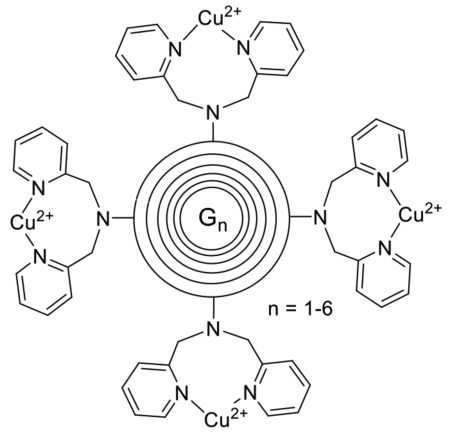

112

Figure 65. Polyamidoamine Cu^{2+} dendrimer complexes used in ref 321. Each concentric ring represents another generation of dendrimer.

catalytic activity across the dendrimer generations. Although all generations contained a large number of catalytically active Cu^{2+} ions (on average 4.8, 7.6, 22.2, 57.3, and 81.7 for G2−G6 dendrimers, respectively), G2−G4 utilized monometallic active sites, while G5 and G6 operated with bimetallic active sites. For G5 and G6, the authors proposed that initial reduction of $Cu^{II}Cu^{II}$ to $Cu^{I}Cu^{I}$ with dithiothreitol was followed by reduction of O_2 to $O_2^{\bullet-}$ at the active site. Generated $O_2^{\bullet-}$ then reacted with catechol in solution to yield H_2O_2.

4.5.4. Complexes of Other Transition Metals. Dinuclear cobalt complexes containing terpyridine ligands (**113** and **114a,b**, Figure 66) have been reported to selectively reduce O_2 to H_2O.[322,323] Catalysis with **113** was observed in MeCN solutions containing TFA and Me_8Fc, and similar results were obtained with **114a,b** in PhCN containing $HClO_4$ and Fc. The authors proposed that **113** reacted via rate-determining PCET to yield a $Co^{III}(OH)Co^{III}(O^{\bullet})$ complex, which was rapidly reduced and protonated to yield H_2O and complete the catalytic cycle.[322] For **114a,b**, $(^{18}O)_2$ experiments supported the intermediacy of peroxo complexes, which the authors reported as being advantageous for $4H^{+}/4e^{-}$ selectivity.

Two related nickel−ruthenium complexes (**115** and **116**, Figure 67), originally designed as functional models of [NiFe]hydrogenases, have been reported to perform the $4H^{+}/4e^{-}$ ORR in H_2O.[185,186] Complex **115** was used as a homogeneous catalyst to both oxidize H_2 and reduce O_2 in an operative fuel cell (0.32 V open-circuit voltage; 17 μA cm^{-2} maximum current density). Only after reacting with H_2 to form a Ni−Ru bridging hydride was **115** sensitive to O_2. Aqueous RRDE measurements of the ORR with AcOH indicated no production of H_2O_2.[185] The related complex **116** did not require formation of a Ni−Ru hydride and rapidly reacted with O_2 in the absence of H_2 or acid to form an Ru^{IV} η^2-peroxo complex.[186] Under N_2 in acidic water (pH 2) containing excess *para*-hydroquinone and $NaBH_4$, the η^2-peroxo complex was slowly reduced to H_2O and **116** ($k_{obs} = 2.4 \times 10^{-3}$ s^{-1}).

Reactions of noble metal complexes with O_2 have been extensively used for catalytic oxidations of organic substrates. However, to our knowledge, there are only two reports focused on the catalytic homogeneous ORR. Cp*IrH(Ts-DPEN) (**117**, Figure 68; DPEN = 1,2-diphenyl-1,2-ethylenediamine) was reported to catalyze the $4H^{+}/4e^{-}$ ORR with H_2 as the

DOI: 10.1021/acs.chemrev.7b00542
Chem. Rev. XXXX, XXX, XXX−XXX

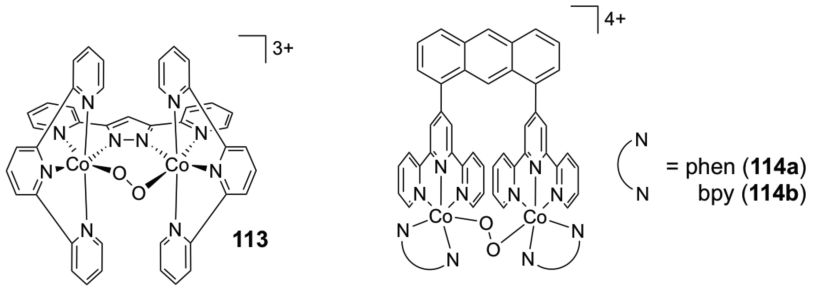

Figure 66. Dinuclear cobalt complexes used as ORR catalysts in refs 322 and 323.

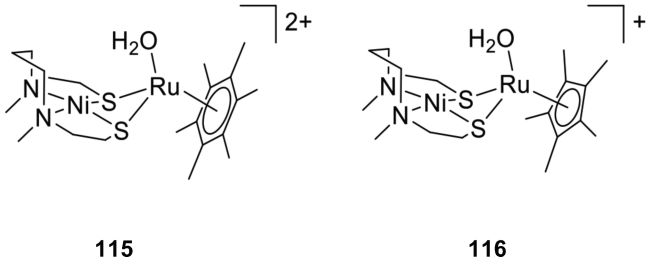

Figure 67. Bimetallic RuNi complexes used as ORR catalysts in refs 185 and 186.

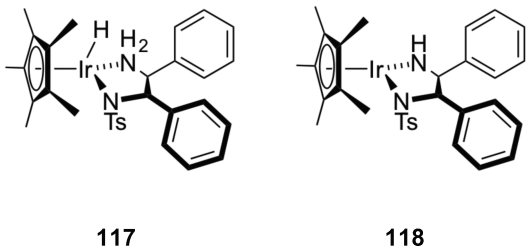

Figure 68. Ir catalyst used for oxygen reduction in ref 324, shown in its reduced (**117**) and oxidized (**118**) form.

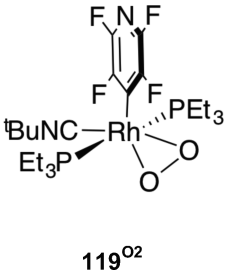

Figure 69. Rh complex used as an ORR catalyst in ref 187.

reductant.[324] This system is thus related to the Ni/Ru catalysts in the previous paragraph that were developed for H_2 catalysis. A "ping-pong" mechanism was suggested involving (i) oxidation of **117** by O_2 to form a hydroperoxo intermediate, (ii) reaction of the hydroperoxo intermediate with another equivalent of **117** to yield H_2O and a hydroxo complex (Cp*Ir(OH)(Ts-DPEN)), (iii) loss of H_2O to form **118**, and, finally, (iv) hydrogenation of **118** by H_2 to regenerate **117**. In CH_2Cl_2, quantitative oxidation of **117** occurred within minutes. Hydrogenation of **118** was slow but could be accelerated by addition of 10 mol % $[H(OEt_2)_2]$-$BAr^F{}_4$. H_2O was produced with a TON of 4.26 over 300 h from a CD_2Cl_2 solution with 10 mol % **117** cycled under 0.13 atm O_2 and then separately under 0.30 atm H_2. Similar TONs for H_2O production were achieved using amine boranes or alcohols as hydrogen donors in place of H_2. The low TONs were attributed in part to a competitive catalyst-degradation pathway involving intramolecular hydrogen atom abstraction from a methyl group of the Cp* ring. Still, the report provides a very unusual example of using a metal hydride to perform catalytic oxygen reduction.

Meier and Braun showed that the *trans*-$[Rh(O_2)(4\text{-}C_5F_4N)(CNtBu)(PEt_3)_2]$ (**119**^{O2}, Figure 69) catalyzed the $2H^+/2e^-$ ORR with $[NH_4][HCO_2^-]$ as a source of protons and electrons.[187] A hydroperoxo-formato intermediate was isolable at low temperatures and decomposed into H_2O_2, CO_2, and an O_2-sensitive four-coordinate Rh(I) complex. In a THF/H_2O solution containing O_2 and $[NH_4][HCO_2^-]$ with 20% **119**, 3.6 turnovers of H_2O_2 were observed.

4.6. Oxygen Reduction with Organic Reductants

As alluded to in several earlier examples, oxygen reduction can also be coupled to the oxidation of organic molecules. This topic is much more commonly described as aerobic oxidation, with an emphasis on conversion of the organic substrate. Aerobic oxidations are practiced on huge scales for commodity chemical production[2,3] and are even performed in the teaching laboratory.[325] This topic is well beyond the scope of this Review, but it is valuable to highlight a few examples to emphasize their similarities to more traditional ORR catalysis.

The Wacker process from the late 1950s uses palladium and copper salts to catalyze the aerobic oxidation of acetylene to acetaldehyde.[2] Much more recently, aerobic oxidations have been developed for organic synthesis and for fine chemical production (e.g., alcohols) using Pd or Cu.[326−329] These reactions typically convert O_2 to H_2O_2, which disproportionates under the reaction conditions. The catalysts are thus mono-oxygenases in the biological terminology, and their mechanisms can involve κ^2-peroxo compounds, κ^1-superoxide ligands, or outer-sphere ET. An elegant and practical example is alcohol oxidation mediated by Cu and (2,2,6,6-tetramethylpiperidin-1-yl)oxyl (TEMPO), which has been widely studied under a variety of conditions.[330−336]

A general mechanism for this transformation, based on experimental and computational evidence, is depicted in Figure 70.

Another example of an aerobic oxidation with implications for ORR catalysis is the Co(salophen)-catalyzed oxidation of *p*-hydroquinone (H_2Q).[337] In this system, 2 equiv of H_2Q were oxidized per molecule of O_2 reduced, indicating the formation of H_2O as the ORR product. Experimental and computational analysis suggested a mechanism involving (i) O_2 binding to Co^{II}(salophen), (ii) HAT from H_2Q to Co^{III}-superoxide to form a hydrogen-bonded semiquinone/Co^{III}-hydroperoxo species, and (iii) turnover-limiting PCET to yield Co^{II}−H_2O_2 and benzoquinone (BQ). Two HAT steps using another equivalent of H_2Q were proposed to account for the formation of H_2O. With these results, the authors emphasize the importance of

DOI: 10.1021/acs.chemrev.7b00542
Chem. Rev. XXXX, XXX, XXX−XXX

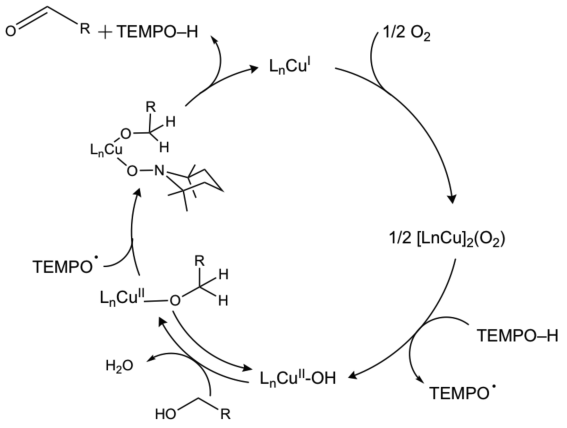

Figure 70. Proposed mechanism for Cu/TEMPO-catalyzed aerobic alcohol oxidation described in refs 330 and 335.

HAT and PCET reactions in promoting efficient ORR catalysis. There are many similarities between these systems and ORR catalysis, although such studies have traditionally not discussed overpotential or used electrochemical approaches.

The anthraquinone (AQ) process is the dominant industrial process for the production of H_2O_2 and is practiced on a very large scale.[12] The AQ process is a free-radical reaction of anthrahydroquinone (AHQ) with O_2 and involves the formation of a hydroxy-hydroperoxy intermediate (Figure 71). The oxidized

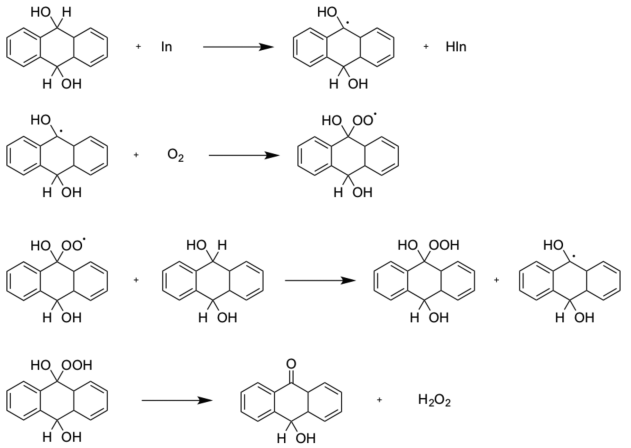

Figure 71. Mechanism of the anthraquinone process for the production of H_2O_2 from O_2, where In is a radical initiator; based on ref 12.

AQ is then typically hydrogenated back to AHQ in a separate vessel, with Pd or Ni catalysts.[338] Reduction of electrode-adsorbed AQ has also been attempted.[339] The AQ process generates very high yields of H_2O_2, but the side reactions and decay of AQ make this a less-than-ideal process. Alternative methods for H_2O_2 production from O_2, some using homogeneous catalysts, have also been explored.[12]

5. CONCLUSIONS

Studies of *homogeneous* ORR catalysis provide important insights that complement studies of heterogeneous ORR electrocatalysts that are closer to current technologies. The use of well-defined molecular species in solution allows precise synthetic control of catalyst properties and facilitates mechanistic studies that reveal the specific rate- and selectivity-determining steps. Traditional analysis of molecular ORR catalysts has involved their adsorption onto an electrode surface; however, investigating these catalysts in solution allows for observation and characterization of reaction intermediates. For solubility reasons, homogeneous ORR catalysts are often evaluated in nonaqueous solutions. The thermochemistry of ORR in both aqueous and nonaqueous solutions is presented (section 2). These data, coupled with the advances in evaluating ORR efficiency (section 2.5), have enabled a more rigorous comparison of catalytic systems. As a result, a more complete understanding of the thermodynamic and kinetic parameters governing the individual mechanistic steps can be developed. The fundamental knowledge gained from these studies provides valuable insight into structure–activity relationships and other approaches to design more efficient ORR catalytic systems.

As summarized earlier, oxygen reduction catalysis can proceed by one of two pathways: via initial outer-sphere electron transfer (ET) to O_2 to form superoxide, $O_2^{\bullet-}$ (section 3), or via initial O_2 binding to a reduced metal center to form a M–O_2 adduct, a type of inner-sphere ET (section 4). Outer-sphere ORR processes are often marked by low efficiencies (high overpotentials) because they often require highly reducing electrode potentials or strong chemical reductants to form $O_2^{\bullet-}$. The final product of outer-sphere ORR processes is typically HO_2^- or H_2O_2 and is largely influenced by reaction conditions, such as solvent, proton source, and the presence of Lewis acids or hydrogen-bonding groups. The vast majority of molecular ORR catalysts proceed via an inner-sphere mechanism, with the most common catalysts being iron and cobalt complexes of N_4 macrocycles. The iron macrocycles are often quite selective for the $4H^+/4e^-$ reduction to H_2O, while the cobalt macrocycles primarily produce H_2O_2. A number of catalysts with nonmacrocyclic ligands have been reported, particularly of manganese and copper. Reports of ORR catalysis with complexes of group Vb and VIb metals or noble metals are limited. However, palladium complexes are commonly used in aerobic oxidation reactions, which are inherently ORR processes even though the focus of these studies is oxidation of the organic substrate.

The performance of molecular ORR catalysts can be evaluated by a number of metrics: rate, selectivity, overpotential, and longevity (section 2.5). Comparisons between catalysts are often challenging due to the wide variety of solvents, acids, and reductants used in ORR catalysis (Tables 11–17). Molecular Tafel plots, which describe a catalyst's TOF as a function of applied potential, were developed by Artero and Savéant to evaluate homogeneous H_2 evolution catalysts[64] but have since been applied to the analysis of CO_2 and O_2 reduction catalysts.[340] Unlike heterogeneous electrocatalysts, the TOF of an ideal homogeneous catalyst reaches a maximum at potentials beyond the catalyst $E_{1/2}$, termed TOF_{max}. Analysis of this TOF_{max} for a series of Fe porphyrin ORR catalysts revealed a linear scaling relationship between this parameter and the overpotential.[66] A more recent publication showed that these linear correlations depend predictably on the experimental parameter varied, whether that be the catalyst $E_{1/2}$, acid pK_a, or concentrations of reactants and products.[85] These and similar methods allow different catalytic ORR systems to be compared, so we encourage authors to apply this analysis to their systems. Careful comparisons among different systems should enable better understanding of how the catalyst and the medium can be tuned to achieve higher ORR efficiency and activity.

DOI: 10.1021/acs.chemrev.7b00542
Chem. Rev. XXXX, XXX, XXX–XXX

AUTHOR INFORMATION

Corresponding Author

*E-mail: james.mayer@yale.edu.

ORCID

Michael L. Pegis: 0000-0001-6686-1717
James M. Mayer: 0000-0002-3943-5250

Author Contributions

†M.L.P. and C.F.W. contributed equally.

Notes

The authors declare no competing financial interest.

Biographies

Michael L. Pegis received his B.S. in Chemistry from Western Washington University in 2012. During his time at Western Washington, he carried out research in Professor John Gilbertson's lab, where he prepared carbon-supported ruthenium and nickel-phosphide nanoparticles for the conversion of cellulosic biomass to sugars. After graduating as a Paul Woodring scholar and student commencement speaker, he began his graduate work in the laboratory of Professor James Mayer at the University of Washington, and then moved to Yale University in 2014. Since 2012, he has worked on molecular systems for electrocatalytic oxygen reduction as part of the Center for Molecular Electrocatalysis. His research interests include electro- and photoelectrocatalytic small-molecule activations.

Catherine F. Wise was born and raised in Richmond, Virginia, and received a B.S. in Chemistry from the College of William and Mary in 2015. She performed undergraduate research with Professor William McNamara, developing nickel catalysts for photo- and electrocatalytic hydrogen generation. Currently, Catherine is a graduate student in the group of Professor James Mayer at Yale University and studies molecular systems for electrocatalytic oxygen reduction and alcohol oxidation.

Daniel J. Martin was born in Johnson City, NY, in 1993 and raised in Charlotte, NC. He received his B.S. in Chemistry with Highest Honors from The University of North Carolina at Chapel Hill in 2015, where he worked with Professor Jillian L. Dempsey on homogeneous electrocatalysts for H_2 production. Currently at Yale University, he works with Professor James M. Mayer on studies of molecular electrocatalysts for the oxygen reduction reaction as a NSF Graduate Research Fellow.

James M. Mayer was born in New York City in 1958 and did undergraduate research at Hunter College CUNY with Edwin Abbott and with William Klemperer while earning his A.B. at Harvard University. He completed a Ph.D. at Caltech under the direction of John Bercaw in 1982. After being a Visiting Scientist at DuPont Central Research and Development for two years, he accepted a faculty position at the University of Washington in Seattle, where he rose through the ranks. In 2014, he moved to Yale University, where he is now the Charlotte Fitch Roberts Professor of Chemistry. His research in redox chemical reactions span inorganic, bioinorganic, organometallic, and physical organic chemistry as well as chemistry at the nanoscale.

ACKNOWLEDGMENTS

This research was supported as part of the Center for Molecular Electrocatalysis, an Energy Frontier Research Center funded by the U.S. Department of Energy, Office of Science, Office of Basic Energy Sciences, and has been tremendously stimulated by interactions among the members of the Center. D.J.M. has been supported since July 2017 by a Graduate Research Fellowship from the National Science Foundation.

ABBREVIATIONS

η	overpotential
η_{eff}	effective overpotential
$2H^+/2e^-$	two proton/two electron
$4H^+/4e^-$	four proton/four electron
ABTS	2,2′-azino-bis-3-ethylbenzothiazoline sulfonate
AcOH	acetic acid
AHQ	anthrahydroquinone
AQ	anthraquinone
BAr^F_4	tetrakis(pentafluorophenyl)borate
BDFE	bond dissociation free energy
Br_2Fc	1,1′-dibromoferrocene
BQ	benzoquinone
C*c*O	cytochrome *c* oxidase
CPET	concerted proton electron transfer
CRRFC	chemically regenerated redox fuel cell
CV	cyclic voltammetry
DCB	1,2-dichlorobenzene
DCE	1,2-dichloroethane
DCM	dichloromethane
DDT	dithiothreitol
DFT	density functional theory
DMA	*N*,*N*-dimethylacetamide
DMF	*N*,*N*-dimethylformamide
DMSO	dimethyl sulfoxide
DPH	diphenylhydrazine
$E^\circ_{O_2/H_2O(X)}$	standard potential for O_2/H_2O in solvent X
EPR	electron paramagnetic resonance
ET	electron transfer
EtOH	ethanol
Fc	ferrocene
GC	glassy carbon electrode
HAT	hydrogen atom transfer
HB	hydrogen-bond assisted
$HO_2^\bullet$	perhydroxyl
HOTf	triflic acid, CF_3SO_3H
$HBAr^F_4$	tetrakis(pentafluorophenyl)boric acid, $[H(Et_2O)_2]$-$[B(C_6F_5)_4]$
^{i}PrOH	2-propanol
MCD	magnetic circular dichroism
MCET	metal-ion coupled electron transfer
$Me_{10}Fc$	decamethylferrocene
Me_2Fc	1,1′-dimethylferrocene
Me_8Fc	octamethylferrocene
MeCN	acetonitrile
MeOH	methanol
MV^{2+}	methylviologen dication
NHE	normal hydrogen electrode
O_2	dioxygen
O^{2-}	oxide
$O_2^{\bullet-}$	superoxide
OAT	oxygen atom transfer
OEP	octaethylporphyrin
ORR	oxygen reduction reaction
OTf^-	triflate anion, $CF_3SO_3^-$
P	porphyrin
Pc	phthalocyanine
PCET	proton-coupled electron transfer
PhCl	chlorobenzene
PhCN	benzonitrile
$PhCO_2H$	benzoic acid
$PhNH_3^+$	anilinium

AQ

PhO^-	phenolate
PhOH	phenol
PI	proton-initiated
PT	proton transfer
*p*TsOH	*p*-toluenesulfonic acid
PyH^+	pyridinium cation
RHE	regular hydrogen electrode
ROS	reactive oxygen species
RRDV	rotating ring disk voltammetry
SCE	saturated calomel electrode
SECM	scanning electrochemical microscopy
SHE	standard hydrogen electrode
TFA	trifluoroacetic acid
THF	tetrahydrofuran
TMPA	tris(2-pyridylmethyl)amine
TMPyP	5,10,15,20-tetrakis(*N*-methylpyridyl)porphyrin
TOF	turnover frequency
TOF_{max}	maximum turnover frequency
TON	turnover number
TPP	5,10,15,20-tetraphenylporphyrin
TTF	tetrathiafulvalene

REFERENCES

(1) Berg, J. M.; Tymoczko, J. L.; Stryer, L. *Biochemistry*, 4th ed.; Palgrave Macmillan: 1988.

(2) Weissermel, K.; Arpe, H.-J. *Industrial Organic Chemistry*, 3rd ed.; VCH Publishers, Inc.: New York, 1997.

(3) Olah, G. A.; Molnar, A. Oxidation-Oxygenation. In *Hydrocarbon Chemistry*; John Wiley & Sons, Inc.: New York, 1995; pp 291−413.

(4) Yoshikawa, S.; Shimada, A. Reaction Mechanism of Cytochrome *c* Oxidase. *Chem. Rev.* **2015**, *115*, 1936−1989.

(5) Gewirth, A. A.; Varnell, J. A.; DiAscro, A. M. Non-Precious Metal Catalysts for Oxygen Reduction in Heterogeneous Aqueous Systems. *Chem. Rev.* DOI: http://dx.doi.org/10.1021/acs.chemrev.7b00335.

(6) Costas, M.; Mehn, M. P.; Jensen, M. P.; Que, L. Dioxygen Activation at Mononuclear Nonheme Iron Active Sites: Enzymes, Models, and Intermediates. *Chem. Rev.* **2004**, *104*, 939−986.

(7) Collman, J. P.; Boulatov, R.; Sunderland, C. J.; Fu, L. Functional Analogues of Cytochrome *c* Oxidase, Myoglobin, and Hemoglobin. *Chem. Rev.* **2004**, *104*, 561−588.

(8) Collman, J. P. Synthetic Models for the Oxygen-Binding Hemoproteins. *Acc. Chem. Res.* **1977**, *10*, 265−272.

(9) Niederhoffer, E. C.; Timmons, J. H.; Martell, A. E. Thermodynamics of Oxygen Binding in Natural and Synthetic Dioxygen Complexes. *Chem. Rev.* **1984**, *84*, 137−203.

(10) Savéant, J.-M. Molecular Catalysis of Electrochemical Reactions. Mechanistic Aspects. *Chem. Rev.* **2008**, *108*, 2348−2378.

(11) Zhang, W.; Lai, W.; Cao, R. Energy-Related Small Molecule Activation Reactions: Oxygen Reduction and Hydrogen and Oxygen Evolution Reactions Catalyzed by Porphyrin- and Corrole-Based Systems. *Chem. Rev.* **2017**, *117*, 3717−3797.

(12) Campos-Martin, J. M.; Blanco-Brieva, G.; Fierro, J. L. G. Hydrogen Peroxide Synthesis: An Outlook beyond the Anthraquinone Process. *Angew. Chem., Int. Ed.* **2006**, *45*, 6962−6984.

(13) Russo, V.; Tesser, R.; Santacesaria, E.; Di Serio, M. Chemical and Technical Aspects of Propene Oxide Production via Hydrogen Peroxide (HPPO Process). *Ind. Eng. Chem. Res.* **2013**, *52*, 1168−1178.

(14) Collier, A.; Wang, H.; Zi Yuan, X.; Zhang, J.; Wilkinson, D. P. Degradation of Polymer Electrolyte Membranes. *Int. J. Hydrogen Energy* **2006**, *31*, 1838−1854.

(15) Valentine, J. S.; Foote, C. S.; Greenberg, A.; Liebman, J. F. *Active Oxygen in Biochemistry*; Valentine, J. S., Foote, C. S., Greenberg, A., Liebman, J. F., Eds.; Springer Science+Business Media: Dordrecht, The Netherlands, 1995.

(16) *Oxygen Radicals in Biology and Medicine*; Simic, M. G., Taylor, K. A., Ward, J. F., Von Sonntag, C., Eds.; Plenum Press: New York, 1988.

(17) Shao, M.; Chang, Q.; Dodelet, J.-P.; Chenitz, R. Recent Advances in Electrocatalysts for Oxygen Reduction Reaction. *Chem. Rev.* **2016**, *116*, 3594−3657.

(18) Dai, L.; Xue, Y.; Qu, L.; Choi, H.-J.; Baek, J.-B. Metal-Free Catalysts for Oxygen Reduction Reaction. *Chem. Rev.* **2015**, *115*, 4823−4892.

(19) Suntivich, J.; Gasteiger, H. A.; Yabuuchi, N.; Nakanishi, H.; Goodenough, J. B.; Shao-Horn, Y. Design Principles for Oxygen-Reduction Activity on Perovskite Oxide Catalysts for Fuel Cells and Metal−air Batteries. *Nat. Chem.* **2011**, *3*, 647−647.

(20) Kaila, V. R.; Verkhovsky, M. I.; Wikström, M. Proton-Coupled Electron Transfer in Cytochrome Oxidase. *Chem. Rev.* **2010**, *110*, 7062−7081.

(21) Thorum, M. S.; Anderson, C. A.; Hatch, J. J.; Campbell, A. S.; Marshall, N. M.; Zimmerman, S. C.; Lu, Y.; Gewirth, A. A. Direct, Electrocatalytic Oxygen Reduction by Laccase on Anthracene-2-Methanethiol-Modified Gold. *J. Phys. Chem. Lett.* **2010**, *1*, 2251−2254.

(22) Cracknell, J. A.; Vincent, K. A.; Armstrong, F. A. Enzymes as Working or Inspirational Electrocatalysts for Fuel Cells and Electrolysis. *Chem. Rev.* **2008**, *108*, 2439−2461.

(23) Chang, C. K.; Liang, Y.; Aviles, G.; Peng, S.-M. Conformational Control of Intramolecular Hydrogen Bonding in Heme Models: Maximal Co^{II}-O_2 Binding in a C-Clamp Porphyrin. *J. Am. Chem. Soc.* **1995**, *117*, 4191−4192.

(24) Mills, I.; Cvitas, T.; Homann, K.; Kallay, N.; Kuchitsu, K. *Quantities, Units and Symbols in Physical Chemistry*, 2nd ed.; Blackwell Science Ltd.: Oxford, U.K., 1993.

(25) Bratsch, S. Standard Electrode Potentials and Temperature Coefficients in Water at 298.15 K. *J. Phys. Chem. Ref. Data* **1989**, *18*, 1−21.

(26) Garsany, Y.; Baturina, O. A.; Swider-Lyons, K. E.; Kocha, S. S. Experimental Methods for Quantifying the Activity of Platinum Electrocatalysts for the Oxygen Reduction Reaction. *Anal. Chem.* **2010**, *82*, 6321−6328.

(27) Gritzner, G. Reference Redox Systems in Nonaqueous Systems and the Relation of Electrode Potentials in Nonaqueous and Mixed Solvents to Standard Potentials in Water. In *Handbook of Reference Electrodes*; Springer-Verlag: Berlin/Heidelberg, 2013; pp 25−32.

(28) Bard, A. J.; Faulkner, L. R. *Electrochemical Methods: Fundamentals and Application*, 2nd ed.; John Wiley & Sons, Inc.: New York, 2000.

(29) Pegis, M. L.; Roberts, J. A. S.; Wasylenko, D. J.; Mader, E. A.; Appel, A. M.; Mayer, J. M. Standard Reduction Potentials for Oxygen and Carbon Dioxide Couples in Acetonitrile and *N*,*N*-Dimethylformamide. *Inorg. Chem.* **2015**, *54*, 11883−11888.

(30) Roberts, J. A. S.; Bullock, R. M. Direct Determination of Equilibrium Potentials for Hydrogen Oxidation/Production by Open Circuit Potential Measurements in Acetonitrile. *Inorg. Chem.* **2013**, *52*, 3823−3835.

(31) Passard, G.; Ullman, A. M.; Brodsky, C. N.; Nocera, D. G. Oxygen Reduction Catalysis at a Dicobalt Center: The Relationship of Faradaic Efficiency to Overpotential. *J. Am. Chem. Soc.* **2016**, *138*, 2925−2928.

(32) Izutsu, K. *Acid-Base Dissociation Constants in Dipolar Aprotic Solvents*; Blackwell Scientific Publications: Oxford, U.K., 1990.

(33) Kütt, A.; Leito, I.; Kaljurand, I.; Sooväli, L.; Vlasov, V. M.; Yagupolskii, L. M.; Koppel, I. A. A Comprehensive Self-Consistent Spectrophotometric Acidity Scale of Neutral Brønsted Acids in Acetonitrile. *J. Org. Chem.* **2006**, *71*, 2829−2838.

(34) Bordwell, F. G. Equilibrium Acidities in Dimethyl Sulfoxide Solution. *Acc. Chem. Res.* **1988**, *21*, 456−463.

(35) McCarthy, B. D.; Martin, D. J.; Rountree, E. S.; Ullman, A. C.; Dempsey, J. L. Electrochemical Reduction of Brønsted Acids by Glassy Carbon in Acetonitrile-Implications for Electrocatalytic Hydrogen Evolution. *Inorg. Chem.* **2014**, *53*, 8350−8361.

(36) Appel, A. M.; Helm, M. L. Determining the Overpotential for a Molecular Electrocatalyst. *ACS Catal.* **2014**, *4*, 630−633.

(37) Fourmond, V.; Jacques, P. A.; Fontecave, M.; Artero, V. H_2 Evolution and Molecular Electrocatalysts: Determination of Overpotentials and Effect of Homoconjugation. *Inorg. Chem.* **2010**, *49*, 10338−10347.

DOI: 10.1021/acs.chemrev.7b00542
Chem. Rev. XXXX, XXX, XXX−XXX

(38) Wiedner, E. S.; Brown, H. J. S.; Helm, M. L. Kinetic Analysis of Competitive Electrocatalytic Pathways: New Insights into Hydrogen Production with Nickel Electrocatalysts. *J. Am. Chem. Soc.* **2016**, *138*, 604−616.
(39) Leito, I.; Kaljurand, I.; Koppel, I. A.; Yagupolskii, L. M.; Vlasov, V. M. Spectrophotometric Acidity Scale of Strong Neutral Bronsted Acids in Acetonitrile. *J. Org. Chem.* **1998**, *63*, 7868−7874.
(40) Elgrishi, N.; McCarthy, B. D.; Rountree, E. S.; Dempsey, J. L. Reaction Pathways of Hydrogen-Evolving Electrocatalysts: Electrochemical and Spectroscopic Studies of Proton-Coupled Electron Transfer Processes. *ACS Catal.* **2016**, *6*, 3644−3659.
(41) Fourmond, V.; Canaguier, S. S.; Golly, B.; Field, M. J.; Fontecave, M.; Artero, V. A Nickel−Manganese Catalyst as a Biomimic of the Active Site of NiFe Hydrogenases: A Combined Electrocatalytical and DFT Mechanistic Study. *Energy Environ. Sci.* **2011**, *4*, 2417.
(42) Izutsu, K. *Electrochemistry in Nonaqueous Solutions*, 2nd ed.; Wiley-VCH Verlag: 2009.
(43) Azcarate, I.; Costentin, C.; Robert, M.; Savéant, J.-M. Through-Space Charge Interaction Substituent Effects in Molecular Catalysis Leading to the Design of the Most Efficient Catalyst of CO_2-to-CO Electrochemical Conversion. *J. Am. Chem. Soc.* **2016**, *138*, 16639−16644.
(44) Gagné, R. R.; Koval, C. A.; Lisensky, G. C. Ferrocene as an Internal Standard for Electrochemical Measurements. *Inorg. Chem.* **1980**, *19*, 2854−2855.
(45) Noviandri, I.; Brown, K. N.; Fleming, D. S.; Gulyas, P. T.; Lay, P. A.; Masters, A. F.; Phillips, L. The Decamethylferrocenium/Decamethylferrocene Redox Couple: A Superior Redox Standard to the Ferrocenium/Ferrocene Redox Couple for Studying Solvent Effects on the Thermodynamics of Electron Transfer. *J. Phys. Chem. B* **1999**, *103*, 6713−6722.
(46) Pavlishchuk, V. V.; Addison, A. W. Conversion Constants for Redox Potentials Measured versus Different Reference Electrodes in Acetonitrile Solutions at 25°C. *Inorg. Chim. Acta* **2000**, *298*, 97−102.
(47) Astruc, D. Electrochemistry. In *Electron Transfer and Radical Processes in Transition-Metal Chemistry*; Wiley-VCH, Inc.: New York, 1995; pp 89−183.
(48) Connelly, N. G.; Geiger, W. E. Chemical Redox Agents for Organometallic Chemistry. *Chem. Rev.* **1996**, *96*, 877−910.
(49) Wallace, J. M.; Hobbs, P. V. *Atmospheric Science: An Introductory Survey*, 2nd ed.; Academic Press: Burlington, MA, 2006.
(50) Li, Q.; Batchelor-Mcauley, C.; Lawrence, N. S.; Hartshorne, R. S.; Compton, R. G. Anomalous Solubility of Oxygen in Acetonitrile/water Mixture Containing Tetra-*N*-Butylammonium Perchlorate Supporting Electrolyte; the Solubility and Diffusion Coefficient of Oxygen in Anhydrous Acetonitrile and Aqueous Mixtures. *J. Electroanal. Chem.* **2013**, *688*, 328−335.
(51) Sander, R. Henry's Law Constants. In *NIST Chemistry WebBook, NIST Standard Reference Database Number 69*; Linstrom, P. J., Mallard, W. G., Eds.; National Institutes of Standards and Technology: Gaithersburg, MD.
(52) Millero, F. J.; Huang, F. Solubility of Oxygen in Aqueous Solutions of KCl, K_2SO_4, and $CaCl_2$ as a Function of Concentration and Temperature. *J. Chem. Eng. Data* **2003**, *48*, 1050−1054.
(53) Valderrama, J. O.; Campusano, R. A.; Forero, L. A. A New Generalized Henry-Setschenow Equation for Predicting the Solubility of Air Gases (Oxygen, Nitrogen and Argon) in Seawater and Saline Solutions. *J. Mol. Liq.* **2016**, *222*, 1218−1227.
(54) Osterberg, P. M.; Niemeier, J. K.; Welch, C. J.; Hawkins, J. M.; Martinelli, J. R.; Johnson, T. E.; Root, T. W.; Stahl, S. S. Experimental Limiting Oxygen Concentrations for Nine Organic Solvents at Temperatures and Pressures Relevant to Aerobic Oxidations in the Pharmaceutical Industry. *Org. Process Res. Dev.* **2015**, *19*, 1537−1543.
(55) Battino, R.; Rettich, T. R.; Tominaga, T. The Solubility of Oxygen and Ozone in Liquids. *J. Phys. Chem. Ref. Data* **1983**, *12*, 163−178.
(56) Sawyer, D.; Chiericato, G. J.; Angelis, C. T.; Nanni, J.; Tsuchiya, T. Effects of Media and Electrode Materials on the Electrochemical Reduction of Dioxygen. *Anal. Chem.* **1982**, *54*, 1720−1724.
(57) James, H. J.; Broman, R. F. Modified Winkler Determination of Oxygen in Dimethylformamide: Oxygen Solubility as a Function of Partial Pressure. *Anal. Chim. Acta* **1969**, *48*, 411−417.
(58) Bertini, I.; Gray, H. B.; Lippard, S. J.; Valentine, J. S. Dioxygen Reactions. In *Bioinorganic Chemistry*; University Science Books: 1994; pp 253−313.
(59) Sawyer, D. T. The Redox Thermodynaics for Dioxygen Species (O_2, O_2^{-}, ·OH, and $^{-}$OH) in Water and Aprotic Solvents. In *Oxygen Radicals in Biology and Medicine*; Plenum Press: New York, 1988; pp 11−20.
(60) Warren, J. J.; Tronic, T. A.; Mayer, J. M. Thermochemistry of Proton-Coupled Electron Transfer Reagents and Its Implications. *Chem. Rev.* **2010**, *110*, 6961−7001.
(61) Sawyer, D. T. *Oxygen Chemistry*; Oxford University Press, Inc.: New York, 1991.
(62) *CRC Handbook of Chemistry and Physics*, 94th ed.; Haynes, W. M., Ed.; CRC Press: Boca Raton, FL, 2013; Vol. *53*.
(63) Waidmann, C. R.; Miller, A. J. M.; Ng, C.-W. A.; Scheuermann, M. L.; Porter, T. R.; Tronic, T. A.; Mayer, J. M. Using Combinations of Oxidants and Bases as PCET Reactants: Thermochemical and Practical Considerations. *Energy Environ. Sci.* **2012**, *5*, 7771.
(64) Artero, V.; Savéant, J.-M. Toward the Rational Benchmarking of Homogeneous H_2-Evolving Catalysts. *Energy Environ. Sci.* **2014**, *7*, 3808−3814.
(65) Costentin, C.; Drouet, S.; Robert, M.; Savéant, J.-M. Turnover Numbers, Turnover Frequencies, and Overpotential in Molecular Catalysis of Electrochemical Reactions. Cyclic Voltammetry and Preparative-Scale Electrolysis. *J. Am. Chem. Soc.* **2012**, *134*, 11235−11242.
(66) Pegis, M. L.; McKeown, B. A.; Kumar, N.; Lang, K.; Wasylenko, D. J.; Zhang, X. P.; Raugei, S.; Mayer, J. M. Homogenous Electrocatalytic Oxygen Reduction Rates Correlate with Reaction Overpotential in Acidic Organic Solutions. *ACS Cent. Sci.* **2016**, *2*, 850−856.
(67) Helm, M. L.; Stewart, M. P.; Bullock, R. M.; DuBois, M. R.; DuBois, D. L. A Synthetic Nickel Electrocatalyst with a Turnover Frequency Above 100,000 s^{-1} for H_2 Production. *Science* **2011**, *333*, 863−866.
(68) Hoffert, W. A.; Roberts, J. A. S.; Bullock, R. M.; Helm, M. L. Production of H_2 at Fast Rates Using a Nickel Electrocatalyst in Water-Acetonitrile Solutions. *Chem. Commun.* **2013**, *49*, 7767−7769.
(69) Costentin, C.; Passard, G.; Savéant, J. M. Benchmarking of Homogeneous Electrocatalysts: Overpotential, Turnover Frequency, Limiting Turnover Number. *J. Am. Chem. Soc.* **2015**, *137*, 5461−5467.
(70) Costentin, C.; Savéant, J.-M. Multielectron, Multistep Molecular Catalysis of Electrochemical Reactions: Benchmarking of Homogeneous Catalysts. *ChemElectroChem* **2014**, *1*, 1226−1236.
(71) Carver, C. T.; Matson, B. D.; Mayer, J. M. Electrocatalytic Oxygen Reduction by Iron Tetra-Arylporphyrins Bearing Pendant Proton Relays. *J. Am. Chem. Soc.* **2012**, *134*, 5444−5447.
(72) Matson, B. D.; Carver, C. T.; Von Ruden, A.; Yang, J. Y.; Raugei, S.; Mayer, J. M. Distant Protonated Pyridine Groups in Water-Soluble Iron Porphyrin Electrocatalysts Promote Selective Oxygen Reduction to Water. *Chem. Commun.* **2012**, *48*, 11100−11102.
(73) Wasylenko, D. J.; Rodríguez, C.; Pegis, M. L.; Mayer, J. M. Direct Comparison of Electrochemical and Spectrochemical Kinetics for Catalytic Oxygen Reduction. *J. Am. Chem. Soc.* **2014**, *136*, 12544−12547.
(74) Rountree, E. S.; McCarthy, B. D.; Eisenhart, T. T.; Dempsey, J. L. Evaluation of Homogeneous Electrocatalysts by Cyclic Voltammetry. *Inorg. Chem.* **2014**, *53*, 9983−10002.
(75) Fukuzumi, S.; Okamoto, K.; Gros, C. P.; Guilard, R. Mechanism of Four-Electron Reduction of Dioxygen to Water by Ferrocene Derivatives in the Presence of Perchloric Acid in Benzonitrile, Catalyzed by Cofacial Dicobalt Porphyrins. *J. Am. Chem. Soc.* **2004**, *126*, 10441−10449.
(76) Honda, T.; Kojima, T.; Fukuzumi, S. Proton-Coupled Electron-Transfer Reduction of Dioxygen Catalyzed by a Saddle-Distorted Cobalt Phthalocyanine. *J. Am. Chem. Soc.* **2012**, *134*, 4196−4206.

DOI: 10.1021/acs.chemrev.7b00542
Chem. Rev. XXXX, XXX, XXX−XXX

(77) Das, D.; Lee, Y. M.; Ohkubo, K.; Nam, W.; Karlin, K. D.; Fukuzumi, S. Temperature-Independent Catalytic Two-Electron Reduction of Dioxygen by Ferrocenes with a Copper(II) tris[2-(2-Pyridyl)ethyl]amine Catalyst in the Presence of Perchloric Acid. *J. Am. Chem. Soc.* **2013**, *135*, 2825−2834.
(78) Tian, F.; Anderson, A. B. Effective Reversible Potential, Energy Loss, and Overpotential on Platinum Fuel Cell Cathodes. *J. Phys. Chem. C* **2011**, *115*, 4076−4088.
(79) Christensen, R.; Hansen, H. A.; Dickens, C. F.; Nørskov, J. K.; Vegge, T. Functional Independent Scaling Relation for ORR/OER Catalysts. *J. Phys. Chem. C* **2016**, *120*, 24910−24916.
(80) Plessow, P. N.; Abild-Pedersen, F. Examining the Linearity of Transition State Scaling Relations. *J. Phys. Chem. C* **2015**, *119*, 10448−10453.
(81) Hansen, J.; Platten, F.; Wagner, D.; Egelhaaf, S. U. Tuning Protein−protein Interactions by Cosolvents: Specific Effects of Ionic and Non-Ionic Additives on Protein Phase Behavior. *Phys. Chem. Chem. Phys.* **2016**, *18*, 10270−10280.
(82) Ramaswamy, N.; Tylus, U.; Jia, Q.; Mukerjee, S. Activity Descriptor Identification for Oxygen Reduction on Nonprecious Electrocatalysts: Linking Surface Science to Coordination Chemistry. *J. Am. Chem. Soc.* **2013**, *135*, 15443−15449.
(83) Koper, M. T. M. Theory of Multiple Proton−Electron Transfer Reactions and Its Implications for Electrocatalysis. *Chem. Sci.* **2013**, *4*, 2710.
(84) Barros, W. R. P.; Ereno, T.; Tavares, A. C.; Lanza, M. R. V. In Situ Electrochemical Generation of Hydrogen Peroxide in Alkaline Aqueous Solution by Using an Unmodified Gas Diffusion Electrode. *ChemElectroChem* **2015**, *2*, 714−719.
(85) Pegis, M. L.; Wise, C. F.; Koronkiewicz, B.; Mayer, J. M. Identifying and Breaking Scaling Relationships for Molecular Catalysis of Electrochemical Reactions. *J. Am. Chem. Soc.* **2017**, *139*, 11000−11003.
(86) Fukuzumi, S.; Ohkubo, K. Metal Ion-Coupled and Decoupled Electron Transfer. *Coord. Chem. Rev.* **2010**, *254*, 372−385.
(87) Fukuzumi, S.; Ohkubo, K.; Morimoto, Y. Mechanisms of Metal Ion-Coupled Electron Transfer. *Phys. Chem. Chem. Phys.* **2012**, *14*, 8472−8484.
(88) Hayyan, M.; Hashim, M. A.; Alnashef, I. M. Superoxide Ion: Generation and Chemical Implications. *Chem. Rev.* **2016**, *116*, 3029−3085.
(89) Ho, R. Y. N.; Liebman, J. F.; Valentine, J. S. Overview of Energetics and Reactivity of Oxygen. In *Active Oxygen in Chemistry*; Foote, C. S., Valentine, J. S., Greenberg, A., Liebman, J. F., Eds.; Blackie Academic & Professional: Glasgow, 1996; pp 1−23.
(90) Stanbury, D.; Haas, O.; Taube, H. Reduction of Oxygen by Ruthenium (II) Ammines. *Inorg. Chem.* **1980**, *19*, 518−524.
(91) Bielski, B. H. J.; Cabelli, D. E.; Arudi, R. L.; Ross, A. B. Reactivity of HO_2/O_2^- Radicals in Aqueous Solution. *J. Phys. Chem. Ref. Data* **1985**, *14*, 1041−1100.
(92) Bielski, B. H. J.; Gebicki, J. M. Species in Irradiated Oxygenated Water. *Adv. Radiat. Chem.* **1970**, *2*, 177−279.
(93) McDowell, M. S.; Bakac, A.; Espenson, J. H. A Convenient Route to Superoxide Ion in Aqueous Solution. *Inorg. Chem.* **1983**, *22*, 847−848.
(94) Stanbury, D. M.; Mulac, W. A.; Sullivan, J. C.; Taube, H. Superoxide Reactions with (isonicotinamide)pentaammineruthenium-(II) and (III). *Inorg. Chem.* **1980**, *19*, 3735−3740.
(95) McDowell, M. S.; Espenson, J. H.; Bakac, A. Kinetics of Aqueous Outer-Sphere Electron-Transfer Reactions of Superoxide Ion. Implications Concerning the O_2/O_2^- Self-Exchange Rate Constant. *Inorg. Chem.* **1984**, *23*, 2232−2236.
(96) Zahir, K.; Espenson, J. H.; Bakac, A. Reactions of Polypyridylchromium(II) Ions with Oxygen: Determination of the Self-Exchange Rate Constant of O_2/O_2^-. *J. Am. Chem. Soc.* **1988**, *110*, 5059−5063.
(97) Lind, J.; Shen, X.; Merenyi, G.; Jonsson, B. O. Determination of the Rate Constant of Self-Exchange of the Oxygen O_2/O_2^- Couple in Water by $^{18}O/^{16}O$ Isotope Marking. *J. Am. Chem. Soc.* **1989**, *111*, 7654−7655.
(98) Roth, J. P.; Wincek, R.; Nodet, G.; Edmondson, D. E.; McIntire, W. S.; Klinman, J. P. Oxygen Isotope Effects on Electron Transfer to O_2 Probed Using Chemically Modified Flavins Bound to Glucose Oxidase. *J. Am. Chem. Soc.* **2004**, *126*, 15120−15131.
(99) Roth, J. P. Oxygen Isotope Effects as Probes of Electron Transfer Mechanisms and Structures of Activated O_2. *Acc. Chem. Res.* **2009**, *42*, 399−408.
(100) Weinstock, I. A. Outer-Sphere Oxidation of the Superoxide Radical Anion. *Inorg. Chem.* **2008**, *47*, 404−406.
(101) Snir, O.; Weinstock, I. A. Complexity in Chemistry and Beyond: Interplay Theory and Experiment. In *Complexity in Chemistry and Beyond: Interplay Theory and Experiment, NATO Science for Peace and Security Series B: Physics and Biophysics*; Hill, C., Musaev, D. G., Eds.; Springer Science+Business Media: Dordrecht, Netherlands, 2012; pp 207−228.
(102) Stanbury, D. M.; Gaswick, D.; Brown, G. M.; Taube, H. Autoxidation of Binuclear Ruthenium(II) Ammines. *Inorg. Chem.* **1983**, *22*, 1975−1982.
(103) Lopez, N.; Graham, D. J.; Mcguire, R.; Alliger, G. E.; Shao-Horn, Y.; Cummins, C. C.; Nocera, D. G. Reversible Reduction of Oxygen to Peroxide Facilitated by Molecular Recognition. *Science* **2012**, *335*, 450−453.
(104) Ullman, A. M.; Sun, X.; Graham, D. J.; Lopez, N.; Nava, M.; De Las Cuevas, R.; Müller, P.; Rybak-Akimova, E. V.; Cummins, C. C.; Nocera, D. G. Electron-Transfer Studies of a Peroxide Dianion. *Inorg. Chem.* **2014**, *53*, 5384−5391.
(105) Anderson, B. L.; Maher, A. G.; Nava, M.; Lopez, N.; Cummins, C. C.; Nocera, D. G. Ultrafast Photoinduced Electron Transfer from Peroxide Dianion. *J. Phys. Chem. B* **2015**, *119*, 7422−7429.
(106) Bernhard, P.; Anson, F. C. Hydrogen Atom Abstraction from Amine Complexes of Iron(II), Cobalt(II), and Ruthenium(II) by Superoxide: Influence of Driving Force on Rate. *Inorg. Chem.* **1988**, *27*, 4574−4577.
(107) Bernhard, P.; Sargeson, A. M.; Anson, F. C. Autoxidation of the (Sarcophagine)ruthenium(2+) Complex Involving Hydrogen Atom Transfer to O_2^-. *Inorg. Chem.* **1988**, *27*, 2754.
(108) Bisselink, R. J. M.; van Erkel, J. *Electrochemical Production of Hydrogen Peroxide*. U.S. Patent 20160222527, 2014.
(109) Kinoshita, K. *Electrochemical Oxygen Technology*; Wiley-Interscience: New York, 1992.
(110) Siahrostami, S.; Verdaguer-Casadevall, A.; Karamad, M.; Deiana, D.; Malacrida, P.; Wickman, B.; Escudero-Escribano, M.; Paoli, E. A.; Frydendal, R.; Hansen, T. W.; et al. Enabling Direct H_2O_2 Production through Rational Electrocatalyst Design. *Nat. Mater.* **2013**, *12*, 1137−1143.
(111) Jirkovský, J. S.; Panas, I.; Ahlberg, E.; Halasa, M.; Romani, S.; Schiffrin, D. J. Single Atom Hot-Spots at Au-Pd Nanoalloys for Electrocatalytic H_2O_2 Production. *J. Am. Chem. Soc.* **2011**, *133*, 19432−19441.
(112) Fellinger, T.-P.; Hasché, F.; Strasser, P.; Antonietti, M. Mesoporous Nitrogen-Doped Carbon for the Electrocatalytic Synthesis of Hydrogen Peroxide. *J. Am. Chem. Soc.* **2012**, *134*, 4072−4075.
(113) Rosso, K. M.; Morgan, J. J. Outer-Sphere Electron Transfer Kinetics of Metal Ion Oxidation by Molecular Oxygen. *Geochim. Cosmochim. Acta* **2002**, *66*, 4223−4233.
(114) Andrieux, C. P.; Hapiot, P.; Savéant, J.-M. Mechanism of Superoxide Ion Disproportionation in Aprotic Solvents. *J. Am. Chem. Soc.* **1987**, *109*, 3768−3775.
(115) Peover, M. E.; White, B. S. Electrolytic Reduction of Oxygen in Aprotic Solvents: The Superoxide Ion. *Electrochim. Acta* **1966**, *11*, 1061−1067.
(116) Sawyer, D. T.; Roberts, J. L. Electrochemistry of Oxygen and Superoxide Ion in Dimethylsulfoxide at Platinum, Gold and Mercury Electrodes. *J. Electroanal. Chem.* **1966**, *12*, 90−101.
(117) Costentin, C.; Robert, M.; Savéant, J.-M. Acceleration of the Homogeneous and Electrochemical Reductions of Dioxygen in Aprotic Media by Ammonium Ions. Is the Driving Force a Function of NH_4^+

DOI: 10.1021/acs.chemrev.7b00542
Chem. Rev. XXXX, XXX, XXX−XXX

Concentration? What Is the Mechanism of the Reaction? *J. Phys. Chem. C* **2007**, *111*, 12877−12880.
(118) Chin, D. H.; Chiericato, G.; Nanni, E. J.; Sawyer, D. T. Proton-Induced Disproportionation of Superoxide Ion in Aprotic Media. *J. Am. Chem. Soc.* **1982**, *104*, 1296−1299.
(119) Cofré, P.; Sawyer, D. T. Electrochemical Reduction of Dioxygen to Perhydroxyl ($HO_2^{\bullet}$) in Aprotic Solvents That Contain Brønsted Acids. *Anal. Chem.* **1986**, *58*, 1057−1062.
(120) Ohkubo, K.; Kitaguchi, H.; Fukuzumi, S. Activation of Electron-Transfer Reduction of Oxygen by Hydrogen Bond Formation of Superoxide Anion with Ammonium Ion. *J. Phys. Chem. A* **2006**, *110*, 11613−11616.
(121) Sawyer, D. T.; Seo, E. T. One-Electron Mechanism for the Electrochemical Reduction of Molecular Oxygen. *Inorg. Chem.* **1977**, *16*, 499−501.
(122) Goolsby, A. D.; Sawyer, D. T. The Electrochemical Reduction of Superoxide Ion and Oxidation of Hydroxide Ion in Dimethyl Sulfoxide. *Anal. Chem.* **1968**, *40*, 83−86.
(123) Vasudevan, D.; Wendt, H. Electroreduction of Oxygen in Aprotic Media. *J. Electroanal. Chem.* **1995**, *392*, 69−74.
(124) Costentin, C.; Evans, D. H.; Robert, M.; Savéant, J.-M.; Singh, P. S. Electrochemical Approach to Concerted Proton and Electron Transfers. Reduction of the Water-Superoxide Ion Complex. *J. Am. Chem. Soc.* **2005**, *127*, 12490−12491.
(125) Singh, P. S.; Evans, D. H. Study of the Electrochemical Reduction of Dioxygen in Acetonitrile in the Presence of Weak Acids. *J. Phys. Chem. B* **2006**, *110*, 637−644.
(126) Savéant, J.-M. Electrochemical Concerted Proton and Electron Transfers. Further Insights in the Reduction Mechanism of Superoxide Ion in the Presence of Water and Other Weak Acids. *J. Phys. Chem. C* **2007**, *111*, 2819−2822.
(127) Dronov, R.; Kurth, D. G.; Scheller, F. W.; Lisdat, F. Direct and Cytochrome *c* Mediated Electrochemistry of Bilirubin Oxidase on Gold. *Electroanalysis* **2007**, *19*, 1642−1646.
(128) Dequaire, M.; Limoges, B.; Moiroux, J.; Savéant, J.-M. Mediated Electrochemistry of Horseradish Peroxidase. Catalysis and Inhibition. *J. Am. Chem. Soc.* **2002**, *124*, 240−253.
(129) Katz, E.; Shipway, A. N.; Willner, I. Mediated Electron-Transfer Between Redox-Enzymes and Electrode Supports. *Encyclopedia of Electrochemistry*; Wiley-VCH Verlag: 2007.
(130) Andrieux, C. P.; Hapiot, P.; Savéant, J.-M. Electron Transfer Coupling of Diffusional Pathways Homogeneous Redox Catalysis of Dioxygen Reduction By the Methylviologen Cation Radical in Acidic Dimethylsulfoxide. *J. Electroanal. Chem. Interfacial Electrochem.* **1985**, *189*, 121−133.
(131) Savéant, J.-M.; Su, K. B. Homogeneous Redox Catalysis of Electrochemical Reaction. *J. Electroanal. Chem. Interfacial Electrochem.* **1984**, *171*, 341−349.
(132) Costentin, C.; Robert, M.; Savéant, J.-M. Molecular Catalysis of Electrochemical Reactions. *Curr. Opin. Electrochem.* **2017**, *2*, 26−31.
(133) Audebert, P.; Hapiot, P. Preparation and Electrochemistry of Several Substituted 9-(4-R-phenyl)-*N*-methylacridinium Salts. Kinetic Analysis of the O_2 Catalytic Reduction in Acidic Dimethylsulfoxide and in Hydrophobic Nafion Gels. *J. Electroanal. Chem.* **1993**, *361*, 177−183.
(134) Evans, R. G.; Klymenko, O. V.; Saddoughi, S. A.; Hardacre, C.; Compton, R. G. Electroreduction of Oxygen in a Series of Room Temperature Ionic Liquids Composed of Group 15-Centered Cations and Anions. *J. Phys. Chem. B* **2004**, *108*, 7878−7886.
(135) René, A.; Hauchard, D.; Lagrost, C.; Hapiot, P. Superoxide Protonation by Weak Acids in Imidazolium Based Ionic Liquids. *J. Phys. Chem. B* **2009**, *113*, 2826−2831.
(136) Switzer, E. E.; Zeller, R.; Chen, Q.; Sieradzki, K.; Buttry, D. A.; Friesen, C. Oxygen Reduction Reaction in Ionic Liquids: The Addition of Protic Species. *J. Phys. Chem. C* **2013**, *117*, 8683−8690.
(137) Katayama, Y.; Onodera, H.; Yamagata, M.; Miura, T. Electrochemical Reduction of Oxygen in Some Hydrophobic Room-Temperature Molten Salt Systems. *J. Electrochem. Soc.* **2004**, *151*, A59.
(138) Yuan, X.-Z.; Alzate, V.; Xie, Z.; Ivey, D. G.; Dy, E.; Qu, W. Effect of Water and Dimethyl Sulfoxide on Oxygen Reduction Reaction in Bis(trifluoromethanesulfonyl)imide-Based Ionic Liquids. *J. Electrochem. Soc.* **2014**, *161*, A458−A466.
(139) Mayer, U.; Gutmann, V.; Gerger, W. The Acceptor Number - A Quantitative Empirical Parameter for the Electrophilic Properties of Solvents. *Monatsh. Chem.* **1975**, *106*, 1235−1257.
(140) Endicott, J. F.; Schroeder, R. R.; Chidester, D. H.; Ferrier, D. R. Correlation of Homogeneous Self-Exchange and Electrochemical Rate Data. Further Evidence for Anomalously Low Reorganizational Barriers in Electron Transfer Reactions of Cobalt Complexes. *J. Phys. Chem.* **1973**, *77*, 2579−2583.
(141) Prins, R.; Kortbeek, A. G. T. G. Electron Spin Resonance Spectra of Ferrocenium. *J. Organomet. Chem.* **1971**, *33*, C33−C34.
(142) Curphey, T. J.; Santer, J. O.; Rosenblum, M.; Richards, J. H. Protonation of Metallocenes by Strong Acids. Structure of the Cation. *J. Am. Chem. Soc.* **1960**, *82*, 5249−5250.
(143) Su, B.; Hatay, I.; Ge, P. Y.; Mendez, M.; Corminboeuf, C.; Samec, Z.; Ersoz, M.; Girault, H. H. Oxygen and Proton Reduction by Decamethylferrocene in Non-Aqueous Acidic Media. *Chem. Commun.* **2010**, *46*, 2918−2919.
(144) Su, B.; Nia, R. P.; Li, F.; Hojeij, M.; Prudent, M.; Corminboeuf, C.; Samec, Z.; Girault, H. H. H_2O_2 Generation by Decamethylferrocene at a Liquid|liquid Interface. *Angew. Chem., Int. Ed.* **2008**, *47*, 4675−4678.
(145) Deng, H.; Peljo, P.; Cortés-Salazar, F.; Ge, P.; Kontturi, K.; Girault, H. H. Oxygen and Hydrogen Peroxide Reduction by 1,2-diferrocenylethane at a Liquid/Liquid Interface. *J. Electroanal. Chem.* **2012**, *681*, 16−23.
(146) Su, B.; Hatay, I.; Li, F.; Partovi-Nia, R.; Méndez, M. A.; Samec, Z.; Ersoz, M.; Girault, H. H. Oxygen Reduction by Decamethylferrocene at Liquid/liquid Interfaces Catalyzed by Dodecylaniline. *J. Electroanal. Chem.* **2010**, *639*, 102−108.
(147) Jane Stockmann, T.; Deng, H.; Peljo, P.; Kontturi, K.; Opallo, M.; Girault, H. H. Mechanism of Oxygen Reduction by Metallocenes near Liquid|liquid Interfaces. *J. Electroanal. Chem.* **2014**, *729*, 43−52.
(148) Jedraszko, J.; Nogala, W.; Adamiak, W.; Rozniecka, E.; Lubarska-Radziejewska, I.; Girault, H. H.; Opallo, M. Hydrogen Peroxide Generation at Liquid|Liquid Interface under Conditions Unfavorable for Proton Transfer from Aqueous to Organic Phase. *J. Phys. Chem. C* **2013**, *117*, 20681−20688.
(149) Li, F.; Su, B.; Salazar, F. C.; Nia, R. P.; Girault, H. H. Detection of Hydrogen Peroxide Produced at a Liquid/Liquid Interface Using Scanning Electrochemical Microscopy. *Electrochem. Commun.* **2009**, *11*, 473−476.
(150) Jedraszko, J.; Nogala, W.; Adamiak, W.; Dongmo, S.; Wittstock, G.; Girault, H. H.; Opallo, M. Catalysis at the Room Temperature Ionic Liquid|water Interface: H_2O_2 Generation. *Chem. Commun.* **2015**, *51*, 6851−6853.
(151) Deng, H.; Peljo, P.; Momotenko, D.; Cortés-Salazar, F.; Jane Stockmann, T.; Kontturi, K.; Opallo, M.; Girault, H. H. Kinetic Differentiation of Bulk/Interfacial Oxygen Reduction Mechanisms At/Near Liquid/Liquid Interfaces Using Scanning Electrochemical Microscopy. *J. Electroanal. Chem.* **2014**, *732*, 101−109.
(152) Deng, H.; Stockmann, T. J.; Peljo, P.; Opallo, M.; Girault, H. H. Electrochemical Oxygen Reduction at Soft Interfaces Catalyzed by the Transfer of Hydrated Lithium Cations. *J. Electroanal. Chem.* **2014**, *731*, 28−35.
(153) Adamiak, W.; Jedraszko, J.; Krysiak, O.; Nogala, W.; Hidalgo-Acosta, J. C.; Girault, H. H.; Opallo, M. Hydrogen and Hydrogen Peroxide Formation in Trifluorotoluene-Water Biphasic Systems. *J. Phys. Chem. C* **2014**, *118*, 23154−23161.
(154) Karlsson, A.; Broo, A.; Ahlberg, P. Regioselective Protonation of Ferrocene in Superacid and Formation of a C−H−Fe Bond. An Experimental and Theoretical Study of the Structure and Dynamics of the Ferrocenonium Ion. *Can. J. Chem.* **1999**, *77*, 628−633.
(155) Lubach, J.; Drenth, W. Enolization and Oxidation: II. Oxidation of Ferrocene by Molecular Oxygen and Hydrogen Peroxide in Acidic Media. *Recl. des Trav. Chim. des Pays-Bas* **1973**, *92*, 586−592.
(156) Fomin, V. M. Common Relationships of Ferrocene Oxidation with Oxygen and Sulfur Dioxide in Acid Solutions and of Its Direct Oxidation with Carboxylic Acids. *Russ. J. Gen. Chem.* **2007**, *77*, 954−960.

DOI: 10.1021/acs.chemrev.7b00542
Chem. Rev. XXXX, XXX, XXX−XXX

(157) Trojánek, A.; Langmaier, J.; Su, B.; Girault, H. H.; Samec, Z. Electrochemical Evidence of Catalysis of Oxygen Reduction at the Polarized Liquid-Liquid Interface by Tetraphenylporphyrin Monoacid and Diacid. *Electrochem. Commun.* **2009**, *11*, 1940−1943.
(158) Trojánek, A.; Langmaier, J.; Šebera, J.; Záliš, S.; Barbe, J.-M.; Girault, H. H.; Samec, Z. Fine Tuning of the Catalytic Effect of a Metal-Free Porphyrin on the Homogeneous Oxygen Reduction. *Chem. Commun.* **2011**, *47*, 5446−5448.
(159) Trojánek, A.; Langmaier, J.; Samec, Z. Thermodynamic Driving Force Effects in the Oxygen Reduction Catalyzed by a Metal-Free Porphyrin. *Electrochim. Acta* **2012**, *82*, 457−462.
(160) Trojánek, A.; Langmaier, J.; Záliš, S.; Samec, Z. Competitive Inhibition of a Metal-Free Porphyrin Oxygen-Reduction Catalyst by Water. *Chem. Commun.* **2012**, *48*, 4094−4096.
(161) Wu, S.; Su, B. Metal-Free-Porphyrin-Catalyzed Oxygen Reduction at Liquid-Liquid Interfaces. *Chem. - Eur. J.* **2012**, *18*, 3169−3173.
(162) Mase, K.; Ohkubo, K.; Xue, Z.; Yamada, H.; Fukuzumi, S. Catalytic Two-Electron Reduction of Dioxygen Catalysed by Metal-Free [14]triphyrin(2.1.1). *Chem. Sci.* **2015**, *6*, 6496−6504.
(163) Hatay, I.; Su, B.; Méndez, M. A.; Corminboeuf, C.; Khoury, T.; Gros, C. P.; Bourdillon, M.; Meyer, M.; Barbe, J.-M.; Ersoz, M.; et al. Oxygen Reduction Catalyzed by a Fluorinated Tetraphenylporphyrin Free Base at Liquid/Liquid Interfaces. *J. Am. Chem. Soc.* **2010**, *132*, 13733−13741.
(164) Fukuzumi, S.; Ohkubo, K.; Lee, Y. M.; Nam, W. Lewis Acid Coupled Electron Transfer of Metal-Oxygen Intermediates. *Chem. - Eur. J.* **2015**, *21*, 17548−17559.
(165) Fukuzumi, S.; Patz, M.; Suenobu, T.; Kuwahara, Y.; Itoh, S. ESR Spectra of Superoxide Anion - Scandium Complexes Detectable in Fluid Solution. *J. Am. Chem. Soc.* **1999**, *121*, 1605−1606.
(166) Fukuzumi, S.; Ohkubo, K. Quantitative Evaluation of Lewis Acidity of Metal Ions Derived from the G Values of ESR Spectra of Superoxide: Metal Ion Complexes in Relation to the Promoting Effects in Electron Transfer Reactions. *Chem. - Eur. J.* **2000**, *6*, 4532−4535.
(167) Ohkubo, K.; Menon, S. C.; Orita, A.; Otera, J.; Fukuzumi, S. Quantitative Evaluation of Lewis Acidity of Metal Ions with Different Ligands and Counterions in Relation to the Promoting Effects of Lewis Acids on Electron Transfer Reduction of Oxygen. *J. Org. Chem.* **2003**, *68*, 4720−4726.
(168) Gubelmann, M. H.; Williams, A. F. The Structure and Reactivity of Dioxygen Complexes of the Transition Metals. In *Structure and Bonding*; Springer-Verlag: Berlin/Heidelberg, 1983; Vol. *55*, pp 2−65.
(169) Zagal, J. H. Metallophthalocyanines Reactions As Catalysts in Electrochemical. *Coord. Chem. Rev.* **1992**, *119*, 89−136.
(170) Elzing, A.; van der Putten, A.; Visscher, W.; Barendrecht, E. Models for the Adsorption of Dioxygen on Metal Chelates. *Recl. Trav. Chim. Pays-Bas* **1990**, *109*, 31−39.
(171) Hong, S.; Lee, Y.-M.; Ray, K.; Nam, W. Dioxygen Activation Chemistry by Synthetic Mononuclear Nonheme Iron, Copper and Chromium Complexes. *Coord. Chem. Rev.* **2017**, *334*, 25−42.
(172) Sahu, S.; Goldberg, D. P. Activation of Dioxygen by Iron and Manganese Complexes: A Heme and Nonheme Perspective. *J. Am. Chem. Soc.* **2016**, *138*, 11410−11428.
(173) Shook, R. L.; Borovik, A. S. Role of the Secondary Coordination Sphere in Metal-Mediated Dioxygen Activation. *Inorg. Chem.* **2010**, *49*, 3646−3660.
(174) Rosenthal, J.; Nocera, D. G. Role of Proton-Coupled Electron Transfer in O-O Bond Activation. *Acc. Chem. Res.* **2007**, *40*, 543−553.
(175) Jones, R. D.; Summerville, D. A.; Basolo, F. Synthetic Oxygen Carriers Related to Biological Systems. *Chem. Rev.* **1979**, *79*, 139−179.
(176) Momenteau, M.; Reed, C. A. Synthetic Heme-Dioxygen Complexes. *Chem. Rev.* **1994**, *94*, 659−698.
(177) Mirica, L. M.; Ottenwaelder, X.; Stack, T. D. P. Structure and Spectroscopy of Copper−Dioxygen Complexes. *Chem. Rev.* **2004**, *104*, 1013−1046.
(178) Lewis, E. A.; Tolman, W. B. Reactivity of Dioxygen−Copper Systems. *Chem. Rev.* **2004**, *104*, 1047−1076.
(179) Elwell, C. E.; Gagnon, N. L.; Neisen, B. D.; Dhar, D.; Spaeth, A. D.; Yee, G. M.; Tolman, W. B. Copper−Oxygen Complexes Revisited: Structures, Spectroscopy, and Reactivity. *Chem. Rev.* **2017**, *117*, 2059−2107.
(180) Griffith, J. S. On the Magnetic Properties of Some Haemoglobin Complexes. *Proc. R. Soc. London, Ser. A* **1956**, *235*, 23−36.
(181) Pauling, L. Nature of the Iron-Oxygen Bond in Oxy-haemoglobin. *Nature* **1964**, *203*, 182−183.
(182) Praetorius, J. M.; Allen, D. P.; Wang, R.; Webb, J. D.; Grein, F.; Kennepohl, P.; Crudden, C. M. N-Heterocyclic Carbene Complexes of Rh: Reaction with Dioxygen without Oxidation. *J. Am. Chem. Soc.* **2008**, *130*, 3724−3725.
(183) Keske, E. C.; Zenkina, O. V.; Asadi, A.; Sun, H.; Praetorius, J. M.; Allen, D. P.; Covelli, D.; Patrick, B. O.; Wang, R.; Kennepohl, P.; et al. Dioxygen Adducts of Rhodium N-Heterocyclic Carbene Complexes. *Dalt. Trans.* **2013**, *42*, 7414−7423.
(184) Shook, R. L.; Peterson, S. M.; Greaves, J.; Moore, C.; Rheingold, A. L.; Borovik, A. S. Catalytic Reduction of Dioxygen to Water with a Monomeric Manganese Complex at Room Temperature. *J. Am. Chem. Soc.* **2011**, *133*, 5810−5817.
(185) Matsumoto, T.; Kim, K.; Ogo, S. Molecular Catalysis in a Fuel Cell. *Angew. Chem., Int. Ed.* **2011**, *50*, 11202−11205.
(186) Kim, K.; Matsumoto, T.; Robertson, A.; Nakai, H.; Ogo, S. Simple Ligand Effects Switch a Hydrogenase Mimic between H_2 and O_2 Activation. *Chem. - Asian J.* **2012**, *7*, 1394−1400.
(187) Meier, G.; Braun, T. Hydrogenation of a Rhodium Peroxido Complex by Formate Derivatives: Mechanistic Studies and the Catalytic Formation of H_2O_2 from O_2. *Angew. Chem., Int. Ed.* **2012**, *51*, 12564−12569.
(188) Shi, Z.; Zhang, J. Density Functional Theory Study of Transitional Metal Macrocyclic Complexes' Dioxygen-Binding Abilities and Their Catalytic Activities toward Oxygen Reduction Reaction. *J. Phys. Chem. C* **2007**, *111*, 7084−7090.
(189) Shubina, T. E. Computational Studies on Properties, Formation, and Complexation of M(II)-Porphyrins. *Adv. Inorg. Chem.* **2010**, *62*, 261−299.
(190) Geiger, T.; Anson, F. C. Homogeneous Catalysis of the Electrochemical Reduction of Dioxygen by a Macrocyclic Cobalt(III) Complex. *J. Am. Chem. Soc.* **1981**, *103*, 7489−7496.
(191) Kang, C.; Anson, F. C. Effects of Coordination to a Macrocyclic Cobalt Complex on the Electrochemistry of Dioxygen, Superoxide, and Hydroperoxide. *Inorg. Chem.* **1995**, *34*, 2771−2780.
(192) Baran, J. D.; Grönbeck, H.; Hellman, A. Analysis of Porphyrines as Catalysts for Electrochemical Reduction of O_2 and Oxidation of H_2O. *J. Am. Chem. Soc.* **2014**, *136*, 1320−1326.
(193) Dawson, J. H. Probing Structure-Function Relations in Heme-Containing Oxygenases and Peroxidases. *Science* **1988**, *240*, 433−439.
(194) Rietjens, I. M. C. M.; Osman, A. M.; Veeger, C.; Zakharieva, O.; Antony, J.; Grodzicki, M.; Trautwein, A. X. On the Role of the Axial Ligand in Heme-Based Catalysis of the Peroxidase and P450 Type. *JBIC, J. Biol. Inorg. Chem.* **1996**, *1*, 372−376.
(195) Poulos, T. L. The Role of the Proximal Ligand in Heme Enzymes. *JBIC, J. Biol. Inorg. Chem.* **1996**, *1*, 356−359.
(196) Goodin, D. B. When an Amide Is More like Histidine than Imidazole: The Role of Axial Ligands in Heme Catalysis. *JBIC, J. Biol. Inorg. Chem.* **1996**, *1*, 360−363.
(197) Solomon, D.; Peretz, P.; Faraggi, Y. Chemical Properties of Water-Soluble Porphyrins. 2. The Reaction of Iron(III)Tetrakis(4-*N*-methylpyridyl)porphyrin with the Superoxide Radical Dioxygen Couple. *J. Phys. Chem.* **1982**, *86*, 1842−1849.
(198) Chlistunoff, J.; Sansiñena, J.-M. Effects of Axial Coordination of the Metal Center on the Activity of Iron Tetraphenylporphyrin as a Nonprecious Catalyst for Oxygen Reduction. *J. Phys. Chem. C* **2014**, *118*, 19139−19149.
(199) Tsuda, M.; Kasai, H. Imidazole Ligand Effect on O_2 Interaction with Metalloporphyrins. *Surf. Sci.* **2007**, *601*, 5200−5206.
(200) Ohta, T.; Nagaraju, P.; Liu, J. G.; Ogura, T.; Naruta, Y. The Secondary Coordination Sphere and Axial Ligand Effects on Oxygen

DOI: 10.1021/acs.chemrev.7b00542
Chem. Rev. XXXX, XXX, XXX−XXX

Reduction Reaction by Iron Porphyrins: A DFT Computational Study. *JBIC, J. Biol. Inorg. Chem.* **2016**, *21*, 745−755.
(201) Sono, M.; Roach, M. P.; Coulter, E. D.; Dawson, J. H. Heme-Containing Oxygenases. *Chem. Rev.* **1996**, *96*, 2841−2888.
(202) Solomon, E. I.; Heppner, D. E.; Johnston, E. M.; Ginsbach, J. W.; Cirera, J.; Qayyum, M.; Kieber-Emmons, M. T.; Kjaergaard, C. H.; Hadt, R. G.; Tian, L. Copper Active Sites in Biology. *Chem. Rev.* **2014**, *114*, 3659−3853.
(203) Gerber, N. C.; Sligar, S. G. Catalytic Mechanism of Cytochrome P-450: Evidence for a Distal Charge Relay. *J. Am. Chem. Soc.* **1992**, *114*, 8742−8743.
(204) Ortiz de Montellano, P. R. Control of the Catalytic Activity of Prosthetic Heme by the Structure of Hemoproteins. *Acc. Chem. Res.* **1987**, *20*, 289−294.
(205) Meunier, B.; de Visser, S. P.; Shaik, S. Mechanism of Oxidation Reactions Catalyzed by Cytochrome P450 Enzymes. *Chem. Rev.* **2004**, *104*, 3947−3980.
(206) Zhao, M.; Wang, H.-B.; Ji, L.-N.; Mao, Z.-W. Insights into Metalloenzyme Microenvironments: Biomimetic Metal Complexes with a Functional Second Coordination Sphere. *Chem. Soc. Rev.* **2013**, *42*, 8360−8375.
(207) Kim, E.; Chufán, E. E.; Kamaraj, K.; Karlin, K. D. Synthetic Models for Heme-Copper Oxidases. *Chem. Rev.* **2004**, *104*, 1077−1133.
(208) Borovik, A. S. Bioinspired Hydrogen Bond Motifs in Ligand Design: The Role of Noncovalent Interactions in Metal Ion Mediated Activation of Dioxygen. *Acc. Chem. Res.* **2005**, *38*, 54−61.
(209) Spiro, T. G.; Zgierski, M. Z.; Kozlowski, P. M. Stereoelectronic Factors in CO, NO and O_2 Binding to Heme from Vibrational Spectroscopy and DFT Analysis. *Coord. Chem. Rev.* **2001**, *219-221*, 923−936.
(210) Sigfridsson, E.; Ryde, U. On the Significance of Hydrogen Bonds for the Discrimination between CO and O_2 by Myoglobin. *JBIC, J. Biol. Inorg. Chem.* **1999**, *4*, 99−110.
(211) Yeh, C.-Y.; Chang, C. J.; Nocera, D. G. "Hangman" Porphyrins for the Assembly of a Model Heme Water Channel. *J. Am. Chem. Soc.* **2001**, *123*, 1513−1514.
(212) Soper, J. D.; Kryatov, S. V.; Rybak-Akimova, E. V.; Nocera, D. G. Proton-Directed Redox Control of O-O Bond Activation by Heme Hydroperoxidase Models. *J. Am. Chem. Soc.* **2007**, *129*, 5069−5075.
(213) Dogutan, D. K.; Stoian, S. A.; Mcguire, R.; Schwalbe, M.; Teets, T. S.; Nocera, D. G. Hangman Corroles ;: Efficient Synthesis and Oxygen Reaction Chemistry. *J. Am. Chem. Soc.* **2011**, *133*, 131−140.
(214) Chng, L. L.; Chang, C. J.; Nocera, D. G. Catalytic O-O Activation Chemistry Mediated by Iron Hangman Porphyrins with a Wide Range of Proton-Donating Abilities. *Org. Lett.* **2003**, *5*, 2421−2424.
(215) Zyska, B.; Schwalbe, M. Synthesis of Sterically Hindered Xanthene-Modified Iron Corroles with Catalase-like Activity. *Chem. Commun.* **2013**, *49*, 3799−3801.
(216) Dogutan, D. K.; McGuire, R.; Nocera, D. G. Electocatalytic Water Oxidation by Cobalt(III) Hangman Beta-Octafluoro Corroles. *J. Am. Chem. Soc.* **2011**, *133*, 9178−9180.
(217) Blomberg, M. R. A.; Siegbahn, P. E. M.; Babcock, G. T.; Wikström, M. O−O Bond Splitting Mechanism in Cytochrome Oxidase. *J. Inorg. Biochem.* **2000**, *80*, 261−269.
(218) Blomberg, M. R. A.; Siegbahn, P. E. M.; Babcock, G. T.; Wikström, M. Modeling Cytochrome Oxidase: A Quantum Chemical Study of the O-O Bond Cleavage Mechanism. *J. Am. Chem. Soc.* **2000**, *122*, 12848−12858.
(219) Schaefer, A. W.; Kieber-Emmons, M. T.; Adam, S. M.; Karlin, K. D.; Solomon, E. I. Phenol-Induced O−O Bond Cleavage in a Low-Spin Heme−Peroxo−Copper Complex: Implications for O_2 Reduction in Heme−Copper Oxidases. *J. Am. Chem. Soc.* **2017**, *139*, 7958−7973.
(220) Costentin, C.; Hajj, V.; Robert, M.; Savéant, J.-M.; Tard, C. Concerted Heavy-Atom Bond Cleavage and Proton and Electron Transfers Illustrated by Proton-Assisted Reductive Cleavage of an O−O Bond. *Proc. Natl. Acad. Sci. U. S. A.* **2011**, *108*, 8559−8564.
(221) McGuire, R., Jr.; Dogutan, D. K.; Teets, T. S.; Suntivich, J.; Shao-Horn, Y.; Nocera, D. G. Oxygen Reduction Reactivity of Cobalt(II) Hangman Porphyrins. *Chem. Sci.* **2010**, *1*, 411−414.
(222) Shook, R. L.; Borovik, A. S. The Effects of Hydrogen Bonds on Metal-Mediated O_2 Activation and Related Processes. *Chem. Commun.* **2008**, *46*, 6095−6107.
(223) Blacquiere, J. M.; Pegis, M. L.; Raugei, S.; Kaminsky, W.; Forget, A.; Cook, S. A.; Taguchi, T.; Mayer, J. M. Synthesis and Reactivity of Tripodal Complexes Containing Pendant Bases. *Inorg. Chem.* **2014**, *53*, 9242−9253.
(224) Nam, W. Synthetic Mononuclear Nonheme Iron−Oxygen Intermediates. *Acc. Chem. Res.* **2015**, *48*, 2415−2423.
(225) Fukuzumi, S.; Kotani, H. Metal Ion-Coupled and Proton-Coupled Electron Transfer in Catalytic Reduction of Dioxygen. In *Proton Coupled Electron Transfer: A Carrefour of Chemical Reactivity Traditions*; Formosinho, S., Barroso, M., Eds.; Royal Society of Chemistry: 2012; pp 89−125.
(226) Ray, K.; Pfaff, F. F.; Wang, B.; Nam, W. Status of Reactive Non-Heme Metal−Oxygen Intermediates in Chemical and Enzymatic Reactions. *J. Am. Chem. Soc.* **2014**, *136*, 13942−13958.
(227) Fukuzumi, S. Electron-Transfer Properties of High-Valent Metal-Oxo Complexes. *Coord. Chem. Rev.* **2013**, *257*, 1564−1575.
(228) Hong, S.; Pfaff, F. F.; Kwon, E.; Wang, Y.; Seo, M.-S.; Bill, E.; Ray, K.; Nam, W. Spectroscopic Capture and Reactivity of a Low-Spin Cobalt(IV)-Oxo Complex Stabilized by Binding Redox-Inactive Metal Ions. *Angew. Chem., Int. Ed.* **2014**, *53*, 10403−10407.
(229) Pfaff, F. F.; Kundu, S.; Risch, M.; Pandian, S.; Heims, F.; Pryjomska-Ray, I.; Haack, P.; Metzinger, R.; Bill, E.; Dau, H.; et al. An Oxocobalt(IV) Complex Stabilized by Lewis Acid Interactions with Scandium(III) Ions. *Angew. Chem., Int. Ed.* **2011**, *50*, 1711−1715.
(230) Nishida, Y.; Lee, Y.-M.; Nam, W.; Fukuzumi, S. Autocatalytic Formation of an Iron(IV)−Oxo Complex via Scandium Ion-Promoted Radical Chain Autoxidation of an Iron(II) Complex with Dioxygen and Tetraphenylborate. *J. Am. Chem. Soc.* **2014**, *136*, 8042−8049.
(231) Li, F.; Van Heuvelen, K. M.; Meier, K. K.; Münck, E.; Que, L. Sc^{3+}-Triggered Oxoiron(IV) Formation from O_2 and Its Non-Heme Iron(II) Precursor via a Sc^{3+}−Peroxo−Fe^{3+} Intermediate. *J. Am. Chem. Soc.* **2013**, *135*, 10198−10201.
(232) Chen, J.; Lee, Y.-M.; Davis, K. M.; Wu, X.; Seo, M. S.; Cho, K.-B.; Yoon, H.; Park, Y. J.; Fukuzumi, S.; Pushkar, Y. N.; et al. A Mononuclear Non-Heme Manganese(IV)-Oxo Complex Binding Redox-Inactive Metal Ions. *J. Am. Chem. Soc.* **2013**, *135*, 6388−6391.
(233) Morimoto, Y.; Kotani, H.; Park, J.; Lee, Y.-M.; Nam, W.; Fukuzumi, S. Metal Ion-Coupled Electron Transfer of a Nonheme Oxoiron(IV) Complex: Remarkable Enhancement of Electron-Transfer Rates by Sc^{3+}. *J. Am. Chem. Soc.* **2011**, *133*, 403−405.
(234) Hong, S.; Lee, Y.-M.; Sankaralingam, M.; Vardhaman, A. K.; Park, Y. J.; Cho, K.-B.; Ogura, T.; Sarangi, R.; Fukuzumi, S.; Nam, W. A Manganese(V)−Oxo Complex: Synthesis by Dioxygen Activation and Enhancement of Its Oxidizing Power by Binding Scandium Ion. *J. Am. Chem. Soc.* **2016**, *138*, 8523−8532.
(235) Zhang, J.; Yang, H.; Sun, T.; Chen, Z.; Yin, G. Nonredox Metal-Ions-Enhanced Dioxygen Activation by Oxidovanadium(IV) Complexes toward Hydrogen Atom Abstraction. *Inorg. Chem.* **2017**, *56*, 834−844.
(236) Lee, Y. M.; Bang, S.; Kim, Y. M.; Cho, J.; Hong, S.; Nomura, T.; Ogura, T.; Troeppner, O.; Ivanovic-Burmazovic, I.; Sarangi, R.; et al. A Mononuclear Non-Heme Manganese(IV)-Oxo Complex Binding Redox-Inactive Metal Ions. *Chem. Sci.* **2013**, *4*, 3917−3923.
(237) Bae, S. H.; Lee, Y.-M.; Fukuzumi, S.; Nam, W. Fine Control of the Redox Reactivity of a Nonheme Iron(III)−Peroxo Complex by Binding Redox-Inactive Metal Ions. *Angew. Chem., Int. Ed.* **2017**, *56*, 801−805.
(238) Bang, S.; Lee, Y.-M.; Hong, S.; Cho, K.-B.; Nishida, Y.; Seo, M. S.; Sarangi, R.; Fukuzumi, S.; Nam, W. Redox-Inactive Metal Ions Modulate the Reactivity and Oxygen Release of Mononuclear Non-Haem Iron(III)-Peroxo Complexes. *Nat. Chem.* **2014**, *6*, 934−940.
(239) Dürr, K.; Macpherson, B. P.; Warratz, R.; Hampel, F.; Tuczek, F.; Helmreich, M.; Jux, N.; Ivanović-Burmazović, I. Iron(III) Complex of a Crown Ether−Porphyrin Conjugate and Reversible Binding of Superoxide to Its Iron(II) Form. *J. Am. Chem. Soc.* **2007**, *129*, 4217−4228.

DOI: 10.1021/acs.chemrev.7b00542
Chem. Rev. XXXX, XXX, XXX−XXX

(240) Dürr, K.; Jux, N.; Zahl, A.; van Eldik, R.; Ivanović-Burmazović, I. Volume Profile Analysis for the Reversible Binding of Superoxide to Form Iron(II)-Superoxo/Iron(III)-Peroxo Porphyrin Complexes. *Inorg. Chem.* **2010**, *49*, 11254−11260.
(241) Duerr, K.; Troeppner, O.; Olah, J.; Li, J.; Zahl, A.; Drewello, T.; Jux, N.; Harvey, J. N.; Ivanovic-Burmazovic, I. Solution Behavior of Iron(III) and Iron(II) Porphyrins in DMSO and Reaction with Superoxide. Effect of Neighboring Positive Charge on Thermodynamics, Kinetics and Nature of Iron-(Su)peroxo Product. *Dalt. Trans.* **2012**, *41*, 546−557.
(242) Schax, F.; Suhr, S.; Bill, E.; Braun, B.; Herwig, C.; Limberg, C. A Heterobimetallic Superoxide Complex Formed through O_2 Activation between Chromium(II) and a Lithium Cation. *Angew. Chem., Int. Ed.* **2015**, *54*, 1352−1356.
(243) Guilard, R.; Brandes, S.; Tardieux, C.; Tabard, A.; L'Her, M.; Miry, C.; Gouerec, P.; Knop, Y.; Collman, J. P. Synthesis and Characterization of Cofacial Metallodiporphyrins Involving Cobalt and Lewis Acid Metals: New Dinuclear Multielectron Redox Catalysts of Dioxygen Reduction. *J. Am. Chem. Soc.* **1995**, *117*, 11721−11729.
(244) Yamamoto, K.; Oyaizu, K.; Tsuchida, E. Catalytic Cycle of a Divanadium Complex with Salen Ligands in O_2 Reduction: Two-Electron Redox Process of the Dinuclear Center (Salen = *N,N'*-ethylenebis(salicylideneamine)). *J. Am. Chem. Soc.* **1996**, *118*, 12665−12672.
(245) Tsuchida, E.; Oyaizu, K.; Dewi, E. L.; Imai, T.; Anson, F. C. Catalysis of the Electroreduction of O_2 to H_2O by Vanadium-Salen Complexes in Acidified Dichloromethane. *Inorg. Chem.* **1999**, *38*, 3704−3708.
(246) Liu, Z.; Anson, F. C. Electrochemical Properties of vanadium-(III,IV,V) - Salen Complexes in Acetonitrile. Four-Electron Reduction of O_2 by V(III)-Salen. *Inorg. Chem.* **2000**, *39*, 274−280.
(247) Liu, Z.; Anson, F. C. Schiff Base Complexes of Vanadium(III, IV, V) as Catalysts for the Electroreduction of O_2 to H_2O in Acetonitrile. *Inorg. Chem.* **2001**, *40*, 1329−1333.
(248) Liu, S.; Mase, K.; Bougher, C.; Hicks, S. D.; Abu-Omar, M. M.; Fukuzumi, S. High-Valent Chromium-Oxo Complex Acting as an Efficient Catalyst Precursor for Selective Two-Electron Reduction of Dioxygen by a Ferrocene Derivative. *Inorg. Chem.* **2014**, *53*, 7780−7788.
(249) Lu, F.; Zarkesh, R. A.; Heyduk, A. F. A Redox-Active Ligand as a Reservoir for Protons and Electrons: O_2 Reduction at Zirconium(IV). *Eur. J. Inorg. Chem.* **2012**, *2012*, 467−470.
(250) Henthorn, J. T.; Lin, S.; Agapie, T. Combination of Redox-Active Ligand and Lewis Acid for Dioxygen Reduction with π-Bound Molybdenum-Quinonoid Complexes. *J. Am. Chem. Soc.* **2015**, *137*, 1458−1464.
(251) Kobayashi, N.; Nevin, W. A. Electrocatalytic Reduction of Oxygen Using Water-Soluble Iron and Cobalt Phthalocyanines and Porphyrins. *Appl. Organomet. Chem.* **1996**, *10*, 579−590.
(252) Sorokin, A. B. Phthalocyanine Metal Complexes in Catalysis. *Chem. Rev.* **2013**, *113*, 8152−8191.
(253) Fang, Y.; Ou, Z.; Kadish, K. M. Electrochemistry of Corroles in Nonaqueous Media. *Chem. Rev.* **2017**, *117*, 3377−3419.
(254) Hiroto, S.; Miyake, Y.; Shinokubo, H. Synthesis and Functionalization of Porphyrins through Organometallic Methodologies. *Chem. Rev.* **2017**, *117*, 2910−3043.
(255) Kuwana, T.; Fujihira, M.; Sunakawa, K.; Osa, T. Catalytic Electroreduction of Molecular Oxygen Using Water Soluble Iron Porphyrin. *J. Electroanal. Chem. Interfacial Electrochem.* **1978**, *88*, 299−303.
(256) Bettelheim, A.; Kuwana, T. Rotating-Ring-Disc Analysis of Iron Tetra(*N*-methylpyridyl)Porphyrin in Electrocatalysis of Oxygen. *Anal. Chem.* **1979**, *51*, 2257−2260.
(257) Forshey, P. A.; Kuwana, T. Electrochemistry of Oxygen Reduction. 4. Oxygen to Water Conversion by Iron(II) Tetrakis(*N*-methyl-4-pyridyl)porphyrin via Hydrogen Peroxide. *Inorg. Chem.* **1983**, *22*, 699−707.
(258) Oliver Su, Y.; Kuwana, T.; Chen, S. M. Electrocatalysis of Oxygen Reduction by Water-Soluble Iron Porphyrins. Thermodynamic and Kinetic Advantage Studies. *J. Electroanal. Chem. Interfacial Electrochem.* **1990**, *288*, 177−195.
(259) Costentin, C.; Dridi, H.; Savéant, J. M. Molecular Catalysis of O_2 Reduction by Iron Porphyrins in Water: Heterogeneous versus Homogeneous Pathways. *J. Am. Chem. Soc.* **2015**, *137*, 13535−13544.
(260) He, Q.; Mugadza, T.; Hwang, G.; Nyokong, T. Mechanisms of Electrocatalysis of Oxygen Reduction by Metal Porphyrins in Trifluoromethane Sulfonic Acid Solution. *Int. J. Electrochem. Sci.* **2012**, *7*, 7045−7064.
(261) Huang, X.; Xuan, Y.; Xie, L.; Su, B. Unraveling the Phase-Transfer Catalysis Mechanism of Oxygen Reduction Catalyzed by Iron (III) *meso*-tetra-(4-*N*-Methyl-pyridyl)porphine at the Liquid/Liquid Interface. *ChemElectroChem* **2016**, *3*, 1781−1786.
(262) Kobayashi, N.; Nishiyama, Y. Catalytic Electroreduction of Molecular Oxygen Using Iron or Cobalt 4,4′, 4′′, 4′′′-tetracarboxyphthalocyanine. *J. Phys. Chem.* **1985**, *89*, 1167−1170.
(263) Han, S. B.; Kwak, D. H.; Park, H. S.; Choi, I. A.; Park, J. Y.; Ma, K. B.; Won, J. E.; Kim, D. H.; Kim, S. J.; Kim, M. C.; et al. Chemically Regenerative Redox Fuel Cells Using Iron Redox Couples as a Liquid Catalyst with Cocatalysts. *ACS Catal.* **2016**, *6*, 5302−5306.
(264) Fukuzumi, S.; Mochizuki, S.; Tanaka, T. Efficient Reduction of Dioxygen with Ferrocene Derivatives, Catalyzed by Metalloporphyrins in the Presence of Perchloric Acid. *Inorg. Chem.* **1989**, *28*, 2459−2465.
(265) Fukuzumi, S.; Mochizuki, S.; Tanaka, T. Metalloporphyrin-Catalyzed Reduction of Dioxygen by Ferrocene Derivatives. *Chem. Lett.* **1989**, *18*, 27−30.
(266) Samanta, S.; Mittra, K.; Sengupta, K.; Chatterjee, S.; Dey, A. Second Sphere Control of Redox Catalysis: Selective Reduction of O_2 to O_2^- or H_2O by an Iron Porphyrin Catalyst. *Inorg. Chem.* **2013**, *52*, 1443−1453.
(267) Mittra, K.; Chatterjee, S.; Samanta, S.; Dey, A. Selective $4e^-/4H^+$ O_2 Reduction by an Iron(tetraferrocenyl)porphyrin Complex: From Proton Transfer Followed by Electron Transfer in Organic Solvent to Proton Coupled Electron Transfer in Aqueous Medium. *Inorg. Chem.* **2013**, *52*, 14317−14325.
(268) Anson, F. C.; Shi, C.; Steiger, B. Novel Multinuclear Catalysts for the Electroreduction of Dioxygen Directly to Water. *Acc. Chem. Res.* **1997**, *30*, 437−444.
(269) Chatterjee, S.; Sengupta, K.; Mondal, B.; Dey, S.; Dey, A. Factors Determining the Rate and Selectivity of $4e^-/4H^+$ Electrocatalytic Reduction of Dioxygen by Iron Porphyrin Complexes. *Acc. Chem. Res.* **2017**, *50*, 1744−1753.
(270) Collman, J.; Ghosh, S.; Dey, A.; Decréau, R. A.; Yang, Y. Catalytic Reduction of O_2 by Cytochrome *c* Using a Synthetic Model of Cytochrome *c* Oxidase. *J. Am. Chem. Soc.* **2009**, *131*, 5034−5035.
(271) Halime, Z.; Kotani, H.; Li, Y.; Fukuzumi, S.; Karlin, K. D. Homogeneous Catalytic O_2 Reduction to Water by a Cytochrome *c* Oxidase Model with Trapping of Intermediates and Mechanistic Insights. *Proc. Natl. Acad. Sci. U. S. A.* **2011**, *108*, 13990−13994.
(272) Pacheco-Londoño, L. C.; Peña, Á. J.; Primera-Pedrozo, O. M.; Hernández-Rivera, S. P.; Mina, N.; García, R.; Chamberlain, R. T.; Lareau, R. T.; et al. An Experimental and Theoretical Study of the Synthesis and Vibrational Spectroscopy of Triacetone Triperoxide (TATP). *Proc. SPIE* **2004**, *5403*, 279−287.
(273) Collman, J. P.; Wagenknecht, P. S.; Hutchison, J. E. Molecular Catalysts for Multielectron Redox Reactions of Small Molecules: The "Cofacial Metallodiporphyrin" Approach. *Angew. Chem., Int. Ed. Engl.* **1994**, *33*, 1537−1554.
(274) Chan, R. J. H.; Su, Y. O.; Kuwana, T. Electrocatalysis of Oxygen Reduction. 5. Oxygen to Hydrogen Peroxide Conversion. *Inorg. Chem.* **1985**, *24*, 3777−3784.
(275) Sazou, D.; Araullo-McAdams, C.; Han, B. C.; Franzen, M. M.; Kadish, K. M. The Use of an Electrogenerated Cobalt(I) Porphyrin for the Homogeneous Catalytic Reduction of Dioxygen in Dimethylformamide. Reactions of $[(TMpyP)Co^{II}]^{4+}$ and $[(TMpyP)Co^{I}]^{3+}$ Where TMpyP = *meso*-tetrakis(1-methylpyridinium-4-yl)porphyrin. *J. Am. Chem. Soc.* **1990**, *112*, 7879−7886.
(276) D'Souza, F.; Deviprasad, R. G.; Hsieh, Y.-Y. Synthesis and Studies on the Electrocatalytic Reduction of Molecular Oxygen by Non-

DOI: 10.1021/acs.chemrev.7b00542
Chem. Rev. XXXX, XXX, XXX−XXX

Planar Cobalt(II) Tetrakis-(*N*-methyl pyridyl)-*β*-octabromoporphyrin. *J. Electroanal. Chem.* **1996**, *411*, 167−171.
(277) D'souza, F.; Hsieh, Y.-V.; Deviprasad, G. R. Electrocatalytic Reduction of Molecular Oxygen Using Non-Planar Cobalt Tetrakis-(4-sulfonatophenyl)-*β*-octabromoporphyrin. *J. Electroanal. Chem.* **1997**, *426*, 17−21.
(278) Trojánek, A.; Langmaier, J.; Kvapilová, H.; Záliš, S.; Samec, Z. Inhibitory Effect of Water on the Oxygen Reduction Catalyzed by Cobalt(II) Tetraphenylporphyrin. *J. Phys. Chem. A* **2014**, *118*, 2018−2028.
(279) Collman, J. P.; Decréau, R. A.; Dey, A.; Yang, Y. Water May Inhibit Oxygen Binding in Hemoprotein Models. *Proc. Natl. Acad. Sci. U. S. A.* **2009**, *106*, 4101−4105.
(280) Wong, C.-L.; Switzer, J. A.; Balakrishnan, K. P.; Endicott, J. F. Oxidation-Reduction Reactions of Complexes with Macrocyclic Ligands. Oxygen Uptake Kinetics, Equilibria, and Intermediates in Aqueous $Co^{II}(N_4)$ Systems. *J. Am. Chem. Soc.* **1980**, *102*, 5511−5518.
(281) Wong, C.-L.; Endicott, J. F. Oxidation-Reduction Reactions of Complexes with Macrocyclic Ligands. Role of Intermediates in Reactions of *μ*-Peroxo-Dicobalt Complexes. *Inorg. Chem.* **1981**, *20*, 2233−2239.
(282) Kumar, K.; Endicott, J. F. Oxidation-Reduction Reactions of Complexes with Macrocyclic Ligands. Electron-Transfer Reactivity of a 1:1 Cobalt(II)-Dioxygen Adduct. *Inorg. Chem.* **1984**, *23*, 2447−2452.
(283) Collman, J. P.; Denisevich, P.; Konai, Y.; Marrocco, M.; Koval, C.; Anson, F. C. Electrode Catalysis of the Four-Electron Reduction of Oxygen to Water by Dicobalt Face-to-Face Porphyrins. *J. Am. Chem. Soc.* **1980**, *102*, 6027−6036.
(284) Bakac, A.; Espenson, J. H. Formation and Homolysis of a Mononuclear Cobalt-Oxygen Adduct. *J. Am. Chem. Soc.* **1990**, *112*, 2273−2278.
(285) Mho, S.; Ortiz, B.; Doddapaneni, N.; Park, S.-M. Electrochemical and Spectroelectrochemical Studies on Metallophthalocyanine-Oxygen Interactions in Nonaqueous Solutions. *J. Electrochem. Soc.* **1995**, *142*, 1047−1053.
(286) Kadish, K. M.; Shen, J.; Frémond, L.; Chen, P.; El Ojaimi, M.; Chkounda, M.; Gros, C. P.; Barbe, J. M.; Ohkubo, K.; Fukuzumi, S.; et al. Clarification of the Oxidation State of Cobalt Corroles in Heterogeneous and Homogeneous Catalytic Reduction of Dioxygen. *Inorg. Chem.* **2008**, *47*, 6726−6737.
(287) Mase, K.; Ohkubo, K.; Fukuzumi, S. Efficient Two-Electron Reduction of Dioxygen to Hydrogen Peroxide with One-Electron Reductants with a Small Overpotential Catalyzed by a Cobalt Chlorin Complex. *J. Am. Chem. Soc.* **2013**, *135*, 2800−2808.
(288) Mase, K.; Ohkubo, K.; Fukuzumi, S. Much Enhanced Catalytic Reactivity of Cobalt Chlorin Derivatives on Two-Electron Reduction of Dioxygen to Produce Hydrogen Peroxide. *Inorg. Chem.* **2015**, *54*, 1808−1815.
(289) Oldacre, A. N.; Friedman, A. E.; Cook, T. R. A Self-Assembled Cofacial Cobalt Porphyrin Prism for Oxygen Reduction Catalysis. *J. Am. Chem. Soc.* **2017**, *139*, 1424−1427.
(290) Collman, J. P.; Anson, F. C.; Barnes, C. E.; Bencosme, C. S.; Geiger, T.; Evitt, E. R.; Kreh, R. P.; Meier, K.; Pettman, R. B. Further Studies of the Dimeric-Linked "Face-to-Face Four" Porphyrin: FTF4. *J. Am. Chem. Soc.* **1983**, *105*, 2694−2699.
(291) Chang, C. K.; Liu, H. Y.; Abdalmuhdi, I. Electroreduction of Oxygen by Pillared Cobalt(II) Cofacial Diporphyrin Catalysts. *J. Am. Chem. Soc.* **1984**, *106*, 2725−2726.
(292) Karaman, R.; Jeon, S.; Almarsson, O.; Bruice, T. C. Symmetrical and Unsymmetrical Quadruply Aza Bridged Closely Interspaced Cofacial bis(5,10,15,20-tetraphenylporphyrins). 3. Interplanar Distances, ^{1}H NMR Chemical Shifts, and the Catalysis of the Electrochemical Reduction of Oxygen. *J. Am. Chem. Soc.* **1992**, *114*, 4899−4905.
(293) Fukuzumi, S.; Okamoto, K.; Tokuda, Y.; Gros, C. P.; Guilard, R. Dehydrogenation versus Oxygenation in Two-Electron and Four-Electron Reduction of Dioxygen by 9-alkyl-10-methyl-9,10-dihydroacridines Catalyzed by Monomeric Cobalt Porphyrins and Cofacial Dicobalt Porphyrins in the Presence of Perchloric Acid. *J. Am. Chem. Soc.* **2004**, *126*, 17059−17066.
(294) Kadish, K. M.; Frémond, L.; Shen, J.; Chen, P.; Ohkubo, K.; Fukuzumi, S.; El Ojaimi, M.; Gros, C. P.; Barbe, J. M.; Guilard, R. Catalytic Activity of Biscobalt Porphyrin-Corrole Dyads toward the Reduction of Dioxygen. *Inorg. Chem.* **2009**, *48*, 2571−2582.
(295) Le Mest, Y.; L'Her, M.; Collman, J. P.; Hendricks, N. H.; McElwee-White, L. Remarkable Oxygen Affinity of a Mixed Valence Dicobalt Cofacial Pophryin $Co^{III}Co^{II}$FTF4. *J. Am. Chem. Soc.* **1986**, *108*, 533−535.
(296) Le Mest, Y.; Inisan, C.; Laouénan, A.; L'Her, M.; Talarmin, J.; El Khalifa, M.; Saillard, J.-Y. Reactivity toward Dioxygen of Dicobalt Face-to-Face Diporphyrins in Aprotic Media. Experimental and Theoretical Aspects. Possible Mechanistic Implication in the Reduction of Dioxygen. *J. Am. Chem. Soc.* **1997**, *119*, 6095−6106.
(297) Givaja, G.; Volpe, M.; Edwards, M. A.; Blake, A. J.; Wilson, C.; Schröder, M.; Love, J. B. Dioxygen Reduction at Dicobalt Complexes of a Schiff Base Calixpyrrole Ligand. *Angew. Chem., Int. Ed.* **2007**, *46*, 584−586.
(298) Volpe, M.; Hartnett, H.; Leeland, J. W.; Wills, K.; Ogunshun, M.; Duncombe, B. J.; Wilson, C.; Blake, A. J.; McMaster, J.; Love, J. B. Binuclear Cobalt Complexes of Schiff-Base Calixpyrroles and Their Roles in the Catalytic Reduction of Dioxygen. *Inorg. Chem.* **2009**, *48*, 5195−5207.
(299) Askarizadeh, E.; Yaghoob, S. B.; Boghaei, D. M.; Slawin, A. M. Z.; Love, J. B. Tailoring Dicobalt Pacman Complexes of Schiff-Base Calixpyrroles Towards Dioxygen Reduction Catalysis. *Chem. Commun.* **2010**, *46*, 710−712.
(300) Devoille, A. M. J.; Love, J. B. Double-Pillared Cobalt Pacman Complexes: Synthesis, Structures and Oxygen Reduction Catalysis. *Dalt. Trans.* **2012**, *41*, 65−72.
(301) Chung, T. D.; Anson, F. C. Catalysis of the Electroreduction of O_2 by Cobalt 5,10,15,20-tetraphenylporphyrin Dissolved in Thin Layers of Benzonitrile on Graphite Electrodes. *J. Electroanal. Chem.* **2001**, *508*, 115−122.
(302) Trojánek, A.; Marecek, V.; Janchenova, H.; Samec, Z. Molecular Electrocatalysis of the Oxygen Reduction at a Polarised Interface between Two Immiscible Electrolyte Solutions by Co(II) Tetraphenylporphyrin. *Electrochem. Commun.* **2007**, *9*, 2185−2190.
(303) Partovi-Nia, R.; Su, B.; Li, F.; Gros, C. P.; Barbe, J. M.; Samec, Z.; Girault, H. H. Proton Pump for O_2 Reduction Catalyzed by 5,10,15,20-tetraphenylporphyrinatocobalt(II). *Chem. - Eur. J.* **2009**, *15*, 2335−2340.
(304) Peljo, P.; Rauhala, T.; Murtomäki, L.; Kallio, T.; Kontturi, K. Oxygen Reduction at a Water-1,2-dichlorobenzene Interface Catalyzed by Cobalt Tetraphenyl Porphyrine - A Fuel Cell Approach. *Int. J. Hydrogen Energy* **2011**, *36*, 10033−10043.
(305) Partovi-Nia, R.; Su, B.; Méndez, M. A.; Habermeyer, B.; Gros, C. P.; Barbe, J. M.; Samec, Z.; Girault, H. H. Dioxygen Reduction by Cobalt(II) Octaethylporphyrin at Liquid | Liquid Interfaces. *ChemPhysChem* **2010**, *11*, 2979−2984.
(306) Peljo, P.; Murtomäki, L.; Kallio, T.; Xu, H. J.; Meyer, M.; Gros, C. P.; Barbe, J. M.; Girault, H. H.; Laasonen, K.; Kontturi, K. Biomimetic Oxygen Reduction by Cofacial Porphyrins at a Liquid-Liquid Interface. *J. Am. Chem. Soc.* **2012**, *134*, 5974−5984.
(307) Li, Y.; Wu, S.; Su, B. Proton-Coupled O_2 Reduction Reaction Catalysed by Cobalt Phthalocyanine at Liquid/Liquid Interfaces. *Chem. - Eur. J.* **2012**, *18*, 7372−7376.
(308) Patir, I. H. Fluorinated-Cobalt Phthalocyanine Catalyzed Oxygen Reduction at Liquid/Liquid Interfaces. *Electrochim. Acta* **2013**, *87*, 788−793.
(309) Jung, J.; Liu, S.; Ohkubo, K.; Abu-Omar, M. M.; Fukuzumi, S. Catalytic Two-Electron Reduction of Dioxygen by Ferrocene Derivatives with Manganese(V) Corroles. *Inorg. Chem.* **2015**, *54*, 4285−4291.
(310) Kobayashi, N.; Saiki, H.; Osa, T. Catalytic Electroreduction of Molecular Oxygen Using [5,10,15,20-Tetrakis-(1-methylpyridinium-4-yl)porphinato] Manganese. *Chem. Lett.* **1985**, *14*, 1917−1920.
(311) Evans, D. F.; Sheriff, T. S. The Production of Hydrogen Peroxide from Dioxygen and Hydroxylamine Catalysed by Manganese Complexes. *J. Chem. Soc., Chem. Commun.* **1985**, 1407.

DOI: 10.1021/acs.chemrev.7b00542
Chem. Rev. XXXX, XXX, XXX−XXX

(312) Sheriff, T. S. Production of Hydrogen Peroxide from Dioxygen and Hydroxylamine or Hydrazine Catalysed by Manganese Complexes. *J. Chem. Soc., Dalton Trans.* **1992**, 1051−1058.
(313) Gennari, M.; Brazzolotto, D.; Pecaut, J.; Cherrier, M. V.; Pollock, C. J.; Debeer, S.; Retegan, M.; Pantazis, D. A.; Neese, F.; Rouzieres, M.; et al. Dioxygen Activation and Catalytic Reduction to Hydrogen Peroxide by a Thiolate-Bridged Dimanganese(II) Complex with a Pendant Thiol. *J. Am. Chem. Soc.* **2015**, *137*, 8644−8653.
(314) Soo, H. S.; Komor, A. C.; Iavarone, A. T.; Chang, C. J. A Hydrogen-Bond Facilitated Cycle for Oxygen Reduction by an Acid- and Base-Compatible Iron Platform. *Inorg. Chem.* **2009**, *48*, 10024−10035.
(315) Fukuzumi, S.; Kotani, H.; Lucas, H. R.; Doi, K.; Suenobu, T.; Peterson, R. L.; Karlin, K. D. Mononuclear Copper Complex-Catalyzed Four-Electron Reduction of Oxygen. *J. Am. Chem. Soc.* **2010**, *132*, 6874−6875.
(316) Kakuda, S.; Peterson, R. L.; Ohkubo, K.; Karlin, K. D.; Fukuzumi, S. Enhanced Catalytic Four-Electron Dioxygen (O_2) and Two-Electron Hydrogen Peroxide (H_2O_2) Reduction with a Copper(II) Complex Possessing a Pendant Ligand Pivalamido Group. *J. Am. Chem. Soc.* **2013**, *135*, 6513−6522.
(317) Kakuda, S.; Rolle, C. J.; Ohkubo, K.; Siegler, M. A.; Karlin, K. D.; Fukuzumi, S. Lewis Acid-Induced Change from Four- to Two-Electron Reduction of Dioxygen Catalyzed by Copper Complexes Using Scandium Triflate. *J. Am. Chem. Soc.* **2015**, *137*, 3330−3337.
(318) Asahi, M.; Yamazaki, S.-I.; Itoh, S.; Ioroi, T. Electrochemical Reduction of Dioxygen by Copper Complexes with Pyridylalkylamine Ligands Dissolved in Aqueous Buffer Solution: The Relationship Between Activity and Redox Potential. *Dalt. Trans.* **2014**, *43*, 10705−10709.
(319) Fukuzumi, S.; Tahsini, L.; Lee, Y. M.; Ohkubo, K.; Nam, W.; Karlin, K. D. Factors That Control Catalytic Two-versus Four-Electron Reduction of Dioxygen by Copper Complexes. *J. Am. Chem. Soc.* **2012**, *134*, 7025−7035.
(320) Tahsini, L.; Kotani, H.; Lee, Y. M.; Cho, J.; Nam, W.; Karlin, K. D.; Fukuzumi, S. Electron-Transfer Reduction of Dinuclear Copper Peroxo and Bis-μ-Oxo Complexes Leading to the Catalytic Four-Electron Reduction of Dioxygen to Water. *Chem. - Eur. J.* **2012**, *18*, 1084−1093.
(321) Tang, Y.-H.; Lin, Y. C.; Hsu, S. C. N.; Liou, S.-T.; Chen, H.-Y.; Hsieh, K.-C.; Chuang, W.-J.; Chiu, L.-T.; Chen, Y.-L.; Kao, C.-L. Cooperative Effects in Copper Polyamidoamine Dendrimer Complexes Catalyzing the Reduction of Molecular Oxygen. *Eur. J. Inorg. Chem.* **2015**, *2015*, 4839−4847.
(322) Fukuzumi, S.; Mandal, S.; Mase, K.; Ohkubo, K.; Park, H.; Benet-Buchholz, J.; Nam, W.; Llobet, A. Catalytic Four-Electron Reduction of O_2 via Rate-Determining Proton-Coupled Electron Transfer to Dinuclear Cobalt-μ-1,2-peroxo Complex. *J. Am. Chem. Soc.* **2012**, *134*, 9906−9909.
(323) Wada, T.; Maki, H.; Imamoto, T.; Yuki, H.; Miyazato, Y. Four-Electron Reduction of Dioxygen Catalysed by Dinuclear Cobalt Complexes Bridged by Bis(terpyridyl)anthracene. *Chem. Commun.* **2013**, *49*, 4394−4396.
(324) Heiden, Z. M.; Rauchfuss, T. B. Homogeneous Catalytic Reduction of Dioxygen Using Transfer Hydrogenation Catalysts. *J. Am. Chem. Soc.* **2007**, *129*, 14303−14310.
(325) Hoover, J. M.; Stahl, S. S. Highly Practical Copper(I)/TEMPO Catalyst System for Chemoselective Aerobic Oxidation of Primary Alcohols. *J. Am. Chem. Soc.* **2011**, *133*, 16901−16910.
(326) Piera, J.; Bäckvall, J.-E. Catalytic Oxidation of Organic Substrates by Molecular Oxygen and Hydrogen Peroxide by Multistep Electron Transfer−a Biomimetic Approach. *Angew. Chem., Int. Ed.* **2008**, *47*, 3506−3523.
(327) Stahl, S. S. Palladium Oxidase Catalysis: Selective Oxidation of Organic Chemicals by Direct Dioxygen-Coupled Turnover. *Angew. Chem., Int. Ed.* **2004**, *43*, 3400−3420.
(328) Stahl, S. S. Palladium-Catalyzed Oxidation of Organic Chemicals with O_2. *Science* **2005**, *309*, 1824−1826.
(329) Allen, S. E.; Walvoord, R. R.; Padilla-Salinas, R.; Kozlowski, M. C. Aerobic Copper-Catalyzed Organic Reactions. *Chem. Rev.* **2013**, *113*, 6234−6458.
(330) Hoover, J. M.; Ryland, B. L.; Stahl, S. S. Copper/TEMPO-Catalyzed Aerobic Alcohol Oxidation: Mechanistic Assessment of Different Catalyst Systems. *ACS Catal.* **2013**, *3*, 2599−2605.
(331) Hoover, J. M.; Ryland, B. L.; Stahl, S. S. Mechanism of Copper(I)/TEMPO-Catalyzed Aerobic Alcohol Oxidation. *J. Am. Chem. Soc.* **2013**, *135*, 2357−2367.
(332) Gamez, P.; Arends, I. W. C. E.; Sheldon, R. A.; Reedijk, J. Room Temperature Aerobic Copper−Catalysed Selective Oxidation of Primary Alcohols to Aldehydes. *Adv. Synth. Catal.* **2004**, *346*, 805−811.
(333) Kumpulainen, E. T. T.; Koskinen, A. M. P. Catalytic Activity Dependency on Catalyst Components in Aerobic Copper−TEMPO Oxidation. *Chem. - Eur. J.* **2009**, *15*, 10901−10911.
(334) Semmelhack, M. F.; Schmid, C. R.; Cortes, D. A.; Chou, C. S. Oxidation of Alcohols to Aldehydes with Oxygen and Cupric Ion, Mediated by Nitrosonium Ion. *J. Am. Chem. Soc.* **1984**, *106*, 3374−3376.
(335) Ryland, B. L.; McCann, S. D.; Brunold, T. C.; Stahl, S. S. Mechanism of Alcohol Oxidation Mediated by Copper(II) and Nitroxyl Radicals. *J. Am. Chem. Soc.* **2014**, *136*, 12166−12173.
(336) Iron, M. A.; Szpilman, A. M. Mechanism of the Copper/TEMPO-Catalyzed Aerobic Oxidation of Alcohols. *Chem. - Eur. J.* **2017**, *23*, 1368−1378.
(337) Anson, C. W.; Ghosh, S.; Hammes-Schiffer, S.; Stahl, S. S. Co(salophen)-Catalyzed Aerobic Oxidation of *p*-Hydroquinone: Mechanism and Implications for Aerobic Oxidation Catalysis. *J. Am. Chem. Soc.* **2016**, *138*, 4186−4193.
(338) Edvinsson Albers, R.; Nyström, M.; Siverström, M.; Sellin, A.; Dellve, A.-C.; Andersson, U.; Herrmann, W.; Berglin, T. Development of a Monolith-Based Process for H_2O_2 Production: From Idea to Large-Scale Implementation. *Catal. Today* **2001**, *69*, 247−252.
(339) Sarapuu, A.; Vaik, K.; Schiffrin, D. J.; Tammeveski, K. Electrochemical Reduction of Oxygen on Anthraquinone-Modified Glassy Carbon Electrodes in Alkaline Solution. *J. Electroanal. Chem.* **2003**, *541*, 23−29.
(340) Costentin, C.; Savéant, J.-M. Homogeneous Molecular Catalysis of Electrochemical Reactions: Catalyst Benchmarking and Optimization Strategies. *J. Am. Chem. Soc.* **2017**, *139*, 8245−8250.

DOI: 10.1021/acs.chemrev.7b00542
Chem. Rev. XXXX, XXX, XXX−XXX